



DEPARTMENT OF MATHEMATICAL SCIENCES

TMA4500 - INDUSTRIAL MATHEMATICS, SPECIALIZATION
PROJECT

**Comparative Analysis of FFT and PINNs for Option
Pricing in a Heston Framework with CIR++ Stochastic
Short Rates**

Author:
Gonchigsuren Bor¹

Supervisor:
Prof. Espen R. Jakobsen

18.12.2025

¹Candidate Number: 10060

Table of Contents

List of Figures	ii
List of Tables	iii
1 Introduction	1
2 A Primer on Financial Theory	3
2.1 Formalities and Setup	3
2.2 Financial Assets and Options	3
2.3 Fixed-Income Instruments	4
2.4 Market Assumptions and Asset Classes	9
2.5 Pricing of European Options	10
3 Interest Rate Models	14
3.1 One-factor Short-rate Models	14
3.2 Pricing of Fixed-Income Instruments under the CIR++ Model	19
4 Option Pricing Model for the Risky Asset	23
4.1 Heston Model with Stochastic Short Rates	23
4.2 Model Specification under the Forward Measure	24
4.3 Backward Parabolic Option Pricing PDE under the Forward Measure	26
5 Option Pricing with the Fast Fourier Transform	29
5.1 Option Pricing using the Characteristic Function	29
5.2 Derivation of the Characteristic Function of $Y(T)$	30
5.3 From Characteristic Functions to the Fast Fourier Transform	36
6 Physics Informed Neural Networks	38
6.1 Formalizing Neural Networks	38
6.2 Sampling Procedure	41
6.3 From PDEs to Loss Functions	45
6.4 Training Procedure	46
7 Numerical Results	48
7.1 Data	48
7.2 Error measures	49
7.3 Calibration of the CIR++ model	50

7.4	Calibration of the option pricing models	53
8	Discussion	61
8.1	Short rate model evaluation	61
8.2	Comparison of the FFT and PINN pricing models	62
9	Conclusion	64
	Bibliography	65
A	Martingales and the martingale representation theorem	67
B	Some Useful Theorems	68
B.1	Itô’s Lemma	68
B.2	The Feynman-Kac Theorem	68
B.3	Girsanov’s Change of Measure Theorem	68
B.4	Bayes’ Theorem	69
C	Numerical simulation of SDEs and Monte Carlo approximation	70
C.1	Euler–Maruyama approximation to SDEs	70
C.2	Monte–Carlo approximation	70
D	Market data	71
D.1	OIS data	71
D.2	Swaptions data	72
D.3	European call option data	77

List of Figures

1	Payoff structure of a zero-coupon bond from the perspective of the bond buyer: The downward facing, red arrow at time τ means that the payer buys the bond for $P(\tau, T)$ and the upward facing, green arrow at time T means that the payer receives 1 at time T	5
2	Example of the cash flow structure for a 4-year swap with start date T_0 , first settlement date T_1 , and strike rate κ . The blue lines represent the floating rates received by the holder of the payer swap contract, whereas the red lines represent the fixed rates paid by the holder of the swap.	7
3	Example of the cash flow structure for a payer swaption with time of maturity τ , notional N , strike rate κ , and a 4-year swap as underlying.	8
4	Feed forward network with five layers (network width), i.e. $l = 5$, and four hidden layers (netwrok depth), i.e. $n_k = 4$ for $k = 2, 3, 4$, with skip connections toward intermediate layers as shown in Hainaut and Casas (2024).	42

5	Sampling procedure for the state variable $s \in [0.1, 1000]$ and the time variable $\tau \in [0, 5]$ with 5000 samples within the rectangular domain (gray dots), 500 samples on the terminal condition boundary (blue dots), and a total of 500 samples on the lower and upper boundaries (red dots).	43
6	Zero-coupon bond prices, yields, and instantaneous forward rates for maturities from 1 to 30 years obtained from the Svensson model with parameter estimates found in table 4.	52
7	Loss landscape of the PINN during the training procedure. The notation "lr" refers to the learning rate used in each training phase. Vertical dashed lines indicate the epoch numbers where a new learning rate is introduced, marking the transition between phases.	55
8	Comparison of FFT and PINN call option prices against market prices (rows 1 and 3) and their respective pricing errors (rows 2 and 4) across strikes for BNPE training and test data.	59
9	Comparison of FFT and PINN call option prices against market prices (rows 1 and 3) and their respective pricing errors (rows 2 and 4) across strikes for SAPE training and test data.	60
10	Monte Carlo estimate of the CIR++ short rate (solid line) compared with the risk-free market instantaneous forward rate $f(0, T)$ (dashed line) implied by the calibrated OIS term structure.	61

List of Tables

1	Details of data set of call option prices for BNPE and SAPE.	49
2	Stock prices at the time of data collection.	49
3	Svensson curve parameters posted by the European Central Bank on October 24th, 2025.	51
4	Optimal Svensson curve parameters on October 24th, 2025.	51
5	CIR++ short-rate model parameters on October 24th, 2025.	53
6	Error measures for the swaptions data set	53
7	Parameter ranges for the training procedure of the PINN.	54
8	Number of samples for the lower, upper and terminal boundaries as well as for the interior domain.	54
9	Learning rates and number of epochs used in the five training phases.	54
10	Approximate times for training and calibration of the FFT and PINN pricing models.	56
11	Comparison of calibrated variance-related parameters for the FFT and PINN option pricing models for European call options on BNPE.	56
12	Comparison of calibrated variance-related parameters for the FFT and PINN option pricing models for European call options on SAPE.	57
13	Error measures for BNPE training and test data sets	57
14	Error measures for SAPE training and test data sets	57
15	EUR OIS par swap rates on October 24th, 2025. The suffixes "W", "M", and "Y" means week, month(s) and year(s), respectively.	71

16	Market and model swaption prices (in percent) on October 24th, 2025. The suffix "Y" means year(s).	72
17	Option data for BNPE on October 24, 2025 for spot stock price $s = 68.72\text{€}$	77
18	Option data for SAPE on October 24, 2025 for spot stock price $s = 242\text{€}$	82

Abstract

This paper compares two numerical approaches for pricing European call options in a Heston framework with CIR++ stochastic short rates. The first approach makes use of the Fast Fourier Transform to price options using characteristic functions derived using affine transforms. The second approach leverages Physics-Informed Neural Networks (PINNs), which embed the governing PDE into the training objective to approximate option prices without the need for market data. By using Eurozone market data for Overnight Indexed Swaps (OIS) and swaptions to calibrate the CIR++ model, as well as by calibrating the FFT and PINN models directly on equity options on BNP Paribas and SAP SE, the accuracy, runtime and robustness of both models is compared. Results indicate that FFT superior pricing accuracy both in-sample and out-of-sample, whereas PINNs offer significantly faster calibration once trained but tend to produce smoother variance dynamics and higher relative errors for extreme strikes. The study highlights trade-offs between accuracy and scalability and suggests improvements for PINNs, such as log-price training and gradient-based penalties, to enhance performance in complex stochastic interest rate settings.

1 Introduction

In 1900, Louis Bachelier’s doctoral thesis, *Theory of Speculation*, introduced a novel framework for modeling asset prices, laying the foundation to what became quantitative finance a century later. Although initially overlooked, the field gained significant traction in the 1970s with the publication of the Black–Scholes–Merton model, see Black and Scholes (1973), for pricing European options. Today, options are an important tool for portfolio managers seeking to hedge risk, and they are typically issued by banks and large financial institutions. Because financial markets are fast-paced and competitive, it is essential that options are priced both fairly and quickly.

A major limitation of the Black–Scholes–Merton model is its assumption that the underlying follows a geometric Brownian motion with constant short rate and volatility. Empirically, both the short rate and especially the volatility vary over time and are stochastic in nature. The crash of the American stock market in 1987, also known as Black Monday, further motivated the use of stochastic volatility models. In this regard, Heston (1993) proposed a way to model the volatility of the underlying asset of a European option. A few years later, Carr and Madan (1999) introduced pricing of European options across multiple strikes using the Fast Fourier Transform (FFT), following Cooley and Tukey (1965), which significantly reduced runtime and marked a shift toward computation-based quantitative finance.

In the late 2010s, Raissi et al. (2017) introduced Physics-Informed Neural Networks (PINNs), a novel, mesh-free, neural-network method for solving PDEs. Since then, several papers have applied PINNs to option pricing, including Hainaut and Casas (2024), where the authors report accuracy comparable to FFT-based models under a Heston-type setup in a non-market environment. However, these studies typically assume a deterministic short rate, which neglects the randomness of the discount factor and its interaction with equity and volatility dynamics, an effect that becomes non-negligible for medium- to long-dated options. As the PINN model developed in the aforementioned work has not yet been tested with stochastic short rates on market data, this paper compares the performance of the FFT model and PINNs under a Heston-type framework with stochastic short rates and real-world data. Specifically, we assume the risky asset follows a geometric Brownian motion with a CIR++ short rate and Heston-type stochastic volatility, and we compare the FFT and PINN models based on calibration speed and fit to market data.

Chapter 2 introduces essential financial theory and financial contracts such as zero-coupon bonds, swaps, and European options on both bonds, swaps and equity, which are used throughout the paper. Additionally, the chapter covers topics such as market assumptions, pricing of European options and the T -forward probability measure which demonstrates to be more practical than the risk-neutral measure. Chapter 3 covers stochastic short-rate models, motivates the use of the CIR++ model, and develops the theory needed to price fixed-income instruments under the CIR++ framework. An example of such instruments are swaptions. In Chapter 4, the option pricing model is first introduced as a system of SDEs under the risk-neutral measure. For computational convenience, the framework is then reformulated under the T -forward measure using Girsanov’s

theorem. The chapter is concluded with the derivation of a backward parabolic option-pricing PDE, which is solved by PINNs in chapter 6. Because there is no available research on the Heston–CIR++ framework, we derive a semi-closed Fourier-based formula to price European call options with FFT in chapter 5 using affine transforms. Numerical results and the discussion are presented in chapters 7 and 8 respectively. The Python scripts used for the numerical experiment can be found in this Github repository.

Finally, unless specified otherwise, variables denoted by capital letters represent stochastic quantities, with the exception of strike prices and time to maturity. Deterministic quantities are written in lowercase. The notation is based on lecture notes from the courses *Martingales in Financial Mathematics*, *Numerical Integration of Stochastic Differential Equations*, and *Interest Rates and Credit Risk Models* given at EPFL², which follow the works of Jarrow (2021), Brigo and Mercurio (2006), Filipović (2009), and Evans (2013), but has been adapted due to variable-naming conflicts.

²École Polytechnique Fédérale de Lausanne

2 A Primer on Financial Theory

Quantitative finance gives the mathematical foundation for today’s financial markets, helping institutions deal with uncertainty and complexity in a structured way. In essence, it focuses on modeling asset prices, interest rates, and derivative payoffs as random processes that change over time. This approach reflects the natural unpredictability of markets while providing tools for pricing and managing risk.

In this chapter, we follow the works of Brigo and Mercurio (2006), Filipović (2009), Delbaen and Schachermayer (2006), and Jarrow (2021), and lay the foundation for pricing financial contracts in a frictionless market by introducing the essential building blocks such as probability spaces and adapted processes. We begin by formalizing the mathematical setting and proceed to define key financial instruments, such as risky and risk-free assets, bonds, and options, within this stochastic environment. Special attention is given to contingent claims, zero-coupon bonds, and interest rate derivatives, as these instruments form the basis for more advanced models discussed later. Lastly, we explore the transition from real-world probabilities to risk-neutral measures and present the tools necessary for valuing European options under both risk-neutral and forward measures.

2.1 Formalities and Setup

For the whole of this paper, we work on a finite time horizon $t \in [\tau, T]$, where τ is the starting time for *all* stochastic processes in this paper, and T denotes the time of expiry of some financial contract. We define the notion of a σ -algebra on Ω which is a collection of subsets closed under complements and countable unions. We say that elements in the σ -algebra are measurable sets. Let $(\Omega, \mathcal{F}, \{\mathcal{F}_t\}_{t \in [\tau, T]}, \mathbb{P})$ be the filtered probability space, where Ω is the sample space, \mathcal{F} the σ -algebra, $\{\mathcal{F}_t\}_{t \in [\tau, T]}$ the set of σ -algebras, and \mathbb{P} the real-world probability measure.

The filtration $\{\mathcal{F}_t\}_{t \in [\tau, T]}$ can be seen as the model’s information flow: for each time t , \mathcal{F}_t contains exactly the events that can be decided from observations up to time t . The filtration is generated by a Brownian motion process, denoted by $W = \{W(t)\}_{t \in [\tau, T]}$, and is an increasing family of σ -algebras containing an increasing amount of information as time goes by. The filtration is assumed to be complete and right-continuous.

In this paper, all defined stochastic processes will be \mathcal{F}_t -adapted by assumption and are assumed to have càdlàg³ paths unless stated otherwise. The notion of an \mathcal{F}_t -adapted process is found in definition 2.1.

Definition 2.1 (\mathcal{F}_t -adapted process). *A stochastic process $\{X(t)\}_{t \in [\tau, T]}$ is adapted to $\{\mathcal{F}_t\}_{t \in [\tau, T]}$ if for every t , the value $X(t)$ is \mathcal{F}_t -measurable.*

2.2 Financial Assets and Options

As before, we assume that the probability space is given as $(\Omega, \mathcal{F}, \{\mathcal{F}_t\}_{t \in [\tau, T]}, \mathbb{P})$. Then, a financial asset is described by an \mathcal{F}_t -adapted stochastic price process $S = \{S(t)\}_{t \in [\tau, T]}$ taking real, positive values.

In addition to assets, we consider options. Options are financial contracts that give the holder the right, but not the obligation, to buy or sell a financial instrument at a specific price over a certain period of time. An option that gives the right but not the obligation to buy a financial instrument at a fixed price is called a *call option*, and an option that gives the right to sell is called a *put option*. We denote the fixed price by $K > 0$ and refer to it as the *strike price*. Furthermore, the financial instrument an option depends on is called the *underlying* and can be anything from bonds or stocks to commodities such as olives presses⁴. We model the dependence of the option on the underlying and K with contingent claims.

³Continue à droite, limite à gauche

⁴The first recorded option buyer was the ancient Greek philosopher Thales of Miletus, who bought the right to use olive presses in advance of an expected high demand.

Definition 2.2 (Contingent Claim). *A contingent claim $H(Z(T))$ is a Borel-measurable function of the time- T price of a financial asset, $Z(T)$, with $\mathbb{E}_{\mathbb{P}}[|H(Z(T))|] < \infty$.*

We note that by definition 2.2, options are contingent claims written on one or multiple underlying assets. We will, however, limit ourselves on contingent claims on a single underlying. One form of a contingent claim are European options, which are contracts that can only be exercised on its expiration date. Definitions 2.3 and 2.4 are a mathematical formalization of the payoffs of European call and put options.

Definition 2.3 (European call option). *For $\tau \leq t \leq T$, denote by $c(t, S(t))$ the time- t price of a European call option, with underlying S , strike price $K > 0$ and time of maturity T . At maturity T , the option has payoff*

$$c(T, S(T)) = (S(T) - K)_+,$$

where $(x)_+ := \max\{x, 0\}$ is the *hockey stick function*.

Definition 2.4 (European put option). *For $\tau \leq t \leq T$, denote by $p(t, S(t))$ the time- t price of a European call option, with underlying S , strike price $K > 0$ and time of maturity T . At maturity T , the option has payoff*

$$p(T, S(T)) = (K - S(T))_+,$$

where $(x)_+ := \max\{x, 0\}$ is the *hockey stick function*.

2.3 Fixed-Income Instruments

Besides financial assets and option contracts, interest rates and other related contracts are key instruments for pricing options. This section, based on works of Brigo and Mercurio (2006) and Filipović (2009), introduces some basic building blocks for instruments observable in the market, such as arbitrage-free zero-coupon bonds and forward rates, as well as interest-rate contracts such as bond options, swaps and swaptions. The instruments will be crucial for estimating parameters in the interest rate model presented in chapter 3.

Interest Rates and Bonds

Interest is often described as the "rent paid for the use of money over a specified period". It is the additional amount a borrower pays to a lender on top of the the borrowed money. For instance, in a mortgage, a bank lends some principal amount N to finance a house purchase, and the borrower repays N together with some pre-determined interest i . Intuitively, since a krone today is worth more than a krone tomorrow, interest compensates for inflation, giving lenders a reason to lend money to borrowers. Conversely, a krone tomorrow is worth less than a krone today. We call this effect the *discount*.

A commonly used discount is the arbitrage-free zero-coupon bond, also referred to as the zero-coupon bond. We define the zero-coupon bond as a financial contract that requires a payment $P(\tau, T)$ at time τ and that pays 1 at time T given some short rate r . We define the short rate and the zero-coupon bond in definitions 2.5 and 2.6. Fig. 1 shows the payoff, or cash flow, structure of $P(\tau, T)$.

Definition 2.5 (Short rates). *We define short rates as the interest rate on a short-term loan be defined by the stochastic short rate process $R = \{R(t)\}_{t \in [\tau, T]}$ with $R(\tau) = r$, where τ is the initial time of the process.*

Definition 2.6 (Zero-coupon bonds). *For $t \geq \tau$, the price of a zero-coupon bond maturing at a future time $T \geq t$ is defined as*

$$P(t, T) = \mathbb{E}_{\mathbb{Q}} \left[e^{- \int_t^T R(u) du} \mid \mathcal{F}_t \right], \quad (1)$$



Figure 1: Payoff structure of a zero-coupon bond from the perspective of the bond buyer: The downward facing, red arrow at time τ means that the payer buys the bond for $P(\tau, T)$ and the upward facing, green arrow at time T means that the payer receives 1 at time T .

where R is the short rate and \mathbb{Q} denotes a no-arbitrage probability measure equivalent to the real-world probability measure \mathbb{P} . The terminal condition of the bond, that is at time $t = T$, is given by

$$P(T, T) = 1.$$

Remark 2.7. Note that in the definition above, we have introduced a new probability measure \mathbb{Q} , also known as the risk-neutral probability measure, which we define in chapter 2.5. However, it is worth mentioning that \mathbb{Q} is not needed to be known as of now.

Remark 2.8. We note that, since a krone at time t is worth more than a krone at time T , we can use zero-coupon bonds as a way to discount a cash flow at time T into the present time⁵. Moreover, we deduce that for positive a short rate R , $P(t, \cdot)$ must be a strictly decreasing function in T .

An important observation that is made from the definition of the zero-coupon bond 2.6 is that for times $t > \tau$, the zero-coupon bond $P(t, T)$ is an \mathcal{F}_t -measurable, stochastic function of time.

Some useful tools are directly derived from zero-coupon bonds. For instance, since 1 krone at time T is worth $P(\tau, T)$ at time τ , we may discount future cash flows with $P(\tau, T)$. Moreover, other useful tools are the instantaneous forward rate, the simple spot rate, and the European option on the zero-coupon bond. Their definitions are as follows:

Definition 2.9 (The instantaneous forward rate). *The instantaneous forward rate is defined as*

$$f(\tau, T) := -\partial_T \log P(\tau, T). \quad (2)$$

Remark 2.10 (Intuition of the instantaneous forward rate). *We will see in chapter 3 that the instantaneous forward rate can be seen as the expected evolution of the interest over time. Moreover, it is a deterministic quantity as long as we consider it at time τ .*

Definition 2.11 (European call option on a zero-coupon bond). *Let T and U be times in the future such that $\tau < T < U$ and let $P(T, U)$ be the time- T price on a zero-coupon bond maturing at time U . Denote by $\mathbf{zbc}(t, T, U, K) \in \mathbb{R}_+$ the time- t price of a European call option on a zero-coupon bond issuing at time T and maturing at time U , with strike price $K > 0$. The time- T payoff of the call option on the bond is the contingent claim*

$$\mathbf{zbc}(T, T, U, K) = H(P(T, U)),$$

where $H(P(T, U)) = (P(T, U) - K)_+$.

Definition 2.12 (European put option on a zero-coupon bond). *Let T and U be times in the future such that $\tau < T < U$ and let $P(T, U)$ be the time- T price on a zero-coupon bond maturing at time U . Denote by $\mathbf{zbp}(t, T, U, K) \in \mathbb{R}_+$ the time- t price of a European put option on a zero-coupon*

⁵This only holds under the arbitrage-free measure \mathbb{Q} . Arbitrage-free in this case means that no market participant can make a non-inflation-based profit from either buying or selling zero-coupon bonds.

bond issuing at time T and maturing at time U , with strike price $K > 0$. The time- T payoff of the put option on the bond is the contingent claim

$$\mathbf{zbp}(T, T, U, K) = H(P(T, U)),$$

where $H(P(T, U)) = (K - P(T, U))_+$.

The Svensson framework

Recall the previously defined instantaneous forward rate $f(\tau, T)$. Forward rates are fundamental to understanding the term structure of interest rates, as they describe the expected evolution of interest rates over time. In practice, market participants often require a smooth and flexible representation of the forward curve that can fit observed data accurately while remaining computationally tractable. The Svensson framework, introduced by Svensson (1994), provides such a parametric approach by extending the functional form of the forward curve to capture both short-term dynamics and long-term behavior. This approach allows us to model the zero-coupon bond prices as a deterministic function of t and T .

Under the Svensson framework, the instantaneous forward rate is assumed to be a deterministic function of t and T . It follows the expression

$$f^{\text{Svensson}}(t, T) = \beta_0 + \beta_1 e^{-a_1(T-t)} + \beta_2 a_1 t e^{-a_1(T-t)} + \beta_3 a_2 (T-t) e^{-a_2(T-t)}, \quad (3)$$

with constant parameters $\beta_0, \beta_1, \beta_2, \beta_3, a_1, a_2 \in \mathbb{R}$. Then, by definition 2.9, the zero-coupon bond is priced with

$$P^{\text{Svensson}}(t, T) = e^{-\int_t^T f^{\text{Svensson}}(t, u) du}.$$

We define the yield of the bond on the time interval $[t, T]$ as

$$y^{\text{Svensson}}(t, T) = -\frac{1}{T-t} \log P^{\text{Svensson}}(t, T)$$

so that

$$y^{\text{Svensson}}(t, T) = \frac{1}{T-t} \int_t^T f^{\text{Svensson}}(t, u) du.$$

With the instantaneous forward rate given by (3), solving the integral above gives

$$\begin{aligned} y^{\text{Svensson}}(t, T) &= \beta_0 + \beta_1 \frac{1 - e^{-a_1(T-t)}}{a_1(T-t)} + \beta_2 \left(\frac{1 - e^{-a_1(T-t)}}{a_1(T-t)} - e^{-a_1(T-t)} \right) \\ &\quad + \beta_3 \left(\frac{1 - e^{-a_2(T-t)}}{a_2(T-t)} - e^{-a_2(T-t)} \right), \end{aligned} \quad (4)$$

which is then substituted into (5)

$$P^{\text{Svensson}}(t, T) = e^{-(T-t)y^{\text{Svensson}}(t, T)}. \quad (5)$$

Interest rate swaps

An interest rate swap, or simply swap, is a scheme where one exchanges a payment stream at a fixed rate of interest for payment stream at a floating rate, that is, an interest rate that changes over time. At the time T_0 , the swap is settled in arrears specified by:

- a number of future dates $\tau \leq T_0 < T_1 < \dots < T_n$ with $\delta_i := T_i - T_{i-1}$ and T_n being the maturity of the swap, and
- a fixed rate $\kappa \in \mathbb{R}$.

Cash flows take place only at the dates T_1, \dots, T_n . At T_i , the holder of the contract:

- pays fixed $\delta_i \kappa$,
- and receives the floating rate $\frac{1}{P(T_{i-1}, T_i)} - 1$.

Such a swap is also known as a *fixed-for-floating* swap as one party pays a fixed interest rate and receives a floating rate such as the Euro Short-Term Rate (€STR), while the counterparty does the opposite.

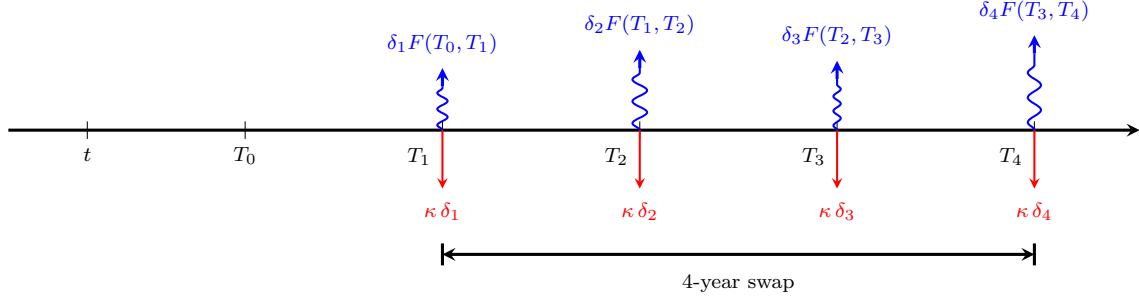


Figure 2: Example of the cash flow structure for a 4-year swap with start date T_0 , first settlement date T_1 , and strike rate κ . The blue lines represent the floating rates received by the holder of the payer swap contract, whereas the red lines represent the fixed rates paid by the holder of the swap.

From the payer's point of view, the net cash flow at T_i is given by

$$\left[\left(\frac{1}{P(T_{i-1}, T_i)} - 1 \right) - \delta_i \kappa \right].$$

To simplify our notation, we define

$$F(T_{i-1}, T_i) := \frac{1}{\delta_i} \left(\frac{1}{P(T_{i-1}, T_i)} - 1 \right),$$

which is also known as the simple forward rate. Then, the net cash flow at T_i of a swap is

$$\delta_i (F(T_{i-1}, T_i) - \kappa).$$

Figure 2 illustrates an example cash flow structure for a 4-year swap contract beginning at T_0 and with first settlement date T_1 . We note that in the illustration, the net cash flow remains positive at all years, but is allowed to be negative as well. The time- T_0 value of the net cash flow is given by

$$(P(T_0, T_{i-1}) - P(T_0, T_i) - \kappa \delta_i P(T_0, T_i)).$$

Then, summing the net cash flows from $T_1 < \dots < T_n$, the total value of the payer interest swap is

$$\begin{aligned} \Pi_{\text{swap}}(T_0) &= \sum_{i=1}^n (P(T_0, T_{i-1}) - P(T_0, T_i)) - \kappa \sum_{i=1}^n \delta_i P(T_0, T_i) \\ &= 1 - P(T_0, T_n) - \kappa \sum_{i=1}^n \delta_i P(T_0, T_i), \end{aligned} \tag{6}$$

where $P(T_0, T_0) = 1$ per definition.

In (6), the fixed rate κ is arbitrary and the holder of the swap can either profit or make a loss from the swap. Under the arbitrage-free framework⁶, only the fair swap rate is of interest to us. We denote the fair rate of a swap beginning at T_0 and maturing at T_n by $r_{\text{swap}}(T_0, T_n)$. The fair rate is, by definition, the rate at which the holder of the swap does not make a profit, and we determine it by setting the present value of the payer swap in (6) equal to zero, that is,

$$\Pi_{\text{swap}}(T_0, T_n) = 1 - P(T_0, T_n) - r_{\text{swap}}(T_0, T_n) \sum_{i=1}^n \delta_i P(T_0, T_i) = 0,$$

⁶The arbitrage-free framework is introduced in 2.5.

which implies that the fair strike rate at time T_0 is

$$r_{\text{swap}}(T_0, T_n) = \frac{1 - P(T_0, T_n)}{\sum_{i=1}^n \delta_i P(T_0, T_i)}.$$

If the swap is to start immediately at the initial time τ , the fair rate reads as

$$r_{\text{swap}}(\tau, T_n) = \frac{1 - P(\tau, T_n)}{\sum_{i=1}^n \delta_i P(\tau, T_i)}. \quad (7)$$

European Swaptions

As its name suggests European swaptions, or simply *swaptions*, are European options on swaps. Swaptions are highly liquid derivatives, meaning that the market prices we observe on swaptions are very likely to be priced in a fair way. Moreover, the data available for swaptions is very large in comparison to many other fixed-income derivatives, so that swaptions are often the go-to instruments for estimating short-rate models. In this section, we give a basic definition of swaptions and explain its cash flow structure. A swaption pricing formula is then introduced in chapter 3 which will later be used for estimating parameters in the short-rate model of our choice.

We differentiate between two types of swaptions: payer and receiver. A payer swaption with strike rate κ gives the holder the right, but not the obligation, to enter into a swap at the maturity of the swaption and can be seen as a European call option on interest rates. This gives the holder of the contract the possibility to pay a fixed rate κ and receive some floating rate in return. This structure works well when the holder of the payer swaption expects the interest rate to rise, profiting from the difference between the floating and fixed rates. Figure 3 depicts the cash flow structure for a payer swaption with time of maturity T_0 , strike rate κ , and a 4-year swap contract with first settlement date T_1 as underlying.

Conversely, a receiver swaption gives the holder the right to enter into a swap as the receiver of the fixed rate κ and the floating rate payer, i.e. a European put option on interest rates. In this case, the structure works well when the holder expects interest rates to fall. Receiver swaptions are often used by pension funds and insurance companies that require stable, predictable income streams and would like to capitalize on favorable rate adjustments.

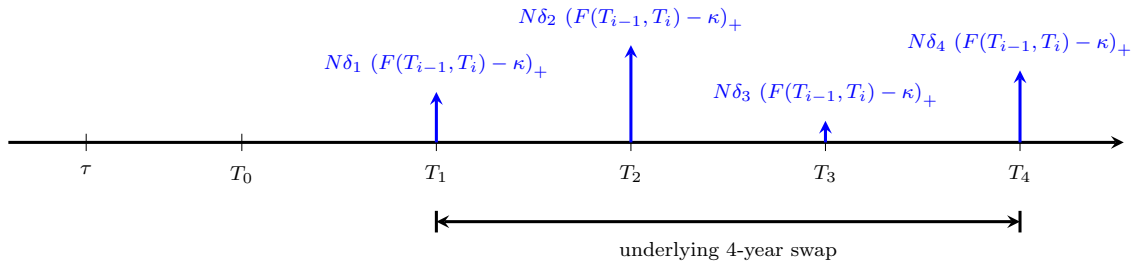


Figure 3: Example of the cash flow structure for a payer swaption with time of maturity τ , notional N , strike rate κ , and a 4-year swap as underlying.

We denote by $\mathbf{ps}(t, T_0, T_n) \in \mathbb{R}_+$ and $\mathbf{ps}(t, T_0, T_n) \in \mathbb{R}_+$ the time- t price of the payer and receiver swaptions, respectively, with strike rate κ that mature at time T_0 and whose underlying swap matures at time T_n . The time- T_0 payoff of a swaption under the no-arbitrage setting is

$$\mathbf{ps}(T_0, T_0, T_n) = \left\{ \sum_{i=1}^n P(T_0, T_i) \left[\left(\frac{1}{P(T_{i-1}, T_i)} - 1 \right) - \delta_i \kappa \right] \right\}_+ = -\mathbf{rs}(T_0, T_0, T_n). \quad (8)$$

We note that the expression of the T_0 -payoff of the swaption is related to the swap rate at T_0 , as lemma 2.13 puts into perspective.

Lemma 2.13 (Relation between swap rates and swaptions). *Let N be the notional amount on the swaption and κ be a positive, real-valued strike rate. Furthermore, recall that the fair swap rate is*

as in (7). Then, the time T_0 payoff of the swaption (8) is given by

$$\mathbf{ps}(T_0, T_0, T_n) = (r_{\text{swap}}(T_0, T_n) - \kappa)_+ \sum_{i=1}^n \delta_i P(T_0, T_i),$$

assuming that $P(T_0, T_{i-1})P(T_{i-1}, T_i) = P(T_0, T_i)$ ⁷.

Proof. Recall the time- T_0 payoff of a swaption (8). With $P(T_0, T_{i-1})P(T_{i-1}, T_i) = P(T_0, T_i)$, one finds

$$\begin{aligned} \mathbf{ps}(T_0, T_0, T_n) &= \left\{ \sum_{i=1}^n P(T_0, T_i) \left[\left(\frac{1}{P(T_{i-1}, T_i)} - 1 \right) - \delta_i \kappa \right] \right\}_+ \\ &= \left(\sum_{i=1}^n P(T_0, T_{i-1}) - P(T_0, T_i) - \kappa \delta_i P(T_0, T_i) \right)_+ \\ &= \left(P(T_0, T_0) - P(T_0, T_n) - \kappa \sum_{i=1}^n \delta_i P(T_0, T_i) \right)_+ \\ &= \left(1 - P(T_0, T_n) - \kappa \sum_{i=1}^n \delta_i P(T_0, T_i) \right)_+ \\ &= \left(\frac{1 - P(T_0, T_n)}{\sum_{i=1}^n \delta_i P(T_0, T_i)} - \kappa \right)_+ \left(\sum_{i=1}^n \delta_i P(T_0, T_i) \right). \end{aligned}$$

Then, with (7), that is,

$$r_{\text{swap}}(T_0, T_n) = \frac{1 - P(T_0, T_n)}{\sum_{i=1}^n \delta_i P(T_0, T_i)},$$

one has

$$\mathbf{ps}(T_0, T_0, T_n) = (r_{\text{swap}}(T_0, T_n) - \kappa)_+ \sum_{i=1}^n \delta_i P(T_0, T_i).$$

□

2.4 Market Assumptions and Asset Classes

In this section, we outline the key market assumptions that form the basis of our model. Following the framework in Jarrow (2021, Chapter 2) we assume a frictionless and perfectly competitive market. Under this assumption, there are no transaction costs, taxes, or liquidity constraints, and information is freely available to all participants. Entry and exit from the market are costless, securities are perfectly divisible, and short-selling is unrestricted. The market is liquid, meaning that any asset can be bought or sold without delay, and the risk-free borrowing and lending rate is the same. Finally, we assume that no financial instruments pay dividends.

Under this setting, we distinguish between two main asset classes: risk-free assets, which evolve deterministically according to the short-rate process, and risky assets, whose dynamics are modeled as stochastic processes. These assumptions provide the foundation for deriving option pricing formulas under the No-Free-Lunch-without-Vanishing-Risk condition, see Delbaen and Schachermayer (2006).

The Perfect Market Hypothesis

Throughout this paper, we assume that the market structure is characterized by a very large number of buyers and sellers of a homogeneous product. Entry and exit from the market, that is the buying and selling of financial assets in the market, is costless, and information is freely available to all market participants. Concretely, we assume the following:

⁷This assumption holds under the T -forward measure which is defined in section 2.5.

-
- (i) No transaction costs or taxes and no bid-ask spread.
 - (ii) No limitations on the quantities of transactions, securities are perfectly divisible and there are no short-selling restrictions.
 - (iii) The market is liquid, i.e. there will always be a buyer to whatever financial asset we sell.
 - (iv) The risk-free lending and borrowing rate is the same.
 - (v) No financial instruments pay dividends.

Risk-free and Risky Assets

We differentiate between two types of financial assets: risk-free assets, such as US Treasury Bonds, and risky assets, i.e. stocks. Suppose that the risk-free asset is described by a stochastic process denoted by $B = \{B(t)\}_{t \in [\tau, T]}$. We assume its dynamic to be described by the ODE

$$dB(t) = R(t)B(t) dt, \quad B(\tau) = 1, \quad (9)$$

with $R(t)$ being the stochastic short rate, see definition 2.5. The solution to the ODE (9) is

$$B(t) = \exp \left(\int_{\tau}^t R(u) du \right), \quad (10)$$

for $\tau \leq t$.

We denote the risky asset's price process by $S = \{S(t)\}_{t \in [\tau, T]}$ and assume that it can be modeled with the geometric Brownian motion (GBM) given by the stochastic differential equation (SDE)

$$dS(t) = \mu(t)S(t) dt + \sqrt{V(t)} S(t) dW^{S, \mathbb{P}}(t), \quad S(\tau) = s, \quad (11)$$

where $W^{S, \mathbb{P}} = \{W^{S, \mathbb{P}}(t)\}_{t \in [\tau, T]}$ is the standard Brownian motion of S under \mathbb{P} , s is a known, deterministic quantity, $\mu = \{\mu(t)\}_{t \in [\tau, T]}$ is the stochastic drift process of S , and $V = \{V(t)\}_{t \in [\tau, T]}$ the stochastic variance process of S . We will see that under the arbitrage-free framework, μ is replaced by the stochastic short-rate R and will concretely define the processes R and V to follow their respective SDEs in chapters 3 and 4 respectively. However, as of now, the only assumption we make about the aforementioned processes is that they are strictly positive, real-valued, and \mathcal{F}_t -adapted processes. Moreover, we assume that $\mu(\tau) = \mu_0$ and $V(\tau) = \nu$ are known constants at the time τ , at which the processes start.

On the interval $[\tau, t]$, the SDE (11) has the solution

$$S(t) = s e^{\int_{\tau}^t (\mu(u) - \frac{1}{2} V(u)) du + \int_{\tau}^t \sqrt{V(u)} dW^{S, \mathbb{P}}(u)}. \quad (12)$$

2.5 Pricing of European Options

Consider the filtered probability space $(\Omega, \mathcal{F}_t, \{\mathcal{F}_t\}_{t \in [\tau, T]}, \mathbb{P})$ for a finite time horizon $T < \infty$. To price options consistently, we need a framework where discounted asset prices behave in a way that rules out arbitrage opportunities. Under the No-Free-Lunch-without-Vanishing-Risk condition, see Delbaen and Schachermayer (2006), such a framework exists and takes the form of a probability measure \mathbb{Q} , equivalent to the real-world probability measure \mathbb{P} , under which discounted asset prices become martingales. The probability measure \mathbb{Q} is called the risk-neutral probability measure⁸.

⁸Also referred to as an equivalent martingale measure or arbitrage-free probability measure depending on the literature.

From the Real-world to the Risk-neutral Probability Measure

The motivation behind changing probability measures comes from the fact that asset prices typically have a drift term which reflects expected returns. In our case, the drift is the unknown stochastic process μ in (12) which makes direct pricing of derivatives complicated. By moving to the risk-neutral measure \mathbb{Q} , we replace this unknown drift with the risk-free rate, which is observable through fixed-instruments like swaptions. This simplifies valuation because the expected discounted payoff of a derivative under \mathbb{Q} gives its fair price.

To perform this change of measure, we apply Girsanov's theorem, see Appendix B.3, which adjusts the Brownian motion driving the asset price. Under \mathbb{Q} , the new Brownian motion of S is denoted by $W^{S,\mathbb{Q}}$. Recalling that R and V stand for the stochastic short-rate and the stochastic variance respectively, define the \mathcal{F}_t -adapted process $\theta := \{\theta(t)\}_{t \in [\tau, T]}$, with

$$\theta(t) := \frac{\mu(t) - R(t)}{\sqrt{V(t)}},$$

with $V(t) > 0$ at any time $t \in [\tau, T]$. Assuming the Novikov condition holds,

$$\mathbb{E}_{\mathbb{P}} \left[\exp \left(\frac{1}{2} \int_{\tau}^T \theta^2(u) du \right) \right] < \infty, \quad (13)$$

the Radon-Nikodym derivative defining \mathbb{Q} on \mathcal{F}_T is

$$\frac{d\mathbb{Q}}{d\mathbb{P}} = e^{-\frac{1}{2} \int_{\tau}^T \theta^2(u) du - \int_{\tau}^T \theta(u) dW^{S,\mathbb{P}}(u)}. \quad (14)$$

By Girsanov's theorem, the Brownian motion under \mathbb{Q} satisfies

$$W^{S,\mathbb{Q}}(t) = W^{S,\mathbb{P}}(t) + \int_{\tau}^T \theta(u) du.$$

Substituting this into the SDE (11), we obtain

$$dS(t) = R(t)S(t) dt + \sqrt{V(t)}S(t) dW^{S,\mathbb{Q}}(t), \quad S(\tau) = s. \quad (15)$$

This representation is crucial as it eliminates the unknown drift $\mu(t)$ and replaces it with the short rate $R(t)$, which can be inferred from fixed-income instruments present in the market such as swaptions.

Pricing European Options under the Risk-neutral Probability Measure

In this section, we present a closed-form formula for pricing contingent claims. We assume that the risk-neutral probability measure \mathbb{Q} exists and consider the probability space $(\Omega, \mathcal{F}, \{\mathcal{F}\}_{t \in [\tau, T]}, \mathbb{Q})$.

We begin by considering the general case of pricing contingent claims such as options on bonds, stocks, or swaptions. Let $Z(T)$ be the time- T price of some asset, such as a bond or a stock, and define the contingent claim, $H(Z(T))$. Under the assumption that $Z(t)$ is \mathcal{F}_t -adapted for times $t \in [\tau, T]$, we price the contingent claim with

$$\Pi(t, Z(t)) = \mathbb{E}_{\mathbb{Q}} \left[\frac{B(t)}{B(T)} H(Z(T)) \mid \mathcal{F}_t \right], \quad (16)$$

where $\Pi(t)$ denotes the time- t price of the contingent claim $H(Z(T))$ and

$$\frac{B(t)}{B(T)} = e^{-\int_t^T R(u) du}$$

discounts the cash flow at time T to the time t . We note that $Z(t)$ exhibits the strong Markov property under \mathbb{Q} and that $\Pi : [\tau, T] \times \mathbb{R}$ is a deterministic function depending on future uncertainty

through the random state $Z(t)$ at time t . Moreover, (16) follows directly from Jarrow (2021, Theorem 17), where the authors establish the risk-neutral valuation formula by invoking the No-Free-Lunch-without-Vanishing-Risk condition and attainable strategies. Since the detailed proof lies beyond the scope of this paper, we adopt the result without further derivation.

For a European call option on the stochastic risky asset process S , the contingent claim is $H(S(T)) = (S(T) - K)_+$. Its price at time $t \in [\tau, T]$ is therefore

$$c(t, S(t), R(t), V(t)) = \mathbb{E}_{\mathbb{Q}} \left[\frac{B(t)}{B(T)} (S(T) - K)_+ \mid \mathcal{F}_t \right], \quad (17)$$

where the random state $(S(t), R(t), V(t))$ at time t reflects the future uncertainty.

Pricing European Call Options under the Forward Measure

We observe that a minor drawback of the option pricing formula (16) is that we cannot move the discounting factor $1/B(T)$ outside of the expectation as the discounting factor may be correlated with the claim H . This makes the pricing process computationally expensive, as we have to compute two integrals to price options. However, Filipović (2009) (see pp.105-107) proposes a neat trick where they define a new risk-free probability measure \mathbb{Q}^T equivalent to \mathbb{Q} . We call \mathbb{Q}^T the T -forward measure. To describe the T -forward measure, we consider lemma 2.14.

Lemma 2.14. *For $t \in [\tau, T]$, assume that the zero-coupon bond, $P(t, T)$, follows the expression (1) and that the risk-free asset, $B(t)$, is modeled with (10). Then, $P(t, T)/B(t)$ is a martingale under \mathbb{Q} .*

Proof. Let s and t be times such that $\tau \leq s \leq t \leq T$. Then,

$$\begin{aligned} \mathbb{E}_{\mathbb{Q}} \left[\frac{P(u, T)}{B(u)} \mid \mathcal{F}_t \right] &= \mathbb{E}_{\mathbb{Q}} \left[\exp \left(- \int_{\tau}^t R(u) du \right) \mathbb{E}_{\mathbb{Q}} \left[\exp \left(- \int_t^T R(u) du \right) \mid \mathcal{F}_t \right] \mid \mathcal{F}_t \right] \\ &= \mathbb{E}_{\mathbb{Q}} \left[\mathbb{E}_{\mathbb{Q}} \left[\exp \left(- \int_{\tau}^T R(u) du \right) \mid \mathcal{F}_t \right] \mid \mathcal{F}_s \right] \\ &= \mathbb{E}_{\mathbb{Q}} \left[\exp \left(- \int_{\tau}^T R(u) du \right) \mid \mathcal{F}_s \right] \\ &= \exp \left(- \int_{\tau}^s R(u) du \right) \mathbb{E}_{\mathbb{Q}} \left[\exp \left(- \int_t^T R(u) du \right) \mid \mathcal{F}_s \right] \\ &= \frac{P(s, T)}{B(s)}, \end{aligned}$$

where we used the tower rule for martingales and the fact that $B(t)$ is \mathcal{F}_t -measurable for all $t \in [\tau, T]$. \square

Using lemma 2.14, we now aim to define the T -forward measure \mathbb{Q}^T . Define the \mathcal{F}_t -measurable, stochastic process

$$L(T) := \frac{P(T, T)}{P(\tau, T)B(T)} \quad \text{on } \mathcal{F}_T$$

such that by lemma 2.14,

$$\mathbb{E}_{\mathbb{Q}}[L(T) \mid \mathcal{F}_{\tau}] = \frac{1}{P(\tau, T)} \mathbb{E}_{\mathbb{Q}} \left[\frac{P(T, T)}{B(T)} \mid \mathcal{F}_{\tau} \right] = 1,$$

since $B(\tau) = 1$ by definition. Furthermore, $L(T)$ is a martingale by construction as $P(\tau, T)$ is a constant. Hence,

$$L(T) = \frac{d\mathbb{Q}^T}{d\mathbb{Q}} = \frac{1}{P(\tau, T)B(T)} \quad \text{on } \mathcal{F}_T \quad (18)$$

is the Radon-Nikodym derivative that defines the T -forward measure. Moreover, as $L(T) > 0$, we have that the T -forward probability measure is equivalent to the risk-neutral probability measure, that is, $\mathbb{Q}^T \sim \mathbb{Q}$.

Proposition 2.15. *Under the T -forward measure defined by the Radon-Nikodym derivative (18), the non-negative, F_T -measurable contingent claim $H(Z(T))$ on an underlying asset Z is priced with*

$$\Pi(t, Z(t)) = P(t, T) \mathbb{E}_{\mathbb{Q}^T} [H(Z(T)) \mid \mathcal{F}_t]. \quad (19)$$

Proof. Recall that a contingent claim $H(Z(T))$ is priced under risk-neutral measure \mathbb{Q} with

$$\Pi(t, Z(t)) = \mathbb{E}_{\mathbb{Q}} \left[\frac{B(t)}{B(T)} H(Z(T)) \mid \mathcal{F}_t \right].$$

Then, (19) can be shown by applying Bayes' theorem for change of measure found in Appendix B.4. This results in

$$\begin{aligned} \Pi(t, Z(t)) &= \mathbb{E}_{\mathbb{Q}} \left[\frac{B(t)}{B(T)} H(Z(T)) \mid \mathcal{F}_t \right] \\ &= P(\tau, T) B(t) \mathbb{E}_{\mathbb{Q}} \left[\frac{H(Z(T))}{P(\tau, T) B(T)} \mid \mathcal{F}_t \right] \\ &= P(\tau, T) B(t) \mathbb{E}_{\mathbb{Q}} \left[\frac{d\mathbb{Q}^T}{d\mathbb{Q}} \mid \mathcal{F}_t \right] \mathbb{E}_{\mathbb{Q}^T} [H(Z(T)) \mid \mathcal{F}_t] \\ &= P(\tau, T) B(t) \frac{P(T, T)}{P(\tau, T) B(t)} \mathbb{E}_{\mathbb{Q}^T} [H(Z(T)) \mid \mathcal{F}_t] \\ &= P(\tau, T) \mathbb{E}_{\mathbb{Q}^T} [H(Z(T)) \mid \mathcal{F}_t]. \end{aligned}$$

□

In view of proposition 2.15, European call options on the risky asset S take the form

$$c(t, S(t), r(t), V(t)) = P(t, T) \mathbb{E}_{\mathbb{Q}^T} [(S(T) - K)_+ \mid \mathcal{F}_t], \quad (20)$$

for times $t \in [\tau, T]$. Comparing the call option pricing formula under the risk-neutral measure (17) to the one under \mathbb{Q}^T (20), one immediately notices that the pricing formula under \mathbb{Q}^T is much simpler to compute as we are not anymore required to compute the stochastic discount $B(t)/B(T)$ within the conditional expectation. Moreover, computing option prices at time τ is merely a task of computing the expectation in the pricing formula, as the discounting factor $P(\tau, T)$ is deterministic and its price is in general frequently updated by the issuing central bank.

3 Interest Rate Models

In the previous chapter, we have defined the risk-neutral probability measure \mathbb{Q} under which pricing contingent claims has proven to be more convenient than under the real-world probability measure \mathbb{P} . This leads to the risky asset price process S , and therefore also the European option price c , being dependent on the stochastic short rate process R .

In this chapter, we seek to price fixed-income securities such as European options on a zero-coupon bond as well as swaptions under the risk-neutral probability measure \mathbb{Q} using R . Focusing on the theory presented in Filipović (2009) (see pp.79–88) and in Brigo and Mercurio (2006) (see pp.102–104), we will see that one-factor, affine short-rate models for R allow analytically tractable models and break down the pricing of European options on zero-coupon bonds and swaptions into a few simple equations. An example of such one-factor short-rate model is the CIR++ model, see Brigo and Mercurio (2001), which we will model R with. The CIR++ model is a so-called deterministic shift extension to the CIR model found in Cox et al. (1985).

3.1 One-factor Short-rate Models

Before delving into the CIR++ model, we begin by considering some general theory about short rate models. Define the filtered probability space $(\Omega, \mathcal{F}, (\mathcal{F}_t)_{t \in [\tau, T]}, \mathbb{Q})$, where τ is the time at which the short rate process starts, T is a finite time horizon, and \mathbb{Q} is the risk-neutral measure. Furthermore, let $\mathcal{Z} \subset \mathbb{R}$ be a closed interval with a non-empty interior, and b and σ continuous functions on $\mathbb{R}_+ \times \mathcal{Z}$. We assume the following:

- (i) Under \mathbb{Q} , the short-rates follow an Itô process

$$dR(t) = \mu(t, R(t)) dt + \sigma(t, R(t)) dW^{R, \mathbb{Q}}(t), \quad R(\tau) = r \quad (21)$$

where $W^{R, \mathbb{Q}} = \{W^{R, \mathbb{Q}}(t)\}_{t \in [\tau, T]}$ is the Brownian motion of R under \mathbb{Q} and R starts at the time τ .

- (ii) Recall that $W^{S, \mathbb{Q}} = \{W^{S, \mathbb{Q}}(t)\}_{t \in [\tau, T]}$ is the Brownian motion of the risky asset S under \mathbb{Q} . We assume that $W^{S, \mathbb{Q}}$ and $W^{R, \mathbb{Q}}$ are correlated, i.e.

$$d\langle W^{S, \mathbb{Q}}(t), W^{R, \mathbb{Q}}(t) \rangle_t = \rho_1 dt, \quad (22)$$

where ρ_1 is the instantaneous correlation coefficient and the operator $\langle \cdot, \cdot \rangle_t$ denotes the quadratic variation.

- (iii) For any $(\tau, r) \in \mathcal{Z}$, where $\tau > 0$ is the starting time of the random process and $R(\tau) = r$, the SDE (21) admits a unique \mathcal{Z} -valued solution $R = R^{(\tau, r)}$.

Remark 3.1. *We note that under assumption (iii), the drift and diffusion functions μ and σ in (21) must be Lipschitz continuous and their respective growths must be linearly bounded. This ensures the existence and uniqueness of the solution R .*

Remark 3.2. *Short-rate models following the general representation (21) are known as one-factor models. Some well-known models are the Vasicek and the CIR models, the latter of which we consider in this chapter.*

General Results for One-factor Short-rate Models

Consider assumptions (i)–(iii). In this section, we derive some important results under these assumptions. These results give further insight about the relation between the instantaneous forward rate f and the short rate R , and a better understanding of the zero-coupon bond $P(t, T)$. The outcomes take the form of propositions 3.3, 3.8 and 3.7. We begin by recalling that the zero-coupon bond, $P(t, T)$, is priced with the formula in definition 2.6, that is,

$$P(t, T) = \mathbb{E}_{\mathbb{Q}} \left[e^{- \int_t^T R(u) du} \mid \mathcal{F}_t \right], \quad P(T, T) = 1,$$

where \mathbb{Q} is the risk-neutral probability measure. The instantaneous forward rate, $f(\tau, T)$, is defined as

$$f(\tau, T) := -\partial_T \log P(\tau, T),$$

which was covered in definition 2.9. Moreover, the T -forward probability measure, \mathbb{Q}^T , is defined via the Radon-Nikodym derivative

$$\frac{d\mathbb{Q}^T}{d\mathbb{Q}} = \frac{P(T, T)}{P(\tau, T)B(T)}, \quad P(T, T) = 1,$$

which also is a \mathbb{Q} -martingale.

In the following proposition, we link the expected value of the short rate at a future time T under \mathbb{Q}^T to the instantaneous forward rate. The result, together with its proof, can be found in Brigo and Mercurio (2006) (see Proposition 2.5.2).

Proposition 3.3 (Expected value of the future short-rate, see Brigo and Mercurio (2006, Proposition 2.5.2)). *The expected value of any future short rate under the corresponding forward measure is equal to the related instantaneous forward rate, i.e.*

$$\mathbb{E}_{\mathbb{Q}^T}[R(T) | \mathcal{F}_\tau] = f(\tau, T).$$

Proof. We apply the result from proposition 2.15 and substitute the contingent claim with $H(R(T)) = R(T) > 0$. Then,

$$E_{\mathbb{Q}^T}[R(T) | \mathcal{F}_\tau] = \frac{1}{P(\tau, T, r)} \mathbb{E} \left[\exp \left(- \int_\tau^T R(u) du \right) R(T) \mid \mathcal{F}_\tau \right].$$

Applying Fubini's theorem to the right-hand side of the equation above,

$$\begin{aligned} E_{\mathbb{Q}^T}[R(T) | \mathcal{F}_\tau] &= -\frac{1}{P(\tau, T)} \mathbb{E}_{\mathbb{Q}} \left[\frac{\partial}{\partial T} \exp \left(- \int_\tau^T R(u) du \right) \mid \mathcal{F}_\tau \right] \\ &= -\frac{1}{P(\tau, T)} \frac{\partial}{\partial T} \mathbb{E}_{\mathbb{Q}} \left[\exp \left(- \int_\tau^T R(u) du \right) \mid \mathcal{F}_\tau \right] \\ &= -\frac{1}{P(\tau, T)} \frac{\partial}{\partial T} P(\tau, T) \\ &= -\frac{\partial}{\partial T} \log P(\tau, T) \\ &= f(\tau, T). \end{aligned}$$

□

Remark 3.4. *We note that the result in proposition 3.3 is not limited to τ and can indeed be applied for any time $t \in [\tau, T]$. In this paper however, we only need to consider $f(\tau, T)$.*

We now turn our attention to the zero-coupon bond, $P(t, T)$. In the way it is defined as of now, computing $P(t, T)$ for different combinations of t and T can be a numerically daunting task. This stresses us to find an analytical expression $P(t, T)$ in the form of an Affine Term Structure (ATS). As a first step in the process of finding an analytical expression for $P(t, T)$, we begin by defining ATS in the definition below.

Definition 3.5 (Affine term structure (ATS)). *Let $a(t, T)$ and $b(t, T)$ be deterministic functions of t and T , once differentiable in t . A short rate model allows an affine term structure (ATS) if*

$$P(t, T, R(t)) = \mathbb{E}_{\mathbb{Q}} \left[e^{- \int_t^T R(u) du} \mid \mathcal{F}_t \right] = e^{-a(t, T) - b(t, T)R(t)}, \quad (23)$$

where $P(T, T) = 1$ implies that $a(T, T) = b(T, T) = 0$.

Remark 3.6. We note that under the ATS, the zero-coupon bond $P(t, T, R(t))$ depends on the short rate at time t , $R(t)$. While in the previous chapter the time- t price of the zero-coupon bond maturing at time T is denoted by $P(t, T)$, we from now write $P(t, T, R(t))$ under the assumption that the short-rate model (21) allows the ATS representation (23). In this paper, we will choose a short-rate model that allows an ATS representation.

Definition 3.5 gives us a simple and efficient way to compute zero-coupon bonds given the times τ and T . However, it is yet unclear what kind of short rate models allow an ATS. We therefore consider the following proposition, which characterizes short-rate models which allows an ATS.

Proposition 3.7 (Characterization of affine term structures, see Filipović (2009, Proposition 5.2)). *The short-rate model (21) provides an ATS if and only if its squared diffusion and drift terms are of form*

$$\sigma^2(t, R(t)) = \alpha_1(t) + \alpha_2(t)R(t) \quad \text{and} \quad \mu(t, R(t)) = \beta_1(t) + \beta_2(t)R(t), \quad (24)$$

for some continuous, deterministic functions $\alpha_1, \alpha_2, \beta_1, \beta_2$, and the deterministic functions a and b satisfy the system of Riccati ODEs, for all $t \in [\tau, T]$,

$$\partial_t a(t, T) = \frac{1}{2}\alpha_1(t)b^2(t, T) - \beta_1(t)b(t, T), \quad a(T, T) = 0, \quad (25)$$

$$\partial_t b(t, T) = \frac{1}{2}\alpha_2(t)b^2(t, T) - \beta_2(t)b(t, T) - 1, \quad b(T, T) = 0. \quad (26)$$

Proof. We refer to Filipović (2009, Proposition 5.2) for the proof. \square

Thus, with proposition 3.7, we may price zero-coupon bonds at time τ without having the need to compute the \mathbb{Q} -expectation of the stochastic exponential. Lastly, we consider another, yet unrelated result about the zero-coupon bond price at time $t \geq \tau$, in which we find the SDE for $P(t, T)$.

Proposition 3.8. *Assume that the short rate process R , expressed with (21), has affine drift and squared diffusion terms. For $t \geq \tau$, the time- t zero-coupon bond maturing at time $T > t$*

$$P(t, T, R(t)) = \mathbb{E}_{\mathbb{Q}} \left[e^{-\int_t^T R(u) du} \mid \mathcal{F}_t \right], \quad P(T, T) = 1,$$

follows the SDE

$$dP(t, T, R(t)) = R(t)P(t, T, R(t)) dt + \sigma(t, R(t), T)\partial_r P(t, T, R(t)) dW^{R, \mathbb{Q}}(t),$$

where $\sigma(t, R(t), T)$ is the diffusion of R .

Proof. Define the continuous function $g(t, r) := P(t, T, r)$. At $t = \tau$, g solves the backward Kolmogorov PDE

$$\partial_t g(t, r) + \mu(t, r)\partial_r g(t, r) + \frac{1}{2}\sigma^2(t, r)g(t, r) - rg(t, r) = 0, \quad (27)$$

with $g(T, r) = 1$. This PDE is a direct result from the Feynman-Kac theorem, see Appendix B.2. Applying Itô's lemma, see Appendix B.1, on $g(P(t, T, R(t)))$ for $t > \tau$ yields

$$\begin{aligned} dg(t, R(t)) &= \left\{ \partial_t g(t, R(t)) + \mu(t, R(t))\partial_r g(t, R(t)) + \frac{1}{2}\sigma^2(t, R(t))\partial_{rr}g(t, R(t)) \right\} dt \\ &\quad + \sigma(t, R(t))\partial_r g(P(t, T, R(t))) dW^{R, \mathbb{Q}}(t). \end{aligned} \quad (28)$$

Since g solves (27), one finds that the drift in the above SDE is

$$\partial_t g(t, R(t)) + \mu(t, r)\partial_r g(t, R(t)) + \frac{1}{2}\sigma^2(t, r)g(t, R(t)) = R(t)g(t, R(t)),$$

such that (28) simplifies to

$$dg(t, R(t)) = R(t)g(t, R(t)) dt + \sigma(t, R(t))\partial_r g(t, R(t)) dW^{R, \mathbb{Q}}(t).$$

Substituting $P(t, T, R(t)) = g(t, R(t))$ into the equation above,

$$dP(t, T, R(t)) = R(t)P(t, T, R(t)) dt + \sigma(t, R(t)) \partial_r P(t, T, R(t)) dW^{R, \mathbb{Q}}(t),$$

which is the SDE for $P(t, T, R(t))$. \square

This concludes this section, in which we have considered some basic theory, which we will base our pricing models on. In the next part of this chapter, we specify the short rate model that we use for the purpose of option pricing.

The CIR Model

The Cox-Ingersoll-Ross model (CIR), see Cox et al. (1985), has long been the go-to model in the financial industry, due to its analytical tractability and the resulting short-rates being non-negative given that some of the parameters are constrained. We discuss the constraint after presenting the CIR model.

The CIR model is defined by the SDE

$$dR(t) = \kappa_r(\theta_r - R(t)) dt + \sigma_r \sqrt{R(t)} dW^{R, \mathbb{Q}}(t), \quad R(\tau) = r, \quad (29)$$

where $\kappa_r, \theta_r, \sigma_r > 0$ are the real-valued, constant parameters belonging to R . The CIR process is a mean-reversion process, where κ_r is the speed of the mean-reversion, θ_r is the long-term mean of the process, and σ_r is the instantaneous volatility of the process.

Considering proposition 3.7, we observe that the model's drift and squared diffusion terms are affine, as

$$\mu(t, R(t)) = \kappa_r\theta_r - \kappa_r R(t)$$

and

$$\sigma^2(t, R(t)) = \sigma_r^2 R(t)$$

such that $\alpha_1(t) = 0$, $\alpha_2(t) = \sigma_r^2$, $\beta_1(t) = \kappa_r\theta_r$, and $\beta_2(t) = -\kappa_r$ in the aforementioned proposition. However, the diffusion in (29) is not globally Lipschitz continuous. This directly contradicts with the assumption that the CIR SDE admits a unique solution. To see this, suppose $X, Y \geq 0$ follow the CIR process (29). Then, at time $t \in [\tau, T]$,

$$\sigma_r \left| \sqrt{X(t)} - \sqrt{Y(t)} \right| \leq \frac{\sigma_r}{\sqrt{X(t)} + \sqrt{Y(t)}} |X(t) - Y(t)| = L(X(t), Y(t)) |X(t) - Y(t)|,$$

where

$$L(X(t), Y(t)) = \frac{\sigma_r}{\sqrt{X(t)} + \sqrt{Y(t)}}.$$

We note that for $X(t) = Y(t) = 0$, L blows up, such that the CIR process is not Lipschitz continuous and its solution is not unique. This poses a problem to us as we can no longer rely on proposition 3.7 for finding the discounting factor $P(t, T, R(t))$, which consequently makes the pricing of many financial derivatives based on the zero-coupon bond difficult. We therefore impose the constraint

$$\sigma_r^2 \leq 2\kappa_r\theta_r \quad (30)$$

such that $R(t) > 0 \ \forall t \in [\tau, T]$ a.s. A proof on why the constraint keeps the short rate process strictly positive can be found in Jeanblanc et al. (2009, Definition 6.1.2.1, and Propositions 6.1.3.1 and 6.3.1.1), where the authors argue that the CIR process follows a squared Bessel process with dimension $4\kappa_r\theta_r/\sigma_r^2$. Since the squared Bessel process is strictly positive for $4\kappa_r\theta_r/\sigma_r^2 \geq 2$, we get the aforementioned positivity constraint $\sigma_r^2 \leq 2\kappa_r\theta_r$. This keeps the CIR model globally Lipschitz continuous and proposition 3.7 holds here as well.

After imposing the constraint (30), we find that the solutions to $a(t, T)$ and $b(t, T)$ in the ATS, see definition 3.5 and proposition 3.7, are

$$a(t, T) = -\frac{2\kappa_r\theta_r}{\sigma_r^2} \log \left(\frac{2he^{(\kappa_r+h)(T-t)/2}}{2h + (\kappa_r + h)(e^{h(T-t)} - 1)} \right), \quad (31)$$

and

$$b(t, T) = \frac{2(e^{h(T-t)} - 1)}{2h + (\kappa_r + h)(e^{h(T-t)} - 1)} \quad (32)$$

where $h = \sqrt{\kappa_r^2 + 2\sigma_r^2}$.

The CIR++ Model

The CIR++ model, first presented by Brigo and Mercurio (2001), extends the previously presented CIR model with the help of a deterministic shift function $\psi(t)$. In theory, this extension seeks to fit the CIR model (29) to perfectly fit the initial term structure. In this paper, we rely on the CIR++ model to model short rates due to its analytical tractability, as well as its simplicity since we are only required to estimate four parameters. Moreover, pricing swaptions and other financial derivatives can be done using simple formulae of closed-form, making the calibration process straightforward.

The short-rate dynamics of the CIR++ process are given by

$$\begin{cases} d\tilde{X}(t) = \kappa_r(\theta_r - \tilde{X}(t)) dt + \sigma_r \sqrt{\tilde{X}(t)} dW^{R,\mathbb{Q}}(t), & \tilde{X}(\tau) = x_0 \\ R(t) = \tilde{X}(t) + \psi(t), & R(\tau) = r \end{cases}$$

where $x_0, \kappa_r, \theta_r, \sigma_r > 0$ are real-valued, constant parameters, $\psi(t)$ is a deterministic function of t and $r = x_0 + \psi(\tau)$. The stochastic, CIR++ short rate R is a mean-reverting process and the parameters x_0, κ_r, θ_r , and σ_r have the same interpretation as for the CIR model (29). Furthermore, we impose the constraint (30), which we have discussed earlier, to keep the CIR process \tilde{X} strictly positive at any time $t \in [\tau, T]$. The SDE for $R(t)$ then reads as

$$dR(t) = (\kappa_r(\theta_r - R(t) + \psi(t)) + \psi'(t)) dt + \sigma_r \sqrt{R(t) - \psi(t)} dW^{R,\mathbb{Q}}(t), \quad (33)$$

where $\psi'(t) = \frac{d}{dt}\psi(t)$. The deterministic function ψ is expressed through

$$\psi(t) = f^{\text{Svensson}}(\tau, t) - f^{\text{CIR}}(\tau, t),$$

with

$$f^{\text{CIR}}(\tau, t) = \frac{2\kappa_r\theta_r(e^{h(t-\tau)} - 1)}{2h + (\kappa_r + h)(e^{h(t-\tau)} - 1)} + x_0 \frac{4h^2 e^{h(t-\tau)}}{[2h + (\kappa_r + h)(e^{h(t-\tau)} - 1)]^2},$$

where $\tau \leq t$, $h = \sqrt{\kappa_r^2 + 2\sigma_r^2}$, and $f^{\text{Svensson}}(\tau, t)$ is the observed instantaneous forward curve in the market between times τ and t . We model the observed forward curve with the help of the Svensson model (3).

When it comes to ψ' in (33), we find that

$$\begin{aligned} \psi'(t) &= \frac{d}{dt} (f^{\text{Svensson}}(\tau, t) - f^{\text{CIR}}(\tau, t)) \\ &= -a_1\beta_1 e^{-a_1(t-\tau)} + \beta_2 a_1 e^{-a_1(t-\tau)} (1 - a_1(t - \tau)) + \beta_3 a_2 e^{-a_2(t-\tau)} (1 - a_2(t - \tau)) \\ &\quad - \frac{4\kappa_r\theta_r h^2 e^{h(t-\tau)}}{[(\kappa_r + h)e^{h(t-\tau)} - \kappa_r + h]^2} + x_0 \frac{4h^3 e^{h(t-\tau)} [(\kappa_r + h)e^{h(t-\tau)} + \kappa_r - h]}{[(\kappa_r + h)e^{h(t-\tau)} - \kappa_r + h]^3}. \end{aligned} \quad (34)$$

Furthermore, we observe that the CIR++ model (33) is affine in view of proposition 3.7, with

$$\sigma^2(t, R(t)) = \sigma_r^2(R(t) - \psi(t)) = \alpha_1(t) + \alpha_2(t)R(t),$$

and

$$\mu(t, R(t)) = \kappa_r(\theta_r - R(t) + \psi(t)) + \psi'(t) = \beta_1(t) + \beta_2(t)R(t),$$

where $\alpha_1(t) = -\sigma_r^2\psi(t)$, $\alpha_2(t) = \sigma_r^2$, $\beta_1(t) = \kappa_r(\theta_r + \psi(t)) + \psi'(t)$, and $\beta_2(t) = -\kappa_r$ characterize the functions a and b present in the ATS. Thus, the time- t price of a zero-coupon bond maturing at time T , $P(t, T, R(T))$, is computed with

$$P(t, T, R(t)) = e^{-\bar{a}(t, T) - b(t, T)R(t)}, \quad (35)$$

where

$$\bar{a}(t, T) = \log \left(\frac{P^{\text{Svensson}}(\tau, t) e^{-a(\tau, T) - b(\tau, T)x_0}}{P^{\text{Svensson}}(\tau, T) e^{-a(\tau, t) - b(\tau, t)x_0}} \right) - a(t, T) - b(t, T)\psi(t), \quad (36)$$

and $a(t, T)$ and $b(t, T)$ are defined as in (31) and (32) respectively, and $P^{\text{Svensson}}(\tau, T)$ is the zero-coupon bond in the Svensson model (5).

With the definition of the CIR++ short rate process (33), we determine the SDE for $P(\tau, T, r)$ for any to be as in the lemma below.

Corollary 3.9 (Zero-coupon bond dynamics under the CIR++ model). *Let $\tau \leq t \leq T$ and assume that the short rate process R is modeled with the CIR++ model following the SDE (33) under \mathbb{Q} . Furthermore, recall that $\psi(\cdot)$ is a deterministic function. Then,*

$$dP(t, T, R(t)) = R(t)P(t, T, R(t)) dt - \sigma_r b(t, T) \sqrt{R(t) - \psi(t)} P(t, T, R(t)) dW^{R, \mathbb{Q}}(t),$$

where $b(t, T)$ is described in (32) and arises from the ATS in definition 3.5.

Proof. For the CIR++ process R following the SDE (33), the diffusion is $\sigma(t, R(t)) = \sigma_r \sqrt{R(t) - \psi(t)}$. Furthermore, since the CIR++ process has affine drift and squared diffusion terms, such that in view of proposition 3.7, the zero-coupon bond is expressed by

$$P(\tau, T, r) = e^{-\bar{a}(\tau, T) - b(\tau, T)r}.$$

The partial derivative of P with respect to r is

$$\partial_r P(\tau, T, r) = -b(\tau, T)P(\tau, T, r).$$

Hence for $t > \tau$,

$$\partial_r P(t, T, R(t)) = -b(t, T)P(t, T, R(t))$$

Then inserting the expressions for $\sigma(t, R(t))$ and $\partial_r P(t, T, R(t))$ into the SDE in proposition 3.8 yields

$$dP(t, T, R(t)) = R(t)P(t, T, R(t)) dt - \sigma_r b(t, T) \sqrt{R(t) - \psi(t)} P(t, T, R(t)) dW^{R, \mathbb{Q}}(t),$$

which was to be proven. \square

3.2 Pricing of Fixed-Income Instruments under the CIR++ Model

So far, we have studied the cash flow structure of swaptions, derived a pricing formula for European options and chosen an affine short rate model that allows an ATS. As previously mentioned, our aim is to estimate the parameters in the CIR++ model with the help of market data for swaptions, which presents a motivation for the derivation of a closed-form pricing formula for the CIR++ model (33). By applying theory and notation presented in Brigo and Mercurio (2006) (see pp.102-104), we develop a pricing model for European bond options used to price swaptions.

European Options on Zero-coupon Bonds

Recall the CIR++ short-rate model (33), where the quantities $\tilde{X}(\tau) = x_0$ and $R(\tau) = r$ are constants. Under the model and at the present time τ , the price of a European call option, with maturity $T \geq \tau$ and strike price $K > 0$, on a zero-coupon bond maturing at $U \geq T$ is

$$\begin{aligned} \text{zbc}(\tau, T, U, K) &= P(\tau, T, r) \mathbb{E}_{\mathbb{Q}^T} [(P(T, U, R(T)) - K)_+ | \mathcal{F}_\tau] \\ &= P(\tau, U, r) \chi^2 \left(2\hat{r}(\rho + \omega + b(T, U)); \frac{4\kappa_r \theta_r}{\sigma_r^2}, \frac{2\rho^2[r - \psi(\tau)]e^{h(T-\tau)}}{\rho + \omega + b(T, U)} \right) - \\ &\quad K P(\tau, T, r) \chi^2 \left(2\hat{r}(\rho + \omega); \frac{4\kappa_r \theta_r}{\sigma_r^2}, \frac{2\rho^2[r - \psi(\tau)]e^{h(T-\tau)}}{\rho + \omega} \right), \end{aligned} \quad (37)$$

where $\chi^2(k; \ell, m)$ denotes the non-central χ^2 -distribution with k degrees of freedom, non-centrality parameter ℓ and scale m . Furthermore, the constants $P(\tau, U, r)$, \hat{r} , ρ , and ω in (37) are

$$P(\tau, U, r) = e^{-\bar{a}(\tau, U) - b(\tau, U)r},$$

$$\hat{r} = \frac{1}{B(T, U)} \left(\log \frac{A(T, U)}{K} - \log \frac{P^{\text{Svensson}}(\tau, T) A(\tau, T) e^{-B(\tau, U)x_0}}{P^{\text{Svensson}}(\tau, U) A(\tau, U) e^{-B(\tau, T)x_0}} \right)$$

$$\rho = \frac{2h}{\sigma_r^2 (e^{h(T-\tau)} - 1)},$$

and

$$\omega = \frac{\kappa_r + h}{\sigma_r^2}.$$

The equations above can be found in Brigo and Mercurio (2006), see pp.102-104. To price European put options on a zero-coupon bond, i.e. **zbp**, we rely on the put-call parity for European options on zero-coupon bonds presented in proposition 3.10.

Proposition 3.10 (Put-call parity for European options on zero-coupon bonds). *Let $\tau \leq T \leq U$. The put-call parity for European options on zero-coupon bonds is given by*

$$\mathbf{zbc}(\tau, T, U, K) + KP(\tau, T, r) = \mathbf{zbp}(\tau, T, U, K) + P(\tau, U, r), \quad (38)$$

for some constant, finite and non-negative strike price K , and under the assumption $P(T, U, R(T)) < \infty$.

Proof. Recall that the payoffs at time T of European options with maturity T on zero-coupon bonds maturing at time U are given by

$$(P(T, U, R(T)) - K)_+,$$

for call options, and

$$(K - P(T, U, R(T)))_+$$

for put options respectively. Moreover, the following identity for hockey stick functions is relevant:

$$(P(T, U, R(T)) - K)_+ - (K - P(T, U, R(T)))_+ = P(T, U, R(T)) - K.$$

Since the contingent claim is non-negative, \mathcal{F}_T -measurable, and finite by assumption, applying proposition 2.15 on the equation above yields

$$\begin{aligned} P(\tau, T, r) \mathbb{E}_{\mathbb{Q}^T} [(P(T, U, R(T)) - K)_+ \mid \mathcal{F}_\tau] - P(\tau, T, r) \mathbb{E}_{\mathbb{Q}^T} [(K - P(T, U, R(T)))_+ \mid \mathcal{F}_\tau] &= \\ &= P(\tau, T, r) \mathbb{E}_{\mathbb{Q}^T} [P(T, U, R(T)) - K \mid \mathcal{F}_\tau]. \end{aligned} \quad (39)$$

Recalling that under the T -forward probability measure, \mathbb{Q}^T , defined with the Radon-Nikodym derivative

$$\frac{d\mathbb{Q}^T}{d\mathbb{Q}} = \frac{1}{P(\tau, T, r) B(T)},$$

we have by Bayes' theorem for change of measures, see Appendix B.4,

$$\begin{aligned} P(\tau, T, r) \mathbb{E}_{\mathbb{Q}^T} [P(T, U, R(T)) - K \mid \mathcal{F}_\tau] &= \mathbb{E}_{\mathbb{Q}} \left[\frac{B(\tau)}{B(T)} P(T, U, R(T)) \mid \mathcal{F}_t \right] - KP(\tau, T, r) \\ &= \mathbb{E}_{\mathbb{Q}} \left[e^{-\int_\tau^U R(u) du} \mid \mathcal{F}_t \right] - KP(\tau, T, r) \\ &= P(\tau, U, r) - KP(\tau, T, r). \end{aligned}$$

Inserting the result above into (39),

$$\begin{aligned} P(\tau, T, r) \mathbb{E}_{\mathbb{Q}^T} [(P(T, U, R(T)) - K)_+ \mid \mathcal{F}_\tau] - P(\tau, T, r) \mathbb{E}_{\mathbb{Q}^T} [(K - P(T, U, R(T)))_+ \mid \mathcal{F}_\tau] &= \\ &= P(\tau, U, r) - KP(\tau, T, r). \end{aligned}$$

As the prices of the bond options are given by

$$\mathbf{zbc}(\tau, T, U, K) = P(\tau, T, r) \mathbb{E}_{\mathbb{Q}^T}[(P(T, U, R(T)) - K)_+ \mid \mathcal{F}_\tau],$$

and

$$\mathbf{zbp}(\tau, T, U, K) = P(\tau, T, r) \mathbb{E}_{\mathbb{Q}^T}[(K - P(T, U, R(T)))_+ \mid \mathcal{F}_\tau],$$

the put-call parity of European bond options is

$$\mathbf{zbc}(\tau, T, U, K) - \mathbf{zbp}(\tau, T, U, K) = P(\tau, U, r) - KP(\tau, T, r).$$

□

Hence, under the CIR++ model, the time- τ value of a European put option with maturity $T \geq \tau$, and strike price K on a zero-coupon bond maturing at $U \geq T$ is

$$\begin{aligned} \mathbf{zbp}(\tau, T, U, K) = & KP(\tau, T, r) \left[1 - \chi^2 \left(2\hat{r}[\rho + \omega]; \frac{4\kappa_r \theta_r}{\sigma_r^2}, \frac{2\rho^2[r - \psi(\tau)]e^{h(T-t)}}{\rho + \omega} \right) \right] - \\ & P(\tau, U, r) \left[1 - \chi^2 \left(2\hat{r}[\rho + \omega + b(T, U)]; \frac{4\kappa_r \theta_r}{\sigma_r^2}, \frac{2\rho^2[r - \psi(\tau)]e^{h(T-\tau)}}{\rho + \omega + b(T, U)} \right) \right], \end{aligned} \quad (40)$$

where the constants ρ , ω , and \hat{r} are as before.

Swaptions

The pricing of swaptions is not a straightforward process as with many other fixed-income derivatives, but an analytical formula is found with the help of Jamshidian's trick, see Jamshidian (1989). We recall that the payoff at maturity T_0 of a payer swaption with a fixed notional amount N and a fixed strike rate κ is given by lemma 2.13, that is,

$$\mathbf{ps}(T_0, T_0, T_n) = (r_{\text{swap}}(T_0, T_n) - \kappa)_+ \sum_{i=1}^n \delta_i P(T_0, T_i),$$

where T_i for $i = 1, \dots, n$ are dates in the future at which the swap is paid, $\delta_i := T_i - T_{i-1}$, r_{swap} denotes the fair swap rate and R is the stochastic short rate. We also recall that for some time $T \geq \tau$, the T -forward measure, \mathbb{Q}^T , is defined with the Radon-Nikodym derivative

$$\frac{d\mathbb{Q}^T}{d\mathbb{Q}} = \frac{P(T, T)}{P(\tau, T, r)B(T)} = \frac{1}{P(\tau, T, r)B(T)}.$$

Under proposition 2.15, the price of a payer swaption maturing at $T_0 \geq \tau$ is then given under the T_0 -forward measure, \mathbb{Q}^{T_0} by

$$\mathbf{ps}(\tau, T_0, T_n) = P(\tau, T_0) \mathbb{E}_{\mathbb{Q}^{T_0}} \left[(r_{\text{swap}}(T_0, T_n) - \kappa)_+ \sum_{i=1}^n \delta_i P(T_0, T_i) \mid \mathcal{F}_\tau \right].$$

The swap rate $r_{\text{swap}}(T_0, T_n)$ is as in (7), so the equation above becomes

$$\mathbf{ps}(\tau, T_0, T_n) = P(\tau, T_0) \mathbb{E}_{\mathbb{Q}^{T_0}} \left[\left(1 - P(T_0, T_n) - \kappa \sum_{i=1}^n \delta_i P(T_0, T_i) \right)_+ \mid \mathcal{F}_\tau \right].$$

Define $c_i := \kappa \delta_i$ for $i = 1, \dots, n-1$ and $c_n = 1 + \kappa \delta_n$. Then, applying a logic similar to the one in the put-call parity for European bond options (38), we find

$$\begin{aligned} \mathbf{ps}(\tau, T_0, T_n) &= P(\tau, T_0) \mathbb{E}_{\mathbb{Q}^{T_0}} \left[\left(1 - \sum_{i=1}^n c_i P(T_0, T_i) \right)_+ \mid \mathcal{F}_\tau \right] \\ &= P(\tau, T_0) \left(1 - \sum_{i=1}^n \mathbb{E}_{\mathbb{Q}^{T_0}} [c_i P(T_0, T_i) \mid \mathcal{F}_\tau] \right) + P(\tau, T_0) \mathbb{E}_{\mathbb{Q}^{T_0}} \left[\left(\sum_{i=1}^n c_i P(T_0, T_i) - 1 \right)_+ \mid \mathcal{F}_\tau \right] \\ &= P(\tau, T_0) \left(1 - \sum_{i=1}^n \mathbb{E}_{\mathbb{Q}^{T_0}} [c_i P(T_0, T_i) \mid \mathcal{F}_\tau] \right) + \mathbf{rs}(\tau, T_0, T_n), \end{aligned} \quad (41)$$

where

$$\mathbf{rs}(\tau, T_0, T_n) = P(\tau, T_0) \mathbb{E}_{\mathbb{Q}^{T_0}} \left[\left(\sum_{i=1}^n c_i P(T_0, T_i) - 1 \right)_+ \mid \mathcal{F}_\tau \right], \quad (42)$$

is the price of the receiver swaption. Recalling that the CIR++ model has affine drift and squared diffusion terms, bonds are priced with the ATS (23). In the ATS, for fixed maturity T , the map $R(t) \mapsto P(t, T, R(t))$ is continuous and strictly decreasing in $R(t)$. By Jamshidian (1989), there consequently exist a unique and constant $r^* > 0$ such that

$$\sum_{i=1}^n c_i P(T_0, T_i; r^*) = 1.$$

To apply this identity, define the deterministic bond strikes⁹

$$x_i := P(T_0, T_i; r^*) = e^{-\bar{a}(T_0, T_i) - b(T_0, T_i)r^*},$$

so that

$$\sum_{i=1}^n c_i x_i = 1.$$

Then, pathwise at T_0 ,

$$\left(\sum_{i=1}^n c_i P(T_0, T_i) - 1 \right)_+ = \left(\sum_{i=1}^n c_i (P(T_0, T_i) - x_i) \right)_+ = \sum_{i=1}^n c_i (P(T_0, T_i) - x_i)_+,$$

by Jamshidian's trick. Therefore, the receiver swaption's price is

$$\begin{aligned} \mathbf{rs}(\tau, T_0, T_n) &= P(\tau, T_0) \mathbb{E}_{\mathbb{Q}^{T_0}} \left[\left(\sum_{i=1}^n c_i P(T_0, T_i) - 1 \right)_+ \mid \mathcal{F}_\tau \right] \\ &= P(\tau, T_0) \sum_{i=1}^n c_i \mathbb{E}_{\mathbb{Q}^{T_0}} [(P(T_0, T_i) - x_i)_+] \mid \mathcal{F}_\tau \\ &= \sum_{i=1}^n c_i \mathbf{zbc}(\tau, T_0, T_i, x_i), \end{aligned}$$

where

$$\mathbf{zbc}(\tau, T_0, T_i, x_i) = P(\tau, T_0) \mathbb{E}_{\mathbb{Q}^{T_0}} [(P(T_0, T_i) - x_i)_+] \mid \mathcal{F}_\tau.$$

Applying the bond option and swaption put-call parities (38) and (41), we find that the time- τ price of a swaption with maturity T_0 , notional amount N and strike rate κ is

$$\mathbf{ps}(\tau, T_0, T_n) = \sum_{i=1}^n c_i \mathbf{zbp}(\tau, T_0, T_i, x_i), \quad (43)$$

where $c_i = \kappa \delta_i$ for $i = 1, \dots, n-1$ and $c_n = 1 + \kappa \delta_n$, and the European put option on a zero-coupon bond, $\mathbf{zbp}(\tau, T_0, T_i, x_i)$, is priced by (40).

With the derivation of a closed form formula for the payer swaptions, the task of estimating the parameters within the CIR++ model (33) is done by finding the optimal parameters x_0^* , κ_r^* , θ_r^* , and σ_r^* that minimize the L^2 -distance between the market data and the model prices (43).

⁹The bond strikes are deterministic since r^* is a constant and \bar{a} and b are deterministic functions of t and T .

4 Option Pricing Model for the Risky Asset

In this chapter, we bring together theory developed in chapters 2 and 3 into a PDE-based framework for option pricing. We begin by specifying a Heston-type stochastic variance model for the underlying asset, combined with a CIR++ short-rate model, so that the option price depends on the joint evolution of the risky asset price, the short rate and the variance. This joint model is specified as a system of SDEs under the risk-neutral probability measure \mathbb{Q} . As seen in proposition 2.15, pricing under the T -forward numéraire has proven to be convenient and the system of SDEs is therefore reformulated to be under \mathbb{Q}^T . Lastly, by applying Itô's lemma, we derive a parabolic backward option pricing PDE in the variables (τ, s, r, ν) , which will form the analytical foundation for the numerical methods presented in the subsequent chapter.

4.1 Heston Model with Stochastic Short Rates

So far, we have priced European call options under the risk-neutral measure \mathbb{Q} without considering a particular model for the underlying asset price process S . In this chapter, we specify a Heston-type model for the asset's variance, combined with a CIR++ short-rate model. We work on the filtered probability space $(\Omega, \mathcal{F}, \{\mathcal{F}_t\}_{t \in [\tau, T]}, \mathbb{Q})$, where \mathbb{Q} is the risk-neutral probability measure. Under \mathbb{Q} , we consider the \mathcal{F}_t -adapted processes $S = \{S(t)\}_{t \in [\tau, T]}$, $R = \{R(t)\}_{t \in [\tau, T]}$ and $V = \{V(t)\}_{t \in [\tau, T]}$ representing the risky asset price, the short rate and the variance respectively. Let $\tau > 0$ be the starting time for all three processes and assume that

$$S(\tau) = s > 0, \quad R(\tau) = r > 0, \quad V(\tau) = \nu > 0,$$

are given, real-valued constants. As seen chapter 2, for constant strike price $K > 0$ and maturity $T > \tau$, the time- τ price of a European call option with underlying S is given by

$$c(\tau, s, r, \nu) = \mathbb{E}_{\mathbb{Q}} \left[\frac{B(\tau)}{B(T)} (S(T) - K)_+ \mid \mathcal{F}_\tau \right],$$

where $s = S(\tau)$ and the stochastic risk-free asset $B(\cdot)$ is determined by

$$B(t) = \exp \left(\int_\tau^t R(u) \, du \right), \quad B(\tau) = 1,$$

so that in particular,

$$\frac{B(\tau)}{B(T)} = \exp \left(- \int_\tau^T R(u) \, du \right).$$

For $t \in [\tau, T]$ and under the probability measure \mathbb{Q} , we assume that the random processes S , R , and V follow the SDEs

$$\begin{cases} dS(t) = R(t)S(t) \, dt + \sqrt{V(t)} S(t) \, dW^{S,\mathbb{Q}}(t), & S(\tau) = s \\ dR(t) = (\kappa_r(\theta_r - R(t)) + \psi(t)) \, dt + \sigma_r \sqrt{R(t) - \psi(t)} \, dW^{R,\mathbb{Q}}(t), & r(\tau) = r \\ dV(t) = \kappa_\nu(\theta_\nu - V(t)) \, dt + \sigma_\nu \sqrt{V(t)} \, dW^{V,\mathbb{Q}}(t), & V(\tau) = \nu \end{cases} \quad (44)$$

where $\kappa_r, \theta_r, \sigma_r, \kappa_\nu, \theta_\nu, \sigma_\nu > 0$ are constant parameters and $W^{S,\mathbb{Q}} = \{W^{S,\mathbb{Q}}(t)\}_{t \in [\tau, T]}$, $W^{R,\mathbb{Q}} = \{W^{R,\mathbb{Q}}(t)\}_{t \in [\tau, T]}$, and $W^{V,\mathbb{Q}} = \{W^{V,\mathbb{Q}}(t)\}_{t \in [\tau, T]}$ are the one-dimensional Brownian motions of S , r and V , respectively, under \mathbb{Q} . The Brownian motions are allowed to be correlated and we assume that

$$\begin{cases} d\langle W^{S,\mathbb{Q}}(t), W^{R,\mathbb{Q}}(t) \rangle_t = \rho_1 \, dt, \\ d\langle W^{S,\mathbb{Q}}(t), W^{V,\mathbb{Q}}(t) \rangle_t = \rho_2 \, dt, \\ d\langle W^{R,\mathbb{Q}}(t), W^{V,\mathbb{Q}}(t) \rangle_t = \rho_3 \, dt, \end{cases} \quad (45)$$

with constant instantaneous correlation coefficients $\rho_1, \rho_2, \rho_3 \in (-1, 1)$. In this specification, the asset price S follows a geometric Brownian motion with stochastic variance V , the short rate R

follows a CIR++ process, and the variance process V follows a CIR type process¹⁰. To ensure that the SDEs for R and V have a unique solution, we impose the constraints

$$\sigma_r \leq 2\kappa_r \theta_r \quad \text{and} \quad \sigma_\nu \leq 2\kappa_\nu \theta_\nu,$$

which keep the respective diffusions of R and V Lipschitz continuous as discussed in chapter 3.1.

4.2 Model Specification under the Forward Measure

As discussed in section 2.5, working under the T -forward measure \mathbb{Q}^T , as opposed to the risk-neutral measure \mathbb{Q} , is convenient because discounting is absorbed into the numéraire and the option price reduces to a single conditional expectation. We therefore resort on applying the option pricing model for the risky asset S (19) under \mathbb{Q}^T to price options throughout this paper. However, this means that the model under \mathbb{Q} (44) is no longer valid under \mathbb{Q}^T and we need to seek a new set of Brownian motions under \mathbb{Q}^T which are denoted by $W^{\mathbb{Q}^T}$. This task is done by applying Girsanov's theorem covered in Appendix B.3.

We begin by recollecting necessary theory. For $t \in [\tau, T]$, recall (19), where the time- t price of the European call option under the T -forward measure \mathbb{Q}^T is

$$c(t, S(t), R(t), V(t)) = P(t, T, R(t)) \mathbb{E}_{\mathbb{Q}^T} [(S(T) - K)_+ | \mathcal{F}_t].$$

For $t > \tau$, $P(t, T, R(t))$ denotes the stochastic, time- t price of the zero-coupon bond maturing at T , which under the CIR++ framework is priced with

$$P(t, T, R(t)) = \mathbb{E}_{\mathbb{Q}} \left[\exp \left(- \int_t^T R(u) du \right) \middle| \mathcal{F}_t \right] = \exp(-\bar{a}(t, T) - b(t, T)R(t)),$$

with deterministic functions \bar{a} and b described in (36) and (32) respectively. Lastly, recall that the T -forward measure is specified with the Radon-Nikodym derivative

$$\frac{d\mathbb{Q}^T}{d\mathbb{Q}} = \frac{P(t, T, R(t))}{P(\tau, T, r)B(T)},$$

such that by lemma 2.14

$$\mathbb{E}_{\mathbb{Q}^T} \left[\frac{d\mathbb{Q}^T}{d\mathbb{Q}} \middle| \mathcal{F}_t \right] = \frac{P(t, T, R(t))}{P(\tau, T, r)B(t)}.$$

We then obtain the Brownian motion under \mathbb{Q}^T by applying Girsanov's theorem

$$W^{R, \mathbb{Q}^T}(t) = W^{R, \mathbb{Q}}(t) + \int_{\tau}^t \theta(u) du,$$

where $\theta = \{\theta(t)\}_{t \in [\tau, T]}$ an \mathcal{F}_t -adapted process characterized by

$$\mathbb{E}_{\mathbb{Q}} \left[\frac{d\mathbb{Q}^T}{d\mathbb{Q}} \middle| \mathcal{F}_t \right] = \frac{P(t, T, R(t))}{P(\tau, T, r)B(t)} = \exp \left(-\frac{1}{2} \int_{\tau}^t \theta^2(u) du - \int_{\tau}^t \theta(u) dW^{R, \mathbb{Q}}(u) \right). \quad (46)$$

As θ is not yet specified, its explicit form will be derived in Proposition 4.1.

Proposition 4.1. *Let $t \in [\tau, T]$. Under the CIR++ framework and the T -forward probability measure \mathbb{Q}^T , the \mathcal{F}_t -adapted process $\theta = \{\theta(t)\}_{t \in (0, T)}$ is*

$$\theta(t) = \sigma_r \sqrt{R(t) - \psi(t)} b(t, T),$$

where $b(t, T)$ is the deterministic function (32).

¹⁰A model with a CIR-type variance process is commonly referred to as a Heston model.

Proof. Consider the \mathbb{Q} -martingale $P(t, T, R(t))/B(t)$ and define the function

$$g(b, p) = \frac{p}{b}.$$

Then, applying Itô's lemma, see Appendix B.1, on $g := g(B(t), P(t, T, R(t)))$, yields

$$\begin{aligned} dg &= \partial_p g dP(t, T, R(t)) + \partial_b g dB(t) + \frac{1}{2} \partial_{pp} g d\langle P(t, T, R(t)), P(t, T, R(t)) \rangle_t \\ &\quad + \partial_{bp} g d\langle B(t), P(t, T, R(t)) \rangle_t + \frac{1}{2} \partial_{bb} g d\langle B(t), B(t) \rangle_t, \end{aligned} \quad (47)$$

where the partial derivatives follow the notation $\partial_b = \frac{\partial}{\partial b}$, $\partial_p = \frac{\partial}{\partial p}$, and so on, and g has the argument $(B(t), P(t, T, R(t)))$.

Now recall that the risk-free asset follows the ODE

$$dB(t) = R(t)B(t) dt, \quad B(\tau) = 1, \quad (48)$$

implying that it does not have a diffusion term. Therefore, one has

$$d\langle B(t), B(t) \rangle_t = 0 \quad (49)$$

and

$$d\langle B(t), P(t, T, R(t)) \rangle_t = 0. \quad (50)$$

Lastly, note that

$$\partial_{pp} g(b, p) = 0. \quad (51)$$

Substituting (48), (49), (50), and (51) into (47), the total derivative of g becomes

$$\begin{aligned} dg &= \partial_p g dP(t, T, R(t)) + \partial_b g R(t)B(t) dt \\ &= \frac{1}{B(t)} dP(t, T, R(t)) - \frac{P(t, T, R(t))}{B(t)} R(t) dt, \end{aligned}$$

where g is evaluated at $(B(t), P(t, T, R(t)))$. Recalling corollary 3.9, the SDE for $P(t, T, R(t))$ under the CIR++ framework is

$$dP(t, T, R(t)) = R(t)P(t, T, R(t)) dt + \sigma_r \sqrt{R(t) - \psi(t)} b(t, T) P(t, T, R(t)) dW^{R, \mathbb{Q}}(t),$$

where $b(t, T)$ is a deterministic function of t and T in equation (32). Therefore, the expression for df simplifies to

$$df(B(t), P(t, T, R(t))) = -\frac{P(t, T, R(t))}{B(t)} \sigma_r \sqrt{R(t) - \psi(t)} b(t, T) dW^{R, \mathbb{Q}}(t).$$

Hence, by integrating the total derivative above on the interval $[\tau, t]$ and substituting $f(B(t), P(t, T, R(t)))$ with $P(t, T, R(t))/B(t)$, one finds

$$\frac{P(t, T, R(t))}{P(\tau, T, r)B(t)} = \exp \left(-\frac{\sigma_r^2}{2} \int_\tau^t \left(\sqrt{r(u) - \psi(u)} b(u, T) \right)^2 du - \sigma_r \int_\tau^t \sqrt{r(u) - \psi(u)} b(u, T) dW^{R, \mathbb{Q}}(u) \right). \quad (52)$$

As

$$\mathbb{E}_{\mathbb{Q}} \left[\frac{d\mathbb{Q}^T}{d\mathbb{Q}} \mid \mathcal{F}_t \right] = \frac{P(t, T, R(t))}{P(\tau, T, r)B(t)} = \exp \left(- \int_t^T \theta^2(u) du - \int_t^T \theta(u) dW^{R, \mathbb{Q}}(u) \right),$$

we infer from (52) that $\theta(t) = \sqrt{R(t) - \psi(t)} b(t, T)$ which completes the proof. \square

By proposition 4.1, a standard construction shows that, under \mathbb{Q}^T , we may define Brownian motions W^{S,\mathbb{Q}^T} , W^{R,\mathbb{Q}^T} and W^{V,\mathbb{Q}^T} by

$$\begin{cases} dW^{S,\mathbb{Q}^T} = dW^{S,\mathbb{Q}} + \rho_1 \sqrt{R(t) - \psi(t)} b(t, T) dt \\ dW^{R,\mathbb{Q}^T} = dW^{R,\mathbb{Q}} + \sqrt{R(t) - \psi(t)} b(t, T) dt \\ dW^{V,\mathbb{Q}^T} = dW^{V,\mathbb{Q}} + \rho_3 \sqrt{R(t) - \psi(t)} b(t, T) dt, \end{cases}$$

where the instantaneous correlation coefficients, ρ_1 and ρ_3 , defined in (45) remain unchanged. Thus for $t \in [\tau, T]$, our model now reads as

$$c(t, S(t), R(t), V(t)) = P(t, T, R(t)) \mathbb{E}_{\mathbb{Q}^T} [(S(T) - K)_+ | \mathcal{F}_t],$$

where

$$\begin{cases} dS(t) = S(t) \left(R(t) - \rho_1 \sigma_r \sqrt{V(t)(R(t) - \psi(t))} b(t, T) \right) dt + \sqrt{V(t)} S(t) dW^{S,\mathbb{Q}^T}(t), \\ dR(t) = \left(\kappa_r (\theta_r - R(t) + \psi(t)) + \psi'(t) - \sigma_r^2 (R(t) - \psi(t)) b^2(t, T) \right) dt + \sigma_r \sqrt{R(t) - \psi(t)} dW^{R,\mathbb{Q}^T}(t), \\ dV(t) = \left(\kappa_\nu (\theta_\nu - V(t)) - \rho_3 \sigma_r \sigma_\nu \sqrt{V(t)(R(t) - \psi(t))} b(t, T) \right) dt + \sigma_\nu \sqrt{V(t)} dW^{V,\mathbb{Q}^T}(t). \end{cases} \quad (53)$$

The strictly positive constants $S(\tau) = s$, $r(\tau) = r$ and $V(\tau) = \nu$ as well as the instantaneous correlation coefficients, ρ_1 , ρ_2 and ρ_3 , defined in (45) remain the same as under \mathbb{Q} . Moreover, under \mathbb{Q}^T , the zero-coupon bond price dynamics become

$$\begin{aligned} dP(t, T, R(t)) &= P(t, T, R(t)) \left(R(t) + \sigma_r^2 (R(t) - \psi(t)) b^2(t, T) \right) dt \\ &\quad - \sigma_r \sqrt{R(t) - \psi(t)} b(t, T) P(t, T, R(t)) dW^{R,\mathbb{Q}}(t) \end{aligned} \quad (54)$$

for $t \in [\tau, T]$.

4.3 Backward Parabolic Option Pricing PDE under the Forward Measure

With the specification of our model under the T -forward measure, our next and last goal is to derive the PDE for the option price which is to be solved with the help of a neural network in chapter 6. Using the martingale representation theorem and Itô's lemma, which can be found in Appendices A and B.1 respectively, we transform the pricing problem into a parabolic, backward PDE that reflects the no-arbitrage condition under the T -forward measure. This result can be found in theorem 4.2.

Theorem 4.2 (Backward parabolic option pricing PDE for European call options). *Consider the filtered probability space $(\Omega, \mathcal{F}, \{\mathcal{F}_t\}_{t \in [\tau, T]}, \mathbb{Q}^T)$ and assume that under the T -forward probability measure, \mathbb{Q}^T , the Markovian processes S , R , and V follow the system of SDEs (53) with initial conditions $S(\tau) = s > 0$, $R(\tau) = r > 0$, and $V(\tau) = \nu > 0$. Let $c(\tau, s, r, \nu)$ denote the time- τ price of a European call option with underlying S , strike price $K > 0$, and maturity T , defined by*

$$c(\tau, s, r, \nu) = P(\tau, T, r) \mathbb{E}_{\mathbb{Q}^T} [(S(T) - K)_+ | \mathcal{F}_\tau].$$

where $P(\tau, T, r)$ is the zero-coupon bond price under the CIR++ short-rate model. Then, $c := c(\tau, s, r, \nu)$ satisfies the backward parabolic PDE

$$\begin{aligned} 0 &= \partial_\tau c + rs \partial_s c + (\kappa_r (\theta_r - r + \psi(\tau)) + \psi'(\tau)) \partial_r c + (\kappa_\nu (\theta_\nu - \nu)) \partial_\nu c \\ &\quad + \frac{1}{2} \left(\nu s^2 \partial_{ss} c + \sigma_r^2 (r - \psi(\tau)) \partial_{rr} c + \sigma_\nu^2 \nu \partial_{\nu\nu} c + 2\rho_1 \sigma_r s \sqrt{\nu(r - \psi(\tau))} \partial_{rs} c \right. \\ &\quad \left. + 2\rho_2 \sigma_\nu \nu s \partial_{s\nu} c + 2\rho_3 \sigma_r \sigma_\nu \sqrt{\nu(r - \psi(\tau))} \partial_{r\nu} c \right) - rc. \end{aligned} \quad (55)$$

with terminal condition $c(T, s) = (s - K)_+$.

Proof. The result follows by applying Itô's lemma and the martingale representation theorem, see Appendix B.1 and A respectively. Begin by considering arbitrary times $t \in [\tau, T]$ and recall that the time- t price of the European call option $c(t, S(t), R(t), V(t))$ is defined by

$$c(t, S(t), R(t), V(t)) = P(t, T, R(t)) \mathbb{E}_{\mathbb{Q}^T} [(S(T) - K)_+ | \mathcal{F}_t]. \quad (56)$$

Furthermore, define the functions g and u by

$$g(h, p) = \frac{h}{p}, \quad (57)$$

and

$$u(t, S(t), R(t), V(t)) := \mathbb{E}_{\mathbb{Q}^T} [(S(T) - K)_+ | \mathcal{F}_t]$$

respectively, where u is a \mathbb{Q}^T -martingale by construction. Then note that

$$\begin{aligned} g(c(t, S(t), R(t), V(t)), P(t, T, R(t))) &:= \frac{c(t, S(t), R(t), V(t))}{P(t, T, R(t))} \\ &= \mathbb{E}_{\mathbb{Q}^T} [(S(T) - K)_+ | \mathcal{F}_t] \\ &=: u(t, S(t), R(t), V(t)). \end{aligned}$$

Equivalently,

$$dg(c(t, S(t), R(t), V(t)), P(t, T, R(t))) = du(t, S(t), R(t), V(t)).$$

With $C := c(t, S(t), R(t), V(t))$ and $P := P(t, T, R(t))$, the total derivative of $g(C, P)$ is found by applying Itô's lemma on $g(c(t, S(t), R(t), V(t)), P(t, T, R(t)))$, which yields

$$\begin{aligned} dg(C, P) &= \partial_h g(C, P) dC + \partial_p g(C, P) dP + \frac{1}{2} \partial_{hh} g(C, P) d\langle C, C \rangle_t \\ &\quad + \frac{1}{2} \partial_{pp} g(C, P) d\langle P, P \rangle_t + \partial_{hp} g(C, P) d\langle C, P \rangle_t, \end{aligned}$$

where the partial derivatives are defined as $\partial_h = \frac{\partial}{\partial h}$, $\partial_p = \frac{\partial}{\partial p}$, and so on. The derivatives of $g(h, p) := \frac{h}{p}$ with respect to h , and p are

$$\partial_h g(h, p) = \frac{1}{p}, \quad \partial_p g(h, p) = -\frac{h}{p^2}, \quad \partial_{hh} g(h, p) = 0, \quad \partial_{hp} g(h, p) = -\frac{1}{p^2}, \quad \partial_{pp} g(h, p) = \frac{h}{p^3}.$$

Therefore, the total derivative of $g(C, P)$ is

$$dg(C, P) = \frac{1}{P} dC - \frac{C}{P^2} dP + \frac{C}{P^3} d\langle P, P \rangle_t - \frac{1}{P^2} d\langle C, P \rangle_t.$$

The dynamics of $P := P(t, T, R(t))$ under \mathbb{Q}^T are given by (54), that is,

$$\frac{dP}{P} = \left(R(t) + \sigma_r^2 (R(t) - \psi(t)) b^2(t, T) \right) dt - \sigma_r \sqrt{R(t) - \psi(t)} b(t, T) dW^{R, \mathbb{Q}}(t), \quad (58)$$

such that the total derivative of the quadratic variation of P is

$$d\langle P, P \rangle_t = \sigma_r^2 (R(t) - \psi(t)) b^2(t, T) P^2 dt. \quad (59)$$

In addition, by applying Itô's lemma on $C := c(t, S(t), R(t), V(t))$,

$$\begin{aligned} dC &= \left\{ \partial_t C + S(t) \left(R(t) - \rho_1 \sigma_r b(t, T) \sqrt{V(t)(R(t) - \psi(t))} \right) \partial_s C \right. \\ &\quad + \left(\kappa_r (\theta_r - R(t) + \psi(t)) + \psi'(t) - \sigma_r^2 (R(t) - \psi(t)) b^2(t, T) \right) \partial_r C \\ &\quad + \left(\kappa_\nu (\theta_\nu - V(t)) - \rho_3 \sigma_r \sigma_\nu b(t, T) \sqrt{V(t)(R(t) - \psi(t))} \right) \partial_\nu C \\ &\quad + \frac{1}{2} \left(V(t) S^2(t) \partial_{ss} C + \sigma_r^2 (R(t) - \psi(t)) \partial_{rr} C + \sigma_\nu^2 V(t) \partial_{\nu\nu} C + 2\rho_1 \sigma_r \sqrt{V(t)(R(t) - \psi(t))} S(t) \partial_{rs} C \right. \\ &\quad \left. + 2\rho_2 \sigma_\nu V(t) S(t) \partial_{s\nu} C + 2\rho_3 \sigma_r \sigma_\nu \sqrt{\nu(R(t) - \psi(t))} \partial_{r\nu} C \right\} dt + \sqrt{V(t)} S(t) \partial_s C dW^{S, \mathbb{Q}^T}(t) \\ &\quad + \sigma_r \sqrt{R(t) - \psi(t)} \partial_r C dW^{R, \mathbb{Q}^T}(t) + \sigma_\nu \sqrt{V(t)} \partial_\nu C dW^{V, \mathbb{Q}^T}(t), \end{aligned} \quad (60)$$

so that the derivative of the quadratic variation between C and P is

$$\begin{aligned} d\langle C, P \rangle_t &= -\sigma_r \sqrt{R(t) - \psi(t)} b(t, T) P \left(\rho_1 \sqrt{V(t)} S(t) \partial_s C + \sigma_r \sqrt{R(t) - \psi(t)} \partial_r C \right. \\ &\quad \left. + \rho_3 \sigma_\nu \sqrt{V(t)} \partial_\nu C \right) dt. \end{aligned} \quad (61)$$

Now recall that

$$dg(c(t, S(t), R(t), V(t)), P(t, T, R(t))) = du(t, S(t), R(t), V(t)).$$

Since u is a \mathbb{Q}^T -martingale, the drift in du must be zero as the martingale representation theorem, see Appendix A, puts into perspective. Roughly speaking, the drift of a stochastic process are all terms multiplied by dt . As a consequence, the sum of all terms multiplied by dt in (58), (59), (60), and (61) must be zero, that is,

$$\begin{aligned} 0 &= \partial_t C + S(t) \left(R(t) - \rho_1 \sigma_r \sqrt{V(t)(R(t) - \psi(t))} b(t, T) \right) \partial_s C \\ &\quad + \left(\kappa_r (\theta_r - R(t) + \psi(t)) + \psi'(t) - \sigma_r^2 (R(t) - \psi(t)) b^2(t, T) \right) \partial_r C \\ &\quad + \left(\kappa_\nu (\theta_\nu - V(t)) - \rho_3 \sigma_r \sigma_\nu \sqrt{V(t)(R(t) - \psi(t))} b(t, T) \right) \partial_\nu C \\ &\quad + \frac{1}{2} \left(V(t) S^2(t) \partial_{ss} C + \sigma_r^2 (R(t) - \psi(t)) \partial_{rr} C + \sigma_\nu^2 V(t) \partial_{\nu\nu} C + 2\rho_1 \sigma_r \sqrt{V(t)(R(t) - \psi(t))} S(t) \partial_{rs} C \right. \\ &\quad \left. + 2\rho_2 \sigma_\nu V(t) S(t) \partial_{s\nu} C + 2\rho_3 \sigma_r \sigma_\nu \sqrt{\nu(R(t) - \psi(t))} \partial_{r\nu} C \right) \\ &\quad - \left(R(t) + \sigma_r^2 (R(t) - \psi(t)) b^2(t, T) \right) C + \sigma_r^2 (R(t) - \psi(t)) b^2(t, T) C \\ &\quad + \sigma_r \sqrt{R(t) - \psi(t)} b(t, T) \left(\rho_1 \sqrt{V(t)} S(t) \partial_s C + \sigma_r \sqrt{R(t) - \psi(t)} b(t, T) \partial_r C + \rho_3 \sigma_\nu \sqrt{V(t)} \partial_\nu C \right). \end{aligned}$$

The expression above simplifies to

$$\begin{aligned} 0 &= \partial_t C + R(t) S(t) \partial_s C + [\kappa_r (\theta_r - R(t) + \psi(t)) + \psi'(t)] \partial_r C + \kappa_\nu (\theta_\nu - V(t)) \partial_\nu C \\ &\quad + \frac{1}{2} \left(V(t) S^2(t) \partial_{ss} C + \sigma_r^2 (R(t) - \psi(t)) \partial_{rr} C + \sigma_\nu^2 V(t) \partial_{\nu\nu} C + 2\rho_1 \sigma_r \sqrt{V(t)(R(t) - \psi(t))} S(t) \partial_{rs} C \right. \\ &\quad \left. + 2\rho_2 \sigma_\nu V(t) S(t) \partial_{s\nu} C + 2\rho_3 \sigma_r \sigma_\nu \sqrt{V(t)(R(t) - \psi(t))} \partial_{r\nu} C \right) - R(t) C, \end{aligned}$$

where $C := c(t, S(t), R(t), V(t))$. At $t = \tau$ and for $c := c(\tau, s, r, \nu)$, the PDE above therefore becomes

$$\begin{aligned} 0 &= \partial_\tau c + rs \partial_s c + (\kappa_r (\theta_r - r + \psi(\tau)) + \psi'(\tau)) \partial_r c + \kappa_\nu (\theta_\nu - \nu) \partial_\nu c \\ &\quad + \frac{1}{2} \left(\nu s^2 \partial_{ss} c + \sigma_r^2 (r - \psi(\tau)) \partial_{rr} c + \sigma_\nu^2 \nu \partial_{\nu\nu} c + 2\rho_1 \sigma_r s \sqrt{\nu(r - \psi(\tau))} \partial_{rs} c \right. \\ &\quad \left. + 2\rho_2 \sigma_\nu \nu s \partial_{s\nu} c + 2\rho_3 \sigma_r \sigma_\nu \sqrt{\nu(r - \psi(\tau))} \partial_{r\nu} c \right) - rc. \end{aligned}$$

and is subject to the terminal condition

$$c(T, s) = (s - K)_+,$$

which was to be proven. \square

The backward parabolic PDE (55) derived in theorem 4.2 provides the analytical foundation for pricing European options under a Heston-like model with the stochastic short rate following the CIR++ model. By utilizing Itô's lemma and the martingale representation theorem, we have transformed the original expectation-based pricing problem into a well-posed backward parabolic PDE. This formulation enables the application of *Physics Informed Neural Networks* (PINNs) for practical implementation. In the next chapters, we introduce numerical solvers to approximate the solution of PDE and compare it to a Fourier transform based, analytical solution.

5 Option Pricing with the Fast Fourier Transform

In previous sections, we have derived a formula to price contingent claims under the T -forward probability measure \mathbb{Q}^T , such as European swaptions and European options on risky assets. This has led to the derivation of the three-factor model under \mathbb{Q}^T (53). In this section, we consider our first pricing method developed by Carr and Madan (1999). The option pricing model in this chapter relies on the use of the characteristic function of the log-prices of the risky asset and on the Fast Fourier Transform (FFT).

5.1 Option Pricing using the Characteristic Function

Throughout this chapter, we consider European call option prices evaluated at the present time τ . Recall that the European call option is priced with

$$c(\tau, s, r, \nu) = P(\tau, T, r) \mathbb{E}_{\mathbb{Q}^T} [(S(T) - K)_+ | \mathcal{F}_\tau]$$

where $P(\tau, T, r)$ is the discounting numéraire from the initial time τ to the time of maturity T , S is the price process of the risky asset, $K > 0$ is the strike price, and $s, r, \nu > 0$ are real-valued constants. We define the quantities $X(T) := \log S(T)$, $x := \log s$, $Y(T) := \log \frac{S(T)}{s} = X(T) - x$, and $k := \log \frac{K}{s}$. Lastly, assume that for a random variable Z ,

$$d\mathbb{Q}^T(z) = q_Z(z) dz,$$

where $q_Z(z)$ is the probability density function for the random variable Z under \mathbb{Q}^T .

We now motivate the use of the Fourier transform on c with respect to k . Considering that the quantities s, r, ν are constants, the European call option is denoted by $c(\tau, k)$ in this chapter. This notation seeks to emphasize the dependence of the time- τ call price function c on k and is of convenient as we aim to take the Fourier transform of the function c with respect to k . Then, the European call option pricing formula becomes

$$\begin{aligned} c(\tau, k) &= sP(\tau, T, r) \mathbb{E}_{\mathbb{Q}^T} \left[\left(\frac{S(T)}{s} - \frac{K}{s} \right)_+ \mid \mathcal{F}_\tau \right] \\ &= sP(\tau, T, r) \mathbb{E}_{\mathbb{Q}^T} \left[(e^{Y(T)} - e^k)_+ \mid \mathcal{F}_\tau \right] \\ &= sP(\tau, T, r) \int_{-\infty}^{\infty} (e^y - e^k)_+ q_{Y_T}(y) dy \\ &= sP(\tau, T, r) \int_k^{\infty} (e^y - e^k) q_{Y_T}(y) dy, \end{aligned}$$

with $q_{Y_T}(y)$ being the probability density function of Y_T under the T -forward measure given the initial conditions s, r , and ν . Define the Fourier transform of c with respect to k as

$$\hat{c}(\tau, u) = \int_{-\infty}^{\infty} c(\tau, k) e^{iuk} dk,$$

and its inverse

$$c(\tau, k) = \frac{1}{2\pi} \int_{-\infty}^{\infty} \hat{c}(\tau, u) e^{-iuk} du,$$

where i is the imaginary number with $i^2 = -1$ and u arises from the Fourier transform. We also define the characteristic function of $Y(T)$ under \mathbb{Q}^T , given s, r and ν , as

$$\phi_{Y_T} := \mathbb{E}_{\mathbb{Q}^T} [e^{iuY(T)} \mid \mathcal{F}_\tau].$$

By applying the Fourier transform on c , we find

$$\begin{aligned}\hat{c}(\tau, u) &= sP(\tau, T, r) \int_{-\infty}^{\infty} e^{iuk} \int_k^{\infty} (e^y - e^k) q_{Y_T}(y) dy dk \\ &= sP(\tau, T, r) \int_{-\infty}^{\infty} q_{Y_T}(y) \int_{-\infty}^y (e^y - e^k) e^{iuk} dk dy \\ &= sP(\tau, T, r) \int_{-\infty}^{\infty} q_{Y_T}(y) \left(\frac{e^{(1+iu)y}}{iu} - \frac{e^{(1+iu)y}}{1+iu} \right) dy \\ &= sP(\tau, T, r) \frac{\phi_{Y_T}(u-i)}{-u^2 + iu},\end{aligned}$$

where Fubini's theorem was applied to alter the integration order. We observe that the Fourier transform, \hat{c} , is singular at $u = 0$ and consequently not L^1 -integrable. This is obviously an issue as inverting the Fourier transform \hat{c} is not possible anymore. To address this, we follow the approach proposed by Carr and Madan (1999), where the authors multiply c by the damping factor $e^{\alpha k}$. Concretely, define

$$c_{\alpha}(\tau, k) := e^{\alpha k} c(\tau, k).$$

Its Fourier transform is

$$\hat{c}_{\alpha}(\tau, u) = \int_{-\infty}^{\infty} c_{\alpha}(\tau, k) e^{iuk} dk,$$

and the inverse counterpart is defined as

$$c_{\alpha}(\tau, k) = \frac{1}{2\pi} \int_{-\infty}^{\infty} \hat{c}_{\alpha}(\tau, u) e^{-iuk} du.$$

We integrate and find that the Fourier transform of c_{α} , \hat{c}_{α} , is

$$\begin{aligned}\hat{c}_{\alpha}(\tau, u) &= \int_{-\infty}^{\infty} c_{\alpha}(\tau, k) e^{iuk} dk \\ &= sP(\tau, T, r) \frac{\phi_{Y_T}(u - (\alpha + 1)i)}{\alpha^2 + \alpha - u^2 + iu(2\alpha + 1)}.\end{aligned}$$

The option price at time τ is whence

$$\begin{aligned}c(\tau, k) &= \frac{e^{-\alpha k}}{2\pi} \int_{-\infty}^{\infty} \hat{c}_{\alpha}(\tau, u) e^{-iuk} du \\ &= sP(\tau, T, r) \frac{e^{-\alpha k}}{2\pi} \int_{-\infty}^{\infty} \frac{\phi_{Y_T}(u - (\alpha + 1)i)}{\alpha^2 + \alpha - u^2 + iu(2\alpha + 1)} e^{-iuk} du.\end{aligned}$$

We note that c is real, implying that it must be odd in its imaginary part and even in its real part. Therefore,

$$\begin{aligned}c(\tau, k) &= sP(\tau, T, r) \frac{e^{-\alpha k}}{2\pi} \int_{-\infty}^{\infty} \frac{\phi_{Y_T}(u - (\alpha + 1)i)}{\alpha^2 + \alpha - u^2 + iu(2\alpha + 1)} e^{-iuk} du \\ &= sP(\tau, T, r) \frac{e^{-\alpha k}}{\pi} \int_0^{\infty} \frac{\phi_{Y_T}(u - (\alpha + 1)i)}{\alpha^2 + \alpha - u^2 + iu(2\alpha + 1)} e^{-iuk} du,\end{aligned}\tag{62}$$

which illustrates the use of characteristic function in the context of option pricing. The pricing formula (62) is, if the characteristic function ϕ_{Y_T} exists, more convenient than the standard expectation representation of option prices since we are no longer required to run computationally expensive Monte Carlo simulations. Instead we price options by solving an integral by, for instance, Riemannian approximation. However, ϕ_{Y_T} remains unknown as of now and we need to find its expression. The next subsection is therefore dedicated to deriving ϕ_{Y_T} .

5.2 Derivation of the Characteristic Function of $Y(T)$

As shown previously, pricing options at time τ can be done through the characteristic function ϕ_{Y_T} . However, since the characteristic function of neither $X(T)$ nor $Y(T)$ are known, the Fourier

pricing formula (62) is not of much value to us as of now. We therefore begin by observing that

$$\phi_{Y_T}(u) := \mathbb{E}_{\mathbb{Q}^T}[e^{iuY(T)} \mid \mathcal{F}_\tau] = e^{-iux} \mathbb{E}_{\mathbb{Q}^T}[e^{iuX(T)} \mid \mathcal{F}_\tau] = e^{-iux} \phi_{X_T}(u), \quad (63)$$

where ϕ_{X_T} is the characteristic function of $X(T) = \log Y(T)$. We then seek to derive an expression for the characteristic function of $X(T)$, and subsequently $\phi_{Y_T}(u)$, the latter of which is needed in the Fourier transform formula (62).

As the derivation of $\phi_{Y_T}(u)$ requires the formalization of infinitesimal generators and particularly of the affine, infinitesimal generator, as well as of the affine transform formula, we begin by introducing the necessary theory.

Definition and Characterization of Affine Generators

Definition 5.1 (Infinitesimal generators, see Evans (2013, Chapter 6.1.3)). Let $\mathbf{Z} = \{\mathbf{Z}(t)\}_{t \in [\tau, T]} \in \mathbb{R}^n$ be a random process residing in the probability space $(\Omega, \mathcal{F}, \{\mathcal{F}_t\}_{t \in [\tau, T]}, \mathbb{Q}^T)$ with $\mathbf{Z}(\tau) = \mathbf{z} = (z_1, \dots, z_n)^\top$ a known constant vector. Assume \mathbf{Z} follows the n -dimensional SDE

$$d\mathbf{Z}(t) = \mathbf{b}(t, \mathbf{Z}) dt + \mathbf{B}(t, \mathbf{Z}) d\mathbf{W}^{\mathbb{Q}^T}(t),$$

where $\mathbf{W}^{\mathbb{Q}^T}$ is the m -dimensional Brownian motion under \mathbb{Q}^T , and $\mathbf{b} \in \mathbb{R}^n$ and $\mathbf{B} \in \mathbb{R}^{n \times m}$ denote the drift and diffusion terms of \mathbf{Z} , both assumed to be Lipschitz continuous and to have a linearly bounded growth. Furthermore, let $u \in C^{2,1}(\mathbb{R}^n \times [\tau, T])$ be a twice-differentiable function with respect to \mathbf{Z} and once differentiable in time with

$$du(t, \mathbf{Z}(t)) = \partial_t u(t, \mathbf{Z}(t)) dt + \sum_{j=1}^n \partial_{z_j} u(t, \mathbf{Z}(t)) d\mathbf{Z}^{(j)}(t) + \frac{1}{2} \sum_{j,k=1}^n \partial_{z_j z_k} u(t, \mathbf{Z}(t)) \sum_{\ell=1}^m \mathbf{B}_{j\ell} \mathbf{B}_{k\ell} dt$$

resulting from Itô's lemma. Then, the generator associated with the process \mathbf{Z} is the partial differential operator

$$\mathcal{G}u(t, \mathbf{Z}(t)) := \sum_{j=1}^n b_i \partial_{z_j} u(t, \mathbf{Z}(t)) + \frac{1}{2} \sum_{j,k=1}^n \mathbf{A}_{jk} \partial_{z_j z_k} u(t, \mathbf{Z}(t))$$

where

$$\mathbf{A}_{jk} = \sum_{\ell=1}^m \mathbf{B}_{j\ell} \mathbf{B}_{k\ell}.$$

Remark 5.2. The above definition of the infinitesimal generator is usually derived in the framework of strongly continuous semi-groups, where one shows that the generator is the derivative at zero of the associated semi-group of operators. As the required functional-analytic semi-group theory lies beyond the scope of this work, we adopt this definition without further justification.

Definition 5.3 (Backward Kolmogorov equation). Let $\mathbf{Z} = \{\mathbf{Z}(t)\}_{t \in [\tau, T]} \in \mathbb{R}^n$ be a random process residing in the probability space $(\Omega, \mathcal{F}, \{\mathcal{F}_t\}_{t \in [\tau, T]}, \mathbb{Q}^T)$ and following the SDE

$$d\mathbf{Z}(t) = \mathbf{b}(t, \mathbf{Z}) dt + \mathbf{B}(t, \mathbf{Z}) d\mathbf{W}^{\mathbb{Q}^T}(t),$$

where $\mathbf{W}^{\mathbb{Q}^T}$ is the m -dimensional Brownian motion under \mathbb{Q}^T , and $\mathbf{b} \in \mathbb{R}^n$ and $\mathbf{B} \in \mathbb{R}^{n \times m}$ denote the drift and diffusion terms of \mathbf{Z} , both assumed to be Lipschitz continuous and to have a linearly bounded growth. Furthermore, let $\phi : \mathbb{R}^n \rightarrow \mathbb{R}$ and $f : \mathbb{R}^n \rightarrow \mathbb{R}$ be continuous functions with polynomial growth. Then, for $u \in C^{2,1}(\mathbb{R})$, the Backward Kolmogorov equation is defined as

$$\begin{aligned} \partial_\tau u(t, \mathbf{z}) + \mathcal{G}u(t, \mathbf{z}) &= f(t, \mathbf{z}), \\ u(T, \mathbf{z}) &= h(\mathbf{z}), \end{aligned}$$

where \mathcal{G} is the infinitesimal generator of the process \mathbf{Z} .

Remark 5.4. We note that the backward Kolmogorov is the deterministic PDE that solves the expectation found in the Feynman-Kac theorem (see Appendix B.2).

Definition 5.5 (Affine infinitesimal generators). Let $\mathbf{Z} \in \mathbb{R}^n$ be an n -dimensional Itô process with $E \subseteq \mathbb{R}^n$ being its state space and denote its infinitesimal generator by \mathcal{G} . Furthermore, define the functions $F : \mathbb{C}^d \rightarrow \mathbb{C}$ and $R : \mathbb{C}^n \rightarrow \mathbb{C}^n$, where $R(\mathbf{v}) = (R_1(\mathbf{v}), \dots, R_d(\mathbf{v}))^\top$. The operator \mathcal{G} is called affine if there exist complex-valued functions F and R such that

$$\mathcal{G}e^{\mathbf{v}^\top \mathbf{z}} = (F(\mathbf{v}) + R(\mathbf{v})^\top \mathbf{z})e^{\mathbf{v}^\top \mathbf{z}}$$

holds for all $\mathbf{z} \in E$ and $\mathbf{v} \in \mathbb{C}^n$. In this case, we call \mathbf{Z} an affine diffusion.

Theorem 5.6 (Affine Transform Formula, see Filipović (2009, Theorem 10.4)). Assume $\mathbf{Z} \in \mathbb{R}^n$ is an affine diffusion. For $\mathbf{v} \in \mathbb{C}^n$ and $\tau \leq t < T$, let $\Phi(T-t) := \Phi(T-t, \mathbf{v})$ and $\Psi(T-t) := (\Psi_1(T-t), \dots, \Psi_n(T-t))^\top = \Psi(T-t, \mathbf{v})$ be functions that solve the system of Riccati equations

$$\begin{aligned}\Phi'(T-t) &= F(\Psi(T-t)), \quad \Phi(0) = 0 \\ \Psi'(T-t) &= R(\Psi(T-t)), \quad \Psi(0) = \mathbf{v}.\end{aligned}$$

If

$$\mathbb{E}_{\mathbb{Q}^T} \left[\int_\tau^T e^{2\Re(\Phi(t)) + 2\Re(\Psi(t)^\top \mathbf{z}(t))} \mathbf{z}(t) \Psi(T-t)^\top \mathbf{B}(\mathbf{Z}, t) \overline{\Psi(T-t)} dt \right] < \infty, \quad (64)$$

where $\mathbf{B}(\mathbf{Z}, \cdot) \in \mathbb{R}^{n \times m}$ denotes the diffusion of \mathbf{Z} for an m -dimensional Brownian motion, then the affine transform formula (ATF) holds, for $t \leq T$,

$$\mathbb{E}_{\mathbb{Q}^T} \left[e^{\mathbf{v}^\top \mathbf{z}(T)} \mid \mathcal{F}_t \right] = e^{\Phi(T-t, \mathbf{v}) + \Psi(T-t, \mathbf{v})^\top \mathbf{z}(t)}.$$

Proof. We refer the interested reader to Filipović (2009, Theorem 10.4) for the proof. \square

Derivation of the Characteristic Function using Affine Generators

We now apply definitions 5.1, 5.3, and 5.5, as well as theorem 5.6, to derive an expression for the characteristic function for the log-price of the risky asset $\phi_{X_T}(u)$ and consequently $\phi_{Y_T}(u)$ at time T . This allows us to characterize ϕ_{X_T} with

$$\phi_{X_T}(u) = \mathbb{E}_{\mathbb{Q}^T} [e^{iuX(T)} \mid \mathcal{F}_\tau] = e^{\Phi(T-\tau, 0) + \Psi_1(T-\tau, iu)x + \Psi_2(T-\tau, 0)r + \Psi_3(T-\tau, 0)\nu},$$

where the functions Φ , Ψ_1 , Ψ_2 and Ψ_3 solve the set of Riccati ODEs in theorem 5.6. We therefore define the random process vector $\mathbf{Z} = (X, R, V)^\top$, where $X := \log S$, and investigate its affinity. As we will see, \mathbf{Z} is not an affine diffusion, but is transformed into one by letting the instantaneous correlations between the Brownian motions of the stochastic short rate with the risky asset process and the variance process respectively, that is ρ_1 and ρ_3 , to be zero. Then, the task of deriving an expression for the characteristic function translates to solving the aforementioned Riccati set ODEs. Let us begin by specifying the dynamics of the log price process $X := \log S$ in the form of lemma 5.7.

Lemma 5.7. Let dynamics of the risky asset process $S = \{S(t)\}_{t \in [\tau, T]}$ be described by the geometric Brownian motion

$$dS(t) = S(t) \left(R(t) - \rho_1 \sigma_r \sqrt{V(t)(R(t) - \psi(t))} b(t, T) \right) dt + \sqrt{V(t)} S(t) dW^{S, \mathbb{Q}^T}(t), \quad S(\tau) = s.$$

Then, the dynamics of $X(t) = \log S(t)$ are given by

$$dX(t) = \left(R(t) - \frac{1}{2} V(t) - \rho_1 \sigma_r \sqrt{V(t)(R(t) - \psi(t))} b(t, T) \right) dt + \sqrt{V(t)} dW^{S, \mathbb{Q}^T}(t), \quad X(\tau) = x.$$

Proof. The proof is done by applying Itô's lemma, see Appendix B.1, on $X = \log S$. Concretely, define the function

$$u(s) = \log s.$$

Then,

$$du(S(t)) = \partial_s u dS(t) + \partial_{ss} u dt.$$

With $\partial_s u(s) = \frac{1}{s}$ and $\partial_{ss} u(s) = -\frac{1}{s^2}$, the total derivative for $du(S(t))$ is

$$du(S(t)) = \left(R(t) - \frac{1}{2}V(t) - \rho_1 \sigma_r \sqrt{V(t)(R(t) - \psi(t))} b(t, T) \right) dt + \sqrt{V(t)} dW^{S, \mathbb{Q}^T}(t).$$

Substituting $X(t) = u(S(t))$ into the SDE above, one has

$$dX(t) = \left(R(t) - \frac{1}{2}V(t) - \rho_1 \sigma_r \sqrt{V(t)(R(t) - \psi(t))} b(t, T) \right) dt + \sqrt{V(t)} dW^{S, \mathbb{Q}^T}(t),$$

which was to be proved. \square

Corollary 5.8. Let $\mathbf{Z} = (X, R, V)$ be a random process vector, with the random processes X , R , and V following the system of SDEs

$$\begin{cases} dX(t) = \left(R(t) - \frac{1}{2}V(t) - \rho_1 \sigma_r b(t, T) \sqrt{V(t)(R(t) - \psi(t))} \right) dt + \sqrt{V(t)} dW^{S, \mathbb{Q}^T}(t), \\ dR(t) = \left(\kappa_r(\theta_r - R(t) + \psi(t)) + \psi'(t) - \sigma_r^2(R(t) - \psi(t))b^2(t, T) \right) dt + \sigma_r \sqrt{R(t) - \psi(t)} dW^{R, \mathbb{Q}^T}(t), \\ dV(t) = \left(\kappa_\nu(\theta_\nu - V(t)) - \rho_3 \sigma_r \sigma_\nu b(t, T) \sqrt{V(t)(R(t) - \psi(t))} \right) dt + \sigma_\nu \sqrt{V(t)} dW^{V, \mathbb{Q}^T}(t), \end{cases}$$

where $X(\tau) = x$, $R(\tau) = r$, and $V(\tau) = \nu$ are strictly positive, real-valued constants such that $\mathbf{z} = (x, r, \nu)^\top$ is constant. Moreover, let $u := u(t, x, r, \nu)$ be a twice differentiable function in its state variables and once differentiable in time. Then, the infinitesimal generator of the process \mathbf{Z} at time τ , denoted by the operator \mathcal{G} , is

$$\begin{aligned} \mathcal{G}u = & \left(r - \frac{1}{2}\nu - \rho_1 \sigma_r b(\tau, T) \sqrt{\nu(r - \psi(\tau))} \right) \partial_x u \\ & + \left(\kappa_r(\theta_r - r + \psi(\tau)) + \psi'(\tau) - \sigma_r^2(r - \psi(\tau))b^2(\tau, T) \right) \partial_r u \\ & + \left(\kappa_\nu(\theta_\nu - \nu) - \rho_3 \sigma_r \sigma_\nu b(\tau, T) \sqrt{\nu(r - \psi(\tau))} \right) \partial_\nu u \\ & + \frac{1}{2} \left[\nu \partial_x u + \sigma_r^2(r - \psi(\tau)) \partial_{rr} u + \sigma_\nu^2 \nu \partial_{\nu\nu} u + 2\rho_1 \sigma_r \sqrt{\nu(r - \psi(\tau))} \partial_{rx} u \right. \\ & \left. + 2\rho_2 \sigma_\nu \nu \partial_{x\nu} u + 2\rho_3 \sigma_r \sigma_\nu \sqrt{\nu(r - \psi(\tau))} \partial_{r\nu} u \right]. \end{aligned} \quad (65)$$

Proof. The proof for the result presented above is straightforward and obtained by applying the definition of the infinitesimal generator, see definition 5.1. \square

Proposition 5.9. The diffusion process $\mathbf{Z} = (X, R, V)$, with the infinitesimal generator \mathcal{G} from corollary 5.8 is affine if and only if $\rho_1 = \rho_3 = 0$. Moreover, the functions $F(\mathbf{v})$ and $R(\mathbf{v}) = (R_1(\mathbf{v}), R_2(\mathbf{v}), R_3(\mathbf{v}))^\top$, where $\mathbf{v} = (v_1, v_2, v_3)^\top \in \mathbb{C}^3$, are

$$\begin{cases} F(\mathbf{v}) = -\frac{1}{2}\sigma_r^2 \psi(\tau) v_2^2 + [\kappa_r(\theta_r + \psi(\tau)) + \psi'(\tau) + \sigma_r^2 b(\tau, T) \psi(\tau)] v_2 + \kappa_\nu \theta_\nu v_3, \\ R_1(\mathbf{v}) = 0, \\ R_2(\mathbf{v}) = v_1 + \frac{1}{2}\sigma_r^2 v_2^2 - (\kappa_r + \sigma_r^2 b(\tau, T)) v_2 \\ R_3(\mathbf{v}) = \frac{1}{2}(v_1^2 - v_1 + \sigma_\nu^2 v_3^2) - \kappa_\nu v_3 + \rho_2 \sigma_\nu v_1 v_3 \end{cases} \quad (66)$$

Proof. We begin by finding expressions for the functions F and R that characterize an affine generator, see definition 5.5. Let $\mathbf{z} = (x, r, \nu)^\top$ and $\mathbf{v} = (v_1, v_2, v_3)^\top \in \mathbb{C}^3$. For $\rho_1, \rho_3 \neq 0$,

$$\mathcal{G}e^{\mathbf{v}^\top \mathbf{z}} = \left(F(\mathbf{v}) + R_1(\mathbf{v})x + R_2(\mathbf{v})r + R_3(\mathbf{v})\nu + R_4(\mathbf{v})\sqrt{\nu(r - \psi(\tau))} \right) e^{\mathbf{v}^\top \mathbf{z}},$$

where

$$\begin{cases} F(\mathbf{v}) = -\frac{1}{2}\sigma_r^2\psi(t)v_2^2 + [\kappa_r(\theta_r + \psi(t)) + \psi'(t) + \sigma_r^2b(\tau, T)\psi(t)]v_2 + \kappa_\nu\theta_\nu v_3, \\ R_1(\mathbf{v}) = 0, \\ R_2(\mathbf{v}) = v_1 + \frac{1}{2}\sigma_r^2v_2^2 - (\kappa_r + \sigma_r^2b(\tau, T))v_2 \\ R_3(\mathbf{v}) = \frac{1}{2}(v_1^2 - v_1 + \sigma_\nu^2v_3^2) - \kappa_\nu v_3 + \rho_2\sigma_\nu v_1 v_3 \\ R_4(\mathbf{v}) = \rho_1\sigma_r(v_2 - b(\tau, T))v_1 + \rho_3\sigma_r\sigma_\nu(v_2 - b(\tau, T))v_3. \end{cases}$$

For $R_4(\mathbf{v}) \neq 0$, one notes that the generator \mathcal{G} is not affine in view of definition 5.5. However, with $\rho_1 = \rho_3 = 0$, R_4 becomes zero and the generator is now affine.

On the other hand, one has $\sigma_r, \sigma_\nu > 0$ and $b(\tau, T) \in \mathbb{R}$, the latter of which implies that $b(\tau, T) \neq v_2$ and $b(\tau, T) \neq v_3$ since $\mathbf{v} \in \mathbb{C}^3$. Therefore, setting $R_4(\mathbf{v}) = 0$ directly implies that $\rho_1 = \rho_3 = 0$. Hence, the generator is affine if and only if $\rho_1 = \rho_3 = 0$. \square

Remark 5.10. *We observe that with $\rho_1 = \rho_3 = 0$, our three-factor model under the T -forward measure, \mathbb{Q}^T , now reads as*

$$\begin{cases} dX(t) = \left(R(t) - \frac{1}{2}V(t) \right) dt + \sqrt{V(t)} dW^{S, \mathbb{Q}^T}(t), \\ dR(t) = \left(\kappa_r(\theta_r - R(t) + \psi(t)) + \psi'(t) - \sigma_r^2(R(t) - \psi(t))b^2(t, T) \right) dt + \sigma_r\sqrt{R(t) - \psi(t)} dW^{R, \mathbb{Q}^T}(t), \\ dV(t) = \kappa_\nu(\theta_\nu - V(t)) dt + \sigma_\nu\sqrt{V(t)} dW^{V, \mathbb{Q}^T}(t), \end{cases} \quad (67)$$

where $X(\tau) = x$, $R(\tau) = r$, and $V(\tau) = \nu$ are real constants. Moreover, for a function u , twice differentiable in (x, r, ν) and once differentiable in time, the affine generator now reads as

$$\begin{aligned} \mathcal{G}u &= \left(r - \frac{1}{2}\nu \right) \partial_x u + \left(\kappa_r(\theta_r - r + \psi(\tau)) + \psi'(\tau) - \sigma_r^2(r - \psi(\tau))b^2(\tau, T) \right) \partial_r u + \left(\kappa_\nu(\theta_\nu - \nu) \right) \partial_\nu u \\ &\quad + \frac{1}{2} \left[\nu \partial_x u + \sigma_r^2(r - \psi(\tau)) \partial_{rr} u + \sigma_\nu^2 \partial_{\nu\nu} u + 2\rho_1\sigma_r\sqrt{\nu(r - \psi(\tau))} \partial_{rx} u + 2\rho_2\sigma_\nu\nu \partial_{x\nu} u \right] \end{aligned} \quad (68)$$

Proposition 5.11 (The characteristic function of the log-prices under the T -forward measure). *Let $\tau \leq T$, $X(T) = \log S(T)$, and $\rho_1 = \rho_3 = 0$. Moreover, assume that $X(\tau) = x$, $R(\tau) = r$ and $V(\tau) = \nu$ are real constants. Then, the characteristic function of $X(T)$ is*

$$\phi_{X_T}(u) = \mathbb{E}_{\mathbb{Q}^T} \left[e^{iuX(T)} \mid \mathcal{F}_\tau \right] = e^{\Phi(T - \tau, \mathbf{v}) + \Psi(T - \tau, \mathbf{v})^\top \mathbf{z}},$$

where $\mathbf{z} = (x, r, \nu)^\top$, $\mathbf{v} = (iu, 0, 0)^\top$, and the functions $\Phi(T - \tau) := \Phi(T - \tau, \mathbf{v})$ and $\Psi(T - \tau, \mathbf{v}) = (\Psi_1(T - \tau, iu), \Psi_2(T - \tau, 0), \Psi_3(T - \tau, 0))^\top$ solve the Riccati set of ODEs

$$\begin{cases} \Phi'(T - \tau) = \frac{1}{2}\sigma_r^2\psi(\tau)\Psi_2^2 - (\kappa_r(\theta_r + \psi(\tau)) + \psi'(\tau) + \sigma_r^2b^2(\tau, T)\psi(\tau))\Psi_2 - \kappa_\nu\theta_\nu\Psi_3, & \Phi(0) = 0 \\ \Psi'_1(T - \tau, iu) = 0, & \Psi_1(0) = iu \\ \Psi'_2(T - \tau, 0) = -\Psi_1 - \frac{1}{2}\sigma_r^2\Psi_2^2 + (\kappa_r + \sigma_r^2b(\tau, T))\Psi_2, & \Psi_2(0) = 0 \\ \Psi'_3(T - \tau, 0) = -\frac{1}{2}(\Psi_1^2 - \Psi_1 + \sigma_\nu^2\Psi_2^2) - \rho_2\sigma_\nu\Psi_1\Psi_3 + \kappa_\nu\Psi_3, & \Psi_3(0) = 0, \end{cases}$$

where $\frac{d}{d\tau}\Phi(\cdot) := \Phi'(\cdot)$, $\frac{d}{d\tau}\Psi(\cdot) := \Psi'(\cdot)$, and $\Psi_1 := \Psi_1(T - \tau, iu)$, $\Psi_2 := \Psi_2(T - \tau, 0)$ and $\Psi_3 := \Psi_3(T - \tau, 0)$.

Proof. Recall that for $\rho_1 = \rho_3 = 0$, the generator \mathcal{G} (68) is affine as seen in proposition 5.9. Define the function

$$M(\tau, \mathbf{z}) := \mathbb{E}_{\mathbb{Q}^T}[e^{\mathbf{v}^\top \mathbf{Z}(T)} \mid \mathcal{F}_\tau] = \mathbb{E}_{\mathbb{Q}^T}[e^{iuX(T)} \mid \mathcal{F}_\tau] := \phi_{X_T}(u),$$

subject to the terminal condition

$$M(T, \mathbf{Z}(T)) = e^{\mathbf{v}^\top \mathbf{Z}(T)}.$$

Applying the Feynman-Kac theorem on $M := M(\tau, \mathbf{z})$, one finds the Kolmogorov backward equation

$$\partial_\tau M + \mathcal{G}M = 0,$$

subject to the terminal condition seen above. As $\rho_1 = \rho_3 = 0$ by assumption, \mathcal{G} is an affine generator by proposition 5.9. Therefore, $M := M(\tau, \mathbf{z})$ has the solution

$$M(\tau, \mathbf{z}) = e^{\Phi(T-\tau, \mathbf{v}) + \Psi(T-\tau, \mathbf{v})^\top \mathbf{z}},$$

by theorem 5.6. Substituting $M(\tau, \mathbf{z}) = \phi_{X_T}(u)$, one finds

$$\phi_{X_T}(u) = e^{\Phi(T-\tau, iu, 0) + \Psi(T-\tau, iu, 0)^\top \mathbf{z}},$$

where the functions $\Phi(T-\tau) := \Phi(T-\tau, \mathbf{v})$ and $\Psi(T-\tau) := (\Psi_1(T-\tau, v_1), \Psi_2(T-\tau, v_2), \Psi_3(T-\tau, v_3))^\top$ are found by solving the Riccati set of ODEs

$$\begin{cases} \Phi'(T-\tau) = -F(\Phi(T-\tau)), & \Phi(0) = 0, \\ \Psi'(T-\tau) = -R(\Psi(T-\tau)), & \Psi(0) = \mathbf{v}, \end{cases}$$

where the functions F and R are as in (66). Substituting for F and R gives

$$\begin{cases} \Phi'(T-\tau) = \frac{1}{2}\sigma_r^2\psi(\tau)\Psi_2^2 - (\kappa_r(\theta_r + \psi(\tau)) + \psi'(\tau) + \sigma_r^2\psi(t)b(\tau, T))\Psi_2 - \kappa_\nu\theta_\nu\Psi_3, & \Phi(0) = 0 \\ \Psi'_1(T-\tau) = 0, & \Psi_1(0) = iu \\ \Psi'_2(T-\tau) = -\Psi_1 - \frac{1}{2}\sigma_r^2\Psi_2^2 + (\kappa_r + \sigma_r^2b(\tau, T))\Psi_2, & \Psi_2(0) = 0 \\ \Psi'_3(T-\tau) = -\frac{1}{2}(\Psi_1^2 - \Psi_1 + \sigma_\nu^2\Psi_2^2) - \rho_2\sigma_\nu\Psi_1\Psi_3 + \kappa_\nu\Psi_3, & \Psi_3(0) = 0. \end{cases}$$

□

We note that in proposition 5.11, we presented the set of Riccati ODEs without ever solving them. As it turns out, only two of the four have a closed-form solution. The solutions of the functions Ψ_1 and Ψ_3 are

$$\Psi_1(T-\tau) = iu,$$

and

$$\Psi_2(T-\tau) = \frac{\beta-d}{\sigma_\nu^2} \frac{1-e^{-(T-\tau)d}}{1-ge^{-(T-\tau)d}},$$

where

$$\begin{aligned} \beta &= \kappa_\nu - iu\rho_2\sigma_\nu, \\ d &= \sqrt{\beta_\nu^2 - 2\sigma_\nu^2(u^2 - iu)}, \\ g &= \frac{\beta-d}{\beta+d}. \end{aligned}$$

The function Ψ_2 can be found in Heston (1993). The remaining two functions, Φ and Ψ_2 do not have a closed-form solution due to the $b(t, T)$ terms making the ODEs time-inhomogeneous. However, the ODEs for Φ and Ψ_2 are well-behaved and are solved numerically using the Runge-Kutta 4-5 method.

Corollary 5.12 (The characteristic function of $Y(T)$ under the T -forward measure). *The characteristic function of $Y(T) = X(T) - x$ is*

$$\phi_{Y_T}(u) = \mathbb{E}_{\mathbb{Q}^T}[e^{iuY(T)} \mid \mathcal{F}_\tau] = e^{\Phi(T-\tau, \mathbf{v}) + \Psi_2(T-\tau, 0)r + \Psi_3(T-\tau, 0)\nu},$$

where $\mathbf{v} = (iu, 0, 0)^\top$.

Proof. By proposition 5.11, the characteristic function of $X(T) = \log S(T)$ is

$$\begin{aligned}\phi_{X_T}(u) &= e^{\Phi(T-\tau, \mathbf{v}) + \Psi(T-\tau, \mathbf{v})^\top \mathbf{z}} \\ &= e^{\Phi(T-\tau, \mathbf{v}) + \Psi_1(T-\tau, iu)x + \Psi_2(T-\tau, 0)r + \Psi_3(T-\tau, 0)\nu}.\end{aligned}$$

As seen in (63),

$$\begin{aligned}\phi_{Y_T}(u) &= e^{-iux}\phi_{X_T}(u) \\ &= e^{-iux + \Phi(T-\tau, \mathbf{v}) + \Psi_1(T-\tau, iu)x + \Psi_2(T-\tau, 0)r + \Psi_3(T-\tau, 0)\nu}\end{aligned}\tag{69}$$

Moreover, as

$$\Psi_1(T-\tau, iu) = iu,$$

the terms $-iux$ and $\Psi_1(T-\tau, iu)x$ in (69) cancel out, leaving

$$\phi_{Y_T}(u) = e^{\Phi(T-\tau, \mathbf{v}) + \Psi_2(T-\tau, 0)r + \Psi_3(T-\tau, 0)\nu}$$

as the expression for the characteristic function for Y_T . \square

Thus, we have derived an expression for the characteristic function of $Y(T)$. This result now allows us to apply the Fourier transform pricing formula (62).

5.3 From Characteristic Functions to the Fast Fourier Transform

A minor issue with (62) is that if we were to partition the real line into N pieces to solve the integral and also evaluate the call option price for N different logarithmic strikes k_m , for $m = 1, \dots, N$, we would end up with a runtime of $\mathcal{O}(N^2)$, without taking into mind the runtime complexity of numerically solving the ODEs Ψ_1 , and Φ . The entire option pricing process can therefore take an infeasible amount of time to price options. As computational speed is crucial in finance, we need to find a faster way to price options. Carr and Madan (1999) show that it is possible to price European call options with the Fast Fourier Transform (FFT), reducing the runtime complexity to $\mathcal{O}(N \log N)$. Using the characteristic function for $Y(T)$ given the initial conditions s , r , and ν for the set of SDEs (67), we now derive the FFT European call option pricing formula.

The FFT, first introduced by Cooley and Tukey (1965), is an efficient algorithm for computing the sum

$$w(m) = \sum_{n=1}^N e^{-i\frac{2\pi}{N}(n-1)(m-1)} f(n) \quad \text{for } m = 1, \dots, N,\tag{70}$$

where N is typically a power of 2. We now present a way to integrate (62) using the FFT.

Recall the time- τ European call option pricing formula (62), that is,

$$c(\tau, k) = \frac{e^{-\alpha k}}{\pi} \int_0^\infty \hat{c}_\alpha(\tau, u) e^{-iuk} du,\tag{71}$$

where

$$\hat{c}_\alpha(\tau, u) = sP(\tau, T, r) \frac{\phi_{Y_T}(u - (\alpha + 1)i)}{\alpha^2 + \alpha - u^2 + iu(2\alpha + 1)},$$

and ϕ_{Y_T} is the characteristic function of $Y(T)$ derived in corollary 5.12. Let $\beta > 0$ be some large cutoff for the integral in the expression for c . Then,

$$c(\tau, k) \approx \frac{e^{-\alpha k}}{\pi} \int_0^\beta \hat{c}_\alpha(\tau, u) e^{-iuk} du.\tag{72}$$

Furthermore, partition the interval $[0, \beta)$ into N equidistant points such that

$$u_n = \eta(n - 1), \quad \text{for } n = 1, \dots, N,$$

so that the upper integration limit $\beta = \eta N$. Since the grid of points u_1, \dots, u_N is equidistant, $\Delta u = u_n - u_{n-1} = \eta$ for any $n = 1, \dots, N$. Approximating (72) with Riemann sums,

$$c(\tau, k) \approx \frac{e^{-\alpha k}}{\pi} \sum_{n=1}^N e^{iu_n k} \hat{c}_\alpha(\tau, u_n) \Delta u = \frac{e^{-\alpha k}}{\pi} \sum_{n=1}^N e^{iu_n k} \hat{c}_\alpha(\tau, u_n) \eta. \quad (73)$$

We also introduce the symmetric grid of k around 0 on the interval $[-\varepsilon, \varepsilon]$ with

$$k_m = -\varepsilon + \lambda(m - 1) \quad \text{for } m = 1, \dots, N. \quad (74)$$

The interval $[-\varepsilon, \varepsilon]$, inside which k_m is defined, is determined by

$$\varepsilon = \frac{\lambda N}{2}. \quad (75)$$

Inserting (74) into (73),

$$\begin{aligned} c(\tau, k_m) &\approx \frac{e^{-\alpha k_m}}{\pi} \sum_{n=1}^N e^{-iu_n(-\varepsilon+\lambda(m+1))} \hat{c}_\alpha(\tau, u_n) \eta \\ &= \frac{e^{-\alpha k_m}}{\pi} \sum_{n=1}^N e^{-i\eta\lambda(n-1)(m-1)} e^{iu_n\varepsilon} \hat{c}_\alpha(\tau, u_n) \eta, \end{aligned}$$

for $m = 1, \dots, N$. To apply the FFT on the formula above, we note from (70) that

$$\lambda\eta = \frac{2\pi}{N}. \quad (76)$$

We see that due to this tradeoff, whenever we want a finer grid size for u_n , λ needs to increase, making the grid for the log-strikes k_m coarser such that only few strikes lie in the desired region near the stock price. Carr and Madan (1999) therefore incorporate Simpson's rule weightings into the summation. Then, we may write our call price as

$$c(\tau, k_m) = \frac{e^{-\alpha k_m}}{\pi} \sum_{n=1}^N e^{-i\frac{2\pi}{N}(n-1)(m-1)} e^{iu_n\varepsilon} \hat{c}_\alpha(\tau, u_n) \frac{\eta}{3} [3 + (-1)^n - \delta_{n-1}],$$

where δ_{n-1} is the Kronecker delta function

$$\delta_{n-1} = \begin{cases} 1, & \text{if } n - 1 = 0, \\ 0, & \text{otherwise.} \end{cases}$$

In view of (70), we see that we must have

$$f(n) = e^{iu_n\varepsilon} \hat{c}_\alpha(\tau, u_n) \frac{\eta}{3} [3 + (-1)^n - \delta_{n-1}], \quad (77)$$

to apply the FFT algorithm. Thus, the time- τ European call option maturing at time T is priced with

$$c(\tau, k_m) = \frac{e^{-\alpha k_m}}{\pi} \sum_{n=1}^N e^{-i\frac{2\pi}{N}(n-1)(m-1)} f(n), \quad (78)$$

where $f(n)$ is described in (77), the Fourier transform of the damped option price, \hat{c} , is

$$\hat{c}_\alpha(\tau, u) = sP(\tau, T, r) \frac{\phi_{Y_T}(u - (\alpha + 1)i)}{\alpha^2 + \alpha - u^2 + iu(2\alpha + 1)},$$

and the characteristic function for $Y(T)$, ϕ_{Y_T} , is as in corollary 5.12. (78) is solved numerically by means of applying the FFT algorithm developed by Cooley and Tukey (1965).

This concludes this chapter, where we have seen that the Fourier transform enables us to price European options with the characteristic function and the Fast Fourier transform.

6 Physics Informed Neural Networks

In the absence of a closed-form solution to the deterministic PDE (55), we have, based on works of Heston (1993) and Carr and Madan (1999), introduced a numerical approach to efficiently price European call options. However, there are several drawbacks with this approach, the most obvious one being that we need to re-calibrate the model for each distinct risky asset since the assets follow their own variance process. For instance, estimating the variables ν , κ_ν , θ_ν , and σ_ν in the option pricing model using market data takes approximately 30 minutes. In theory, pricing European options for all 438 companies listed on the Frankfurt Stock Exchange can therefore take around 9 days – an unfeasible amount of time.

To address this issue, we turn our attention to *physics-informed neural networks* (PINNs), a relatively recent class of mesh-free function approximators for solving PDEs subject to boundary and terminal constraints. Introduced by Raissi et al. (2017), PINNs embed the governing equation of the problem such as PDEs directly into the training objective, the PDE residual, turning pricing into a constrained regression problem enforced at randomly sampled points within the domain of the governing equation. Since their introduction, PINNs have been applied across disciplines such as fluid dynamics Jin et al. (2021) and quantum control Norambuena et al. (2024). For a detailed survey of PINNs, their use and limitations, we refer to Cuomo et al. (2022) and Lawal et al. (2022).

It is therefore natural to apply them to finance, where option values solve PDEs. In this paper, we follow Hainaut and Casas (2024) and extend their setup to include both stochastic short rates as well as stochastic variance. Specifically, we train our PINN to solve a modified version of the backward PDE (55) with the short rate parameters r , κ_r , θ_r , and σ_r as well as the Svensson curve parameters β_0 , β_1 , β_2 , β_3 , a_1 , and a_2 estimated on beforehand to narrow the dimension of the problem. The PINN is then trained over a broad domain for the initial values s , r and ν , as well as for the variance parameters κ_ν , θ_ν , σ_ν , and ρ_2 and for the times τ and T . Furthermore, the PINN architecture in question will be a feedforward neural network with skip connections.

In the context of option pricing, the main advantage of PINNs over purely data-driven Machine Learning methods, like regression or gradient-boosted trees, is that they neither require feature engineering nor labeled market data as the physics enforced by the governing PDE supplies the supervision. We sample parameters over a pre-determined domain and train the network to minimize the PDE residual together with boundary and terminal losses. Once trained, the network evaluates prices in constant runtime across ranges of inputs, without re-running a numerical solver or relying on market data. Empirically, Hainaut and Casas (2024) report accuracy comparable to FFT-based solvers with markedly lower inference time, while avoiding some numerical instabilities of traditional schemes.

6.1 Formalizing Neural Networks

The idea of a neural network first originated from the goal of using a mathematical formulation, called a neuron, to approximate the behaviour of a human brain. The first proposal of this mathematical neuron was published by McCulloch and Pitts (1943) wherein the authors introduce the concept of neuron by virtue of binary thresholding. Soon after, Rosenblatt (1958) applied the neuron to pattern recognition and introduced the concept of a perceptron and proved its convergence, see Rosenblatt et al. (1962). The neural network, which is a complex structure consisting of multiple neurons, was then a natural extension and across the years, many proofs regarding neural networks being universal approximators of functions have been presented. For instance, Hornik (1991) shows that feedforward neural networks¹¹ with as little as one layer can approximate regular functions approximately well given that the activation function is sufficiently smooth.

¹¹Feedforward neural networks are a type of neural network where the information flows in one direction only, generally from input to output neurons.

Scaling the State Variable

We begin by motivating the need to scale the state variables $S(\tau) = s$, $R(\tau) = r$, and $V(\tau) = \nu$, as well as the times τ and T . The mathematical definition of the feedforward neural network will be introduced in the next subsection of this chapter, but it is worth mentioning that neural networks depend on so-called activation functions. In this paper, we rely on the hyperbolic tangent function as the activation function. Since the PDE (55) includes derivatives in the aforementioned state variables, the neural network differentiates the activation function with respect to these variables. Considering the first derivative of the hyperbolic tangent with respect to the variable x

$$\frac{d}{dx} \tanh x = \frac{1}{\cosh^2 x},$$

note that $\cosh x \rightarrow \infty$ as $x \rightarrow \infty$ so that

$$\lim_{x \rightarrow \infty} \frac{d}{dx} \tanh x = 0,$$

As a consequence, for large inputs x , the derivatives of the hyperbolic tangent tend to vanish leading to imprecise function approximations and convergence issues. To address this issue, we scale our state variables to ensure that the derivatives do not vanish. To scale the state vector $\mathbf{z} = (s, r, \nu)^\top$, define the vectors $\mathbf{a}, \mathbf{b} \in \mathbb{R}^3$, where

$$\begin{aligned}\mathbf{a} &= (a_s, a_r, a_\nu)^\top \\ \mathbf{b} &= (b_s, b_r, b_\nu)^\top.\end{aligned}$$

Also, denote the centering constants for the time variables by a_h and b_h . Then, the state variables are scaled with affine standardization, that is,

$$\tilde{\mathbf{z}}(\tau) = \mathbf{a} + \mathbf{b} \odot \mathbf{z}(\tau), \quad (79)$$

where \odot denotes the element-wise product and $\tilde{\mathbf{z}}(\tau)$ is the scaled state variable at the unscaled time τ . The time variables are scaled by

$$\begin{aligned}\tilde{\tau} &= a_h + b_h \tau, \\ \tilde{T} &= a_h + b_h T.\end{aligned}$$

Thus, the scaled state variable is

$$\tilde{\mathbf{z}} = \mathbf{a} + \mathbf{b} \odot \mathbf{z},$$

which, together with $\tilde{\tau}$ and \tilde{T} is fed into the activation function of the PINN. The choice of the scaling parameters a_h , \mathbf{a} , b_h , and \mathbf{b} is addressed in section 6.4.

Option Pricing PDE with Scaled Variables

As discussed in previously, we wish to feed the PINN with scaled variables. This means that the option pricing PDE (55) together with its terminal condition need to be scaled as well. Since we want to compare PINN against FFT call option prices, we set $\rho_1 = \rho_3 = 0$. Therefore, the unscaled, deterministic PDE (55) now reads as

$$\begin{aligned}\partial_\tau c + rs\partial_s c + & \left[\kappa_r(\theta_r - r + \psi(\tau)) + \psi'(\tau) \right] \partial_r c + \kappa_\nu(\theta_\nu - \nu)\partial_\nu c \\ & + \frac{1}{2} \left[\nu s^2 \partial_{ss} c + \sigma_r^2(r - \psi(\tau))\partial_{rr} c + \sigma_\nu^2 \nu \partial_{\nu\nu} c + 2\rho_2 \sigma_\nu s \nu \partial_{s\nu} c \right] - rc = 0,\end{aligned} \quad (80)$$

where $c := c(\tau, s, r, \nu)$. With affine scaling (79), the PDE above becomes

$$\begin{aligned}b_h \partial_{\tilde{\tau}} \tilde{c} + & \frac{\tilde{r} - a_r}{b_r} (\tilde{s} - a_s) \partial_{\tilde{s}} \tilde{c} + \left(\kappa_r(b_r \theta_r - (\tilde{r} - a_r) + b_r \psi(\tau)) + \psi'(\tau) \right) \partial_{\tilde{r}} \tilde{c} \\ & + \kappa_\nu(b_\nu \theta_\nu - (\tilde{\nu} - a_\nu)) \partial_{\tilde{\nu}} \tilde{c} + \frac{1}{2} \left[\frac{\tilde{\nu} - a_\nu}{b_\nu} (\tilde{s} - a_s)^2 \partial_{\tilde{s}\tilde{s}} \tilde{c} + b_r \sigma_r^2 (\tilde{r} - a_r - b_r \psi(\tau)) \partial_{\tilde{r}\tilde{r}} \tilde{c} \right. \\ & \left. + b_\nu \sigma_\nu (\tilde{\nu} - a_\nu) \partial_{\tilde{\nu}\tilde{\nu}} \tilde{c} + 2\rho_2 \sigma_\nu (\tilde{\nu} - a_\nu)(\tilde{s} - a_s) \partial_{\tilde{s}\tilde{\nu}} \tilde{c} \right] - \frac{\tilde{r} - a_r}{b_r} \tilde{c} = 0,\end{aligned} \quad (81)$$

where now

$$\tilde{c} := c(\tilde{\tau}, \tilde{s}, \tilde{r}, \tilde{\nu}).$$

The terminal condition for (81) is

$$c(\tilde{T}, \tilde{s}) = \left(\frac{\tilde{s} - a_s}{b_s} - K \right)_+. \quad (82)$$

To simplify the notation, we define the operator \mathcal{L} containing the scaled state variables such that for a smooth function $u := u(\tilde{s}, \tilde{r}, \tilde{\nu})$, twice differentiable in s, r and ν , $\mathcal{L}u$ reads as

$$\begin{aligned} \mathcal{L}u &= \frac{\tilde{r} - a_r}{b_r} (\tilde{s} - a_s) \partial_{\tilde{s}} u + \left(\kappa_r (b_r \theta_r - (\tilde{r} - a_r) + b_r \psi(\tau)) + \psi'(\tau) \right) \partial_{\tilde{r}} u + \kappa_\nu (b_\nu \theta_\nu - (\tilde{\nu} - a_\nu)) \partial_{\tilde{\nu}} u \\ &+ \frac{1}{2} \left[\frac{\tilde{\nu} - a_\nu}{b_\nu} (\tilde{s} - a_s)^2 \partial_{\tilde{s}\tilde{s}} u + b_r \sigma_r^2 (\tilde{r} - a_r - b_r \psi(\tau)) \partial_{\tilde{r}\tilde{r}} u + b_\nu \sigma_\nu (\tilde{\nu} - a_\nu) \partial_{\tilde{\nu}\tilde{\nu}} u \right. \\ &\left. + 2\rho_2 \sigma_\nu (\tilde{\nu} - a_\nu) (\tilde{s} - a_s) \partial_{\tilde{s}\tilde{\nu}} u \right]. \end{aligned} \quad (83)$$

Expressing (81) in terms of the operator \mathcal{L} , one has, for $\tilde{c} = c(\tilde{\tau}, \tilde{s}, \tilde{r}, \tilde{\nu})$,

$$b_h \partial_{\tilde{\tau}} \tilde{c} + \mathcal{L} \tilde{c} - \frac{\tilde{r} - a_r}{b_r} \tilde{c} = 0, \quad (84)$$

as the scaled option pricing PDE subject to the scaled terminal condition (82).

Pricing Options with a fixed Strike Price

Before delving into the mathematical formulation the PINN, we discuss a practical detail in Hainaut and Casas (2024) to reduce the dimensionality of the PINN training problem. Recalling that our main goal is to use the trained PINN to price options across a broad range of variance parameters, maturities, strike prices and state variables s, r , and ν , the input dimension in this setting reaches 10, which increases the risk of slow convergence or inaccurate solution approximations by the PINN.

To address this, rather than training the network over a wide range of strikes, the authors use the scaling property of European call options. Assume that the PINN has already been trained on the strike price $K > 0$ and let $K' \neq K$ be a strictly positive strike price. For identical initial conditions s, r, ν and maturity T , the prices of two European call options with strikes K_1 and K_2 satisfy

$$c(\tau, s, r, \nu; K') = \frac{K'}{K} c\left(\tau, \frac{K}{K'} s, r, \nu; K\right). \quad (85)$$

By applying this property, we only train the PINN for a single, strictly positive reference strike K and then recover prices any other strike through the transformation (85). This helps reducing the dimensionality of the input space by one and improves training efficiency.

Mathematical Formulation of the PINN

As stated previously, our main focus is to approximate the option pricing PDE (84) across different values for the scaled state variables \tilde{s}, \tilde{r} , and $\tilde{\nu}$, the variance parameters $\kappa_\nu, \theta_\nu, \sigma_\nu$, and ρ_2 , as well as the scaled times $\tilde{\tau}$ and \tilde{T} , using a feedforward neural network. We collect the scaled variables into the vector $\tilde{\mathbf{y}} \in \mathbb{R}^9$, which corresponds to the input vector for the neural network and is defined as

$$\tilde{\mathbf{y}} := (\tilde{\tau}, \tilde{\mathbf{z}}, \Theta, \tilde{T})^\top, \quad (86)$$

where $\mathbf{z} = (\tilde{s}, \tilde{r}, \tilde{\nu})^\top$ and $\Theta = (\kappa_\nu, \theta_\nu, \sigma_\nu, \rho_2)^\top$.

Until now we have named activation functions and neural networks without ever mathematically formalizing them. To make these notions precise, we provide the following definitions:

Definition 6.1 (Activation function). *An activation function is a measurable, non-linear map*

$$\sigma : \mathbb{R} \longrightarrow \mathbb{R},$$

applied componentwise to the affine pre-activations of a neural network layer. Given a vector $u \in \mathbb{R}^m$, we write the vectorized action as

$$\sigma(u) := (\sigma(u_1), \dots, \sigma(u_m))^\top.$$

Remark 6.2 (Regularity assumptions). *For approximation of functions with neural networks, one often assumes that the activation function σ is continuous and non-polynomial. Under these conditions, as shown by Leshno et al. (1993), shallow feed-forward networks are universal approximators on compact sets.*

Remark 6.3 (The choice of the activation function). *As previously mentioned, for our goal of approximating the PDE (81), we choose $\sigma(\cdot) = \tanh(\cdot)$, which is a twice differentiable function, such that the first and second derivatives of the network exist everywhere.*

Definition 6.4 (The feed-forward neural network, see Hainaut and Casas (2024)). *Let $l \in \mathbb{N}$ be the number of layers and $n_0, n_1, \dots, n_l \in \mathbb{N}$ be the number of neurons in each layer, where n_0 denotes the size of the input vector. The activation function of layer $k = 1, 2, \dots, l$ is denoted as $\sigma_k(\cdot) : \mathbb{R} \rightarrow \mathbb{R}$. Furthermore, let $P_1 \in \mathbb{R}^{n_1} \times \mathbb{R}^{n_0}$, $\mathbf{p}_1 \in \mathbb{R}^{n_1}$, $P_k \in \mathbb{R}^{n_k} \times \mathbb{R}^{n_0+n_{k-1}}$, $\mathbf{p}_k \in \mathbb{R}^{n_k}$ for $k = 2, \dots, l-1$, and $P_l \in \mathbb{R}^{n_l} \times \mathbb{R}^{n_{l-1}}$, $\mathbf{p}_l \in \mathbb{R}^{n_l}$ be neural weights defining the input, intermediate and output layers respectively. We define the following functions*

$$\begin{cases} \xi_k(\mathbf{x}) = \sigma_k(P_k \mathbf{x} + \mathbf{p}_k), & k = 1, l, \\ \xi_k(\mathbf{x}, \mathbf{y}) = \sigma_k\left(P_k \begin{pmatrix} \mathbf{x} \\ \mathbf{y} \end{pmatrix} + \mathbf{p}_k\right), & k = 2, \dots, l-1. \end{cases}$$

where $\mathbf{y} \in \mathbb{R}^{n_0}$ is the input variable (86), $\mathbf{x} \in \mathbb{R}^{n_{k-1}}$ are the current hidden activations coming from the previous layer, and activation functions $\sigma_k(\cdot)$ are applied componentwise. Then, the neural network is a function $F : \mathbb{R}^{n_0} \rightarrow \mathbb{R}^{n_l}$ defined by

$$F(\mathbf{z}) = \xi_l \circ \xi_{l-1}(\cdot, \mathbf{z}) \circ \dots \circ \xi_2(\cdot, \mathbf{z}) \circ \xi_1(\mathbf{z}).$$

Network Architecture

Thus far, we have mathematically formalized feed-forward neural networks without ever precising its exact architecture which we now aim to explicitly provide. As previously mentioned, Hornik (1991) showed that even single-layer neural networks can approximate functions arbitrarily well. However, as the PDE we want to solve is non-linear and four dimensional, accurately approximating our option prices will require a very large amount of neurons. Moreover, Hainaut and Casas (2024) argue that feed-forward networks often struggle to replicate non-linear functions with a limited number of layers. One way to address this problem is introduced by Sirignano and Spiliopoulos (2018), where the authors introduce a modification of the Long Short-Term Memory which they call the Deep Galerkin Network (DGM). The DGM can indeed approximate option prices quite well, but due to the complexity of its network architecture, training the DGM on a randomly sampled input of dimension 9 is time-consuming. Therefore, Hainaut and Casas (2024) adopt a simpler architecture where they introduce a "skip connection" feature into the feed-forward neural network. Figure 4 illustrates the feed-forward neural network used in this paper to approximate the PDE (84).

6.2 Sampling Procedure

In the previous section we motivated the use of PINNs by the fact that the network does not require observed option prices in order to approximate the pricing function. Instead, the PINN is trained on synthetically generated inputs $\mathbf{y} \in \mathbb{R}^9$, which are sampled at random from suitable domains

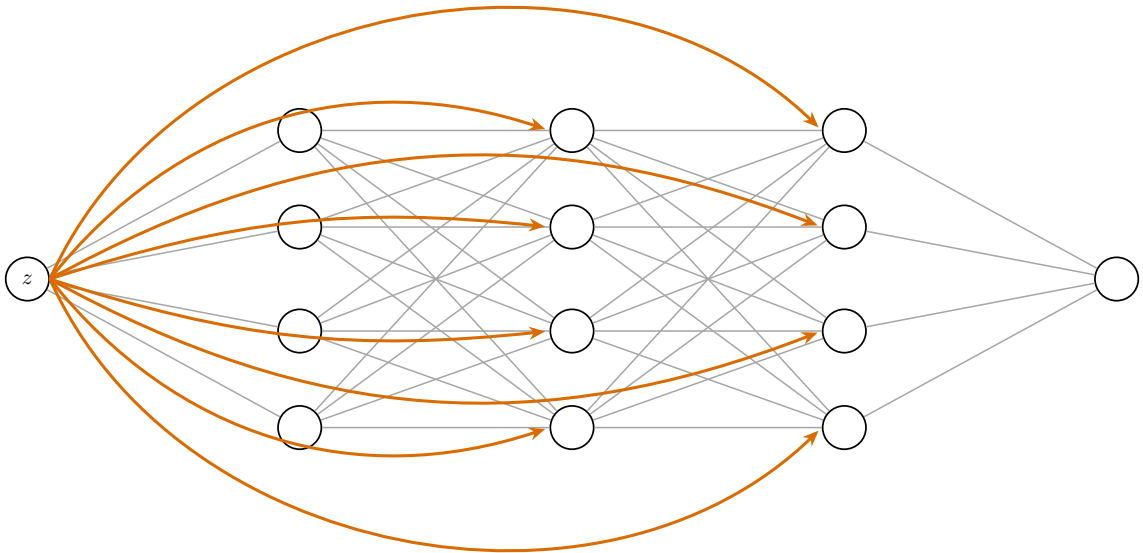


Figure 4: Feed forward network with five layers (network width), i.e. $l = 5$, and four hidden layers (netwrok depth), i.e. $n_k = 4$ for $k = 2, 3, 4$, with skip connections toward intermediate layers as shown in Hainaut and Casas (2024).

using the uniform distribution $\mathcal{U}([a, b])$ on an interval $[a, b]$. In this way, the network learns an approximation of the unknown call price function c on a broad set of states and parameters, and can subsequently be used to price options for a wide range of model inputs. In particular and under our framework, the same trained network can, in principle, be applied to different assets as long as they share the same short-rate dynamics.

The sampling procedure is applied around the three regions in which the PDE and its boundary conditions are imposed:

- (i) Interior domain: the region there the PDE (84) holds.
- (ii) Spatial boundaries: a shell around the domain in the underlying s , consisting of a lower and an upper boundary that reflect the limiting behaviour of call prices. which can be seen as the shell around the domain. We differentiate between lower and upper boundaries in the matter of option pricing, and
- (iii) Terminal boundary:the boundary at maturity T , where the payoff condition is enforced.

Figure 5 illustrates the sampling procedure for the unscaled state variable $s \in [0.1, 1000]$ for times $\tau \in [0, 5]$, showing interior points, boundary points, and terminal points.

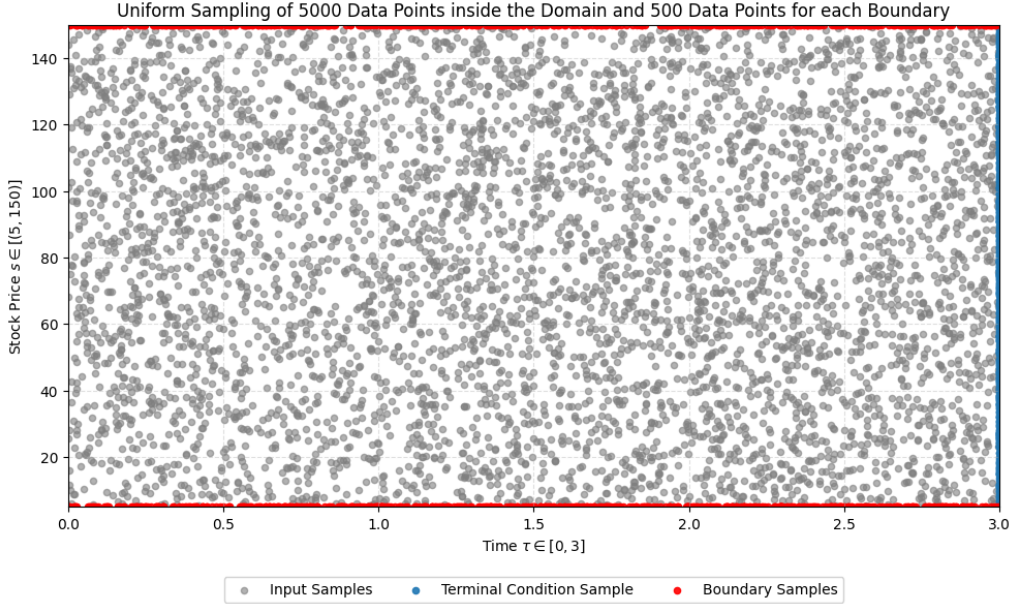
As in the previous chapter, we denote the initial state of the SDE system (53) by $\mathbf{z} = (s, r, \nu)^\top$. The corresponding spatial domain is the Cartesian product

$$\mathcal{D}_{\mathbf{z}} = [s_{\min}, s_{\max}] \times [r_{\min}, r_{\max}] \times [\nu_{\min}, \nu_{\max}],$$

where the subscripts min and max denote lower and upper bounds, respectively. All sampled states \mathbf{z} are constrained to lie in $\mathcal{D}_{\mathbf{z}}$. The maturity T is sampled in an interval $[T_{\min}, T_{\max}]$ and for each sample we draw an initial time τ_j such that $\tau_j \leq T_j$.

The vector of variance parameters is written $\Theta = (\kappa_\nu, \theta_\nu, \sigma_\nu, \rho_2)$. We sample these parameters in

Figure 5: Sampling procedure for the state variable $s \in [0.1, 1000]$ and the time variable $\tau \in [0, 5]$ with 5000 samples within the rectangular domain (gray dots), 500 samples on the terminal condition boundary (blue dots), and a total of 500 samples on the lower and upper boundaries (red dots).



a rectangular parameter domain

$$\mathcal{D}_\Theta = [\kappa_{\nu,\min}, \kappa_{\nu,\max}] \times [\theta_{\nu,\min}, \theta_{\nu,\max}] \times [\sigma_{\nu,\min}, \sigma_{\nu,\max}] \times [\rho_{2,\min}, \rho_{2,\max}].$$

Remark 6.5. The domains \mathcal{D}_z and \mathcal{D}_Θ are design choices and fixed before training. They are not learned by the PINN. Rather, they reflect the range of parameters for which we want the network to be accurate.

As stated in the previous section, recall that to improve numerical stability during training, the components of \mathbf{z} are centered and scaled with affine standardization (79) before being fed into the PINN. We now seek to find suitable scaling vectors \mathbf{a} and \mathbf{b} . Let \mathbf{z}_j denote the j -th realisation of the state variable obtained from the interior samples and let n_D be the number of such samples. We compute the empirical mean vector $\bar{\mathbf{z}}$ and standard deviation vector \mathbf{SD}_z with

$$\bar{\mathbf{z}} = \frac{1}{n_D} \sum_{j=1}^{n_D} \mathbf{z}_j, \quad \mathbf{SD}_z = \sqrt{\frac{1}{n_D - 1} \sum_{j=1}^{n_D} (\mathbf{z}_j - \bar{\mathbf{z}}) \odot (\mathbf{z}_j - \bar{\mathbf{z}})}.$$

The scaling vectors are then defined as

$$\mathbf{a} = -\frac{\bar{\mathbf{z}}}{\mathbf{SD}_z} \quad (87)$$

and

$$\mathbf{b} = \frac{1}{\mathbf{SD}_z}. \quad (88)$$

Furthermore, the time variables τ and T are scaled with

$$a_h = -\frac{1}{2}, \quad b_h = \frac{1}{T_{\max}}.$$

Sampling within the Interior Domain

Let n_D denote the number of training points in the interior domain. For each index $j = 1, \dots, n_D$, we draw

$$T_j \sim \mathcal{U}([T_{\min}, T_{\max}]), \quad \tau_j \sim \mathcal{U}([T_{\min}, T_{\max}])$$

Let $n_{\mathcal{D}}$ denote the number of samples taken inside the interior domain. We sample the times T and τ by

$$T_j \sim \mathcal{U}([T_{\min}, T_{\max}]),$$

and

$$\tau_j \sim \mathcal{U}([0, T_j])$$

and sample \mathbf{z}_j uniformly from $\mathcal{D}_{\mathbf{z}}$ and Θ_j uniformly from \mathcal{D}_{Θ} . The resulting inputs $\mathbf{y}_j = (\tau_j, \mathbf{z}_j, \Theta_j, T_j)$ are then mapped to their scaled counterparts $\tilde{\mathbf{y}}_j$ using the affine transformation (79). The collection of scaled interior points used in the loss for the PDE residual is

$$\tilde{\mathcal{S}}_{\mathcal{D}} = \{\tilde{\mathbf{y}}_j\}_{j=1}^{n_{\mathcal{D}}}.$$

Sampling at the Lower and Upper Boundaries

The lower boundary for the initial variable s corresponds to deep out-of-the-money options which happens for $s \ll K$. Numerically this is implemented at $s = s_{\min}$. For sufficiently small s_{\min} , the call price satisfies

$$c(\tau, s_{\min}, r, \nu) \approx 0.$$

We draw n_{lower} samples on the lower boundary, keeping $s = s_{\min}$ fixed and sampling the remaining components as before. The corresponding scaled inputs are

$$\tilde{\mathbf{z}}_{\text{lower},j} = (\tilde{s}_{\min}, \tilde{r}_j, \tilde{\nu}_j)^{\top},$$

and

$$\tilde{\mathbf{y}}_{\text{lower},j} = (\tilde{\tau}_j, \tilde{\mathbf{z}}_{\text{lower},j}, \Theta_j, \tilde{T}_j)^{\top}.$$

The collection of lower boundary points is

$$\tilde{\mathcal{S}}_{\text{lower}} = \{\tilde{\mathbf{y}}_{\text{lower},j}\}_{j=1}^{n_{\text{lower}}}.$$

The upper boundary corresponds to deep-in-the-money options, that is, $s \gg K$. This boundary is imposed numerically at $s = s_{\max}$. For large s_{\max} , the call price is approximated by

$$c(\tau, s_{\max}, r, \nu) = P(\tau, T) \mathbb{E}_{\mathbb{Q}^T} [(s_{\max} - K)_+ \mid \mathcal{F}_{\tau}] \approx s_{\max} - K P(\tau, T),$$

such that for $s = s_{\max}$

$$\partial_s c(\tau, s, r, \nu) \approx 1.$$

We again draw n_{upper} samples, now with $s = s_{\max}$. The scaled inputs are

$$\tilde{\mathbf{z}}_{\text{upper},j} = (\tilde{\tau}_j, \tilde{\mathbf{z}}_{\text{upper},j}, \Theta_j, \tilde{T}_j)^{\top},$$

and we denote the set of upper boundary points by

$$\tilde{\mathcal{S}}_{\text{upper}} = \{\tilde{\mathbf{y}}_{\text{upper},j}\}_{j=1}^{n_{\text{upper}}}.$$

Sampling at the Terminal Condition

For a European call option, the terminal condition at maturity is

$$c(T, s, r, \nu) = (s - K)_+.$$

Expressed in terms of scaled variables, this becomes

$$c(\tilde{T}, \tilde{s}, \tilde{r}, \tilde{\nu}) = \left(\frac{\tilde{s} - a_s}{b_s} - K \right)_+.$$

On the terminal boundary, we do not sample τ independently, but set $\tau = T$. For each $j = 1, \dots, n_T$ we sample T_j , \mathbf{z}_j , and Θ_j as before, then set $\tau_j = T_j$. The corresponding scaled inputs are

$$\tilde{\mathbf{y}}_{T,j} = (\tilde{T}_j, \tilde{\mathbf{z}}_j, \Theta_j, \tilde{T}_j)^{\top},$$

and the collection of the terminal points used to enforce the payoff is

$$\tilde{\mathcal{S}}_T = \{\tilde{\mathbf{y}}_{T,j}\}_{j=1}^{n_T}.$$

6.3 From PDEs to Loss Functions

Now that the state and time variables have been scaled, the network architecture specified, and the sampling procedure formalized, we turn to the construction of the training objective. The idea is that we replace the unknown solution c in the scaled PDE (84) by the network output and penalize the mismatch between the approximated PDE and zero. This mismatch is also known as the residual. In addition, we enforce terminal and boundary conditions through dedicated penalty terms. The penalty terms are often referred as loss functions, that is, a numerical score that quantifies the error between a model's predictions and the actual target values. In the context of PINNs, the overall loss is thus the sum of the following three penalty terms:

- (i) *the interior loss*: the loss resulting from the PDE residual,
- (ii) *the boundary loss*: the loss resulting from imposing constraints around the boundaries on the PDE. In the context of call option pricing, we have lower and upper losses.
- (iii) *the terminal boundary loss*: the last loss we consider is the terminal loss which comes from the terminal condition, i.e. the contingent claim, of a European option. Although the terminal condition is a boundary condition as it can be seen in figure 5, we present its contribution as a separate loss for the purpose of clarity.

As previously mentioned, all differential operators, both first and second order, are obtained by automatic differentiation, and not finite differences, using the `torch.autograd` function in the PyTorch library for Python. This ensures a mesh-free formulation and makes the derivatives of c less prone to numerical instabilities following from finite differences. For a general survey and theory on automatic differentiation, we refer the interested reader to Baydin et al. (2018).

Domain Loss Function

Let us denote by Λ the vector containing all neural weights $(P_k, \mathbf{p}_k)_{k=1,\dots,l}$, and let F be the network function that approximates the call option prices c . At each interior sample point $\tilde{\mathbf{y}}_j \in \tilde{\mathcal{S}}_{\mathcal{D}}$ for $j = 1, \dots, n_{\mathcal{D}}$, denote by \mathcal{L}_j the operator of c defined by (83) and evaluated at the j -th sample point. Then, the residual of the scaled PDE (84) is given by

$$e_j^{\mathcal{D}}(\Lambda) = b_h \partial_{\tilde{\tau}} F(\tilde{\mathbf{y}}_j) + \mathcal{L}_j F(\tilde{\mathbf{y}}_j) - \frac{\tilde{r}_j - a_r}{b_r} F(\tilde{\mathbf{y}}_j),$$

where \mathcal{L}_j denotes the operator of c defined by (83) and evaluated at the j -th sample point. The residual $e_j(\Lambda)$ can also be referred as the error on the inner domain since it measures the goodness of fit before the expiry time T . The average quadratic loss on $\tilde{\mathcal{S}}_{\mathcal{D}}$ is then the first component of the total loss function used to fit the neural network, formalized by

$$L_{\mathcal{D}}(\Lambda) = \frac{1}{n_{\mathcal{D}}} \sum_{j=1}^{n_{\mathcal{D}}} e_j^{\mathcal{D}}(\Lambda)^2. \quad (89)$$

Boundary Loss Functions

We begin by considering the lower boundary. Recall that when $s \ll K$, the call option has essentially no value. The error for the lower boundary is therefore the output of the neural network itself, that is

$$e_j^{\text{lower}}(\Lambda) = F(\tilde{\mathbf{y}}_{\text{lower},j}),$$

where $\tilde{\mathbf{y}}_{\text{lower},j} \in \tilde{\mathcal{S}}_{\text{lower}}$ for $j = 1, \dots, n_{\text{lower}}$. For the upper boundary, that is when $s \gg K$, the PINN error is described by

$$e_j^{\text{upper}}(\Lambda) = b_s \partial_{\tilde{s}} F(\tilde{\mathbf{y}}_{\text{upper},j}) - 1$$

where $\tilde{\mathbf{y}}_{\text{upper},j} \in \tilde{\mathcal{S}}_{\text{upper}}$ for $j = 1, \dots, n_{\text{upper}}$. Then, the boundary loss is defined as the combination of the mean-squared errors of the errors on the lower and upper boundaries, that is

$$L_{\partial\mathcal{D}}(\boldsymbol{\Lambda}) = \frac{1}{n_{\text{lower}}} \sum_{j=1}^{n_{\text{lower}}} e_j^{\text{lower}}(\boldsymbol{\Lambda})^2 + \frac{1}{n_{\text{upper}}} \sum_{j=1}^{n_{\text{upper}}} e_j^{\text{upper}}(\boldsymbol{\Lambda})^2,$$

where $\partial\mathcal{D}$ denotes the boundary of domain.

Terminal Boundary Loss Function

Lastly, we impose a condition on the boundary at $\tau = T$. For $\tilde{\mathbf{y}}_{T,j} \in \tilde{\mathcal{S}}_T$, where $j = 1, \dots, n_T$, the PINN error on the terminal condition is quantified by

$$e_j^T(\boldsymbol{\Lambda}) = F(\tilde{\mathbf{y}}_{T,j}) - \left(\frac{\tilde{s} - a_s}{b_s} - K \right)_+$$

and the terminal loss is

$$L_T(\boldsymbol{\Lambda}) = \frac{1}{n_T} \sum_{j=1}^{n_T} e_j^T(\boldsymbol{\Lambda})^2.$$

Total Loss Function

Thus, putting all losses together, we end up with the total loss function, which reads as

$$L(\boldsymbol{\Lambda}) = L_{\mathcal{D}}(\boldsymbol{\Lambda}) + L_{\partial\mathcal{D}}(\boldsymbol{\Lambda}) + L_T(\boldsymbol{\Lambda}). \quad (90)$$

The training objective of the PINN is then to find an optimal vector of neural weights, denoted by $\boldsymbol{\Lambda}^*$, such that $L(\boldsymbol{\Lambda}^*)$ is minimal. Mathematically speaking, this translates to the minimization problem

$$\boldsymbol{\Lambda}^* = \arg \min_{\boldsymbol{\Lambda}} L(\boldsymbol{\Lambda}), \quad (91)$$

where $\boldsymbol{\Lambda}^*$ is the optimal vector of the neural network weights.

6.4 Training Procedure

So far, we have focused on the implementation of the neural network. We have formalized neural networks, chosen a network architecture for the PINN, and delved into the sampling procedure and loss functions, without ever mentioning the training procedure of the PINN. We now describe how the PINN is trained to minimize the total loss function L . Throughout, let $\boldsymbol{\Lambda}$ denote the vector containing all neural weights $(P_k, \mathbf{p}_k)_{k=1, \dots, l}$, where $l \in \mathbb{N}$ is the number of layers, i.e. the width of the neural network. Furthermore, recall the previously defined total loss function (90).

In essence, our PINN adjusts the neural weights in $\boldsymbol{\Lambda}$ on the output of each neuron such that for some inputs, for a given input, the weights in $\boldsymbol{\Lambda}$ adjust each neuron's output. To find the optimal weights in $\boldsymbol{\Lambda}^*$, we first let the sample collections $\tilde{\mathcal{S}}_{\mathcal{D}}, \tilde{\mathcal{S}}_{\text{lower}}, \tilde{\mathcal{S}}_{\text{upper}}$, and $\tilde{\mathcal{S}}_T$ pass through the neural network and then compute the total loss with (90). The passing of the data through the neural network is called *epoch*. We then use backpropagation, an algorithm that works by iteratively adjusting the PINN's weights and biases to minimize the total error, such that the neural network adapts the vector of weights $\boldsymbol{\Lambda}$ iteratively for each epoch in the total number of epochs.

Now an explanation the backpropagation algorithm lies beyond the scope of this paper. We therefore refer the interested reader to Damadi et al. (2023) for a clear explanation of the algorithm. In all essence, however, the backpropagation algorithm passes the sample data through the neural network that contains the vector of weights $\boldsymbol{\Lambda}$ and computes the total loss (90). If $\boldsymbol{\Lambda}$ is not optimal, that is, if the total loss is larger than zero, the algorithm re-adjusts the weights in $\boldsymbol{\Lambda}$. Without

delving much into details, this is done by computing the gradient of the loss L with respect to Λ and an optimizer.

In our training procedure, we rely on the Adaptive Moment Estimation (Adam) optimizer introduced by Kingma (2014). It is a stochastic gradient-based method that adapts individual learning rates using first and second moment estimates of past gradients. This improves convergence stability compared to fixed-rate methods such as the L-BFGS algorithm. However, very large learning rates can cause oscillations around the minimum, while overly small rates slow progress. To balance exploration and precision, we adopt a phased schedule, where we start with a high learning rate for broad search and gradually reducing it for fine-tuning near the optimum.

7 Numerical Results

Having established the theoretical foundations of the FFT and PINN approaches, we evaluate their empirical performance. We begin by presenting the market data used for the estimation of parameters present in the option pricing model, as well as the error metrics used to evaluate model performance. We then formalize the calibration procedure as a constrained minimization problem and assess accuracy using standard error metrics. Results are reported through tables and figures, including in-sample and out-of-sample performance and a runtime comparison¹².

7.1 Data

In this study, we consider market data from the Eurozone, where monetary policy and short rates are governed by the European Central Bank (ECB). Consequently, for Eurozone economies such as France, Germany, and Spain, the short rates are assumed to be the same. This assumption is practical as it lets us use the same discount curve for countries in the Eurozone such that the CIR++ short-rate model only needs to be calibrated once and pricing derivatives can be under a unified discounting curve.

The data for the fixed-income instruments and European call options is obtained from the London Stock Exchange Group (LSEG) terminal, which provides standardized templates for interest rate instruments and derivatives. We assume that the data from LSEG’s terminal is accurate.

Overnight Indexed Swaps

For the construction of the discount curve, we used Overnight Indexed Swaps (OIS) quoted under the EURESTOIS template on the LSEG terminal. These instruments represent fixed-for-floating swaps¹³ indexed to the Euro Short-Term Rate (€STR), which serves as the benchmark overnight rate for the Eurozone. The choice of OIS as the basis for the discounting curve $P(\tau, T)$ is motivated by their high liquidity¹⁴ and minimal credit risk¹⁵. Unlike government bonds, which can embed market and credit risks, OIS contracts are standardized and widely traded such that they are most likely to be traded at a fair price. In addition, their link to the overnight €STR rate ensures that the discount curve derived from OIS reflects a near risk-free benchmark. This is essential for the estimation of the discount curve since the swap rate is a function of the discounting factor $P(\tau, T)$, see (7). With the help of OIS contracts, we can estimate the parameters in the Svensson model (5) and, subsequently, estimate the deterministic shift function ψ in the CIR++ model (33).

The dataset we use for OIS contracts was fetched from the LSEG terminal on October 24th, 2025. The dataset spans maturities from one week to thirty years, with fixed rates ranging from approximately 1.93% for short tenors to around 2.75% for the longest maturities. The variation in quoted fixed rates is not economically significant and is primarily due to the way the LSEG terminal reports these values. The full OIS data can be found in appendix D.1.

Swaptions

As discussed earlier, the estimation of the parameters present in the CIR++ model relies on European payer swaptions, that is, European call options on swaps. The data was sampled from the LSEG terminal on October 24th, 2025, and the swaption contracts are quoted under the EUR_AB3E template, where the prefix EUR indicates the currency (Euro), A the annual fixed swap rate, and B3E the floating leg based on EURIBOR 3M (three-month Euro Interbank Offered Rate).

¹²The Python code used in this chapter is available online through this GitHub repository.

¹³Recall that in a fixed-for-floating swap, one party pays a fixed interest rate and receives a floating rate, while the counterparty does the opposite.

¹⁴Liquidity refers to how easily an asset can be converted into cash without affecting its market price. In this case, high liquidity means that the swaps are almost surely likely to have a potential buyer.

¹⁵Credit risk is the chance that a borrower does not repay a loan or fulfill a loan obligation.

The dataset can be found in appendix D.2 and contains a broad range of expiries and underlying swap tenors. Specifically, the option expiries span from 1 year to 15 years, while the underlying swap tenors range from 1 to 15 years. This structure ensures that the calibration of the CIR++ model captures both short-term and long-term dynamics of the term structure.

European call options

For the numerical experiments, we consider European call options written on the stocks of BNP Paribas (BNPE) and SAP SE (SAPE), listed on the Paris and Frankfurt stock exchanges respectively. These two underlyings were selected to represent liquid equities different sectors within the Eurozone.

As with swaps and swaptions, option data was retrieved from the LSEG terminal on October 24, 2025, immediately after market closure. This guarantees that all quoted prices are end-of-day prices, thereby eliminating intraday noise and ensuring consistency across instruments. The dataset spans a broad range of maturities, from short-dated contracts with approximately 27 days to expiry to long-dated options with maturities of up to three years. This range allows us to capture both near-term and medium-term dynamics in option pricing.

An overview of the sample sizes and time-to-maturity distribution for options on BNPE and SAPE is provided in Table 1, while the corresponding end-of-day spot prices for the two underlying assets are reported in Table 2 and the full dataset can be found in appendix D.3.

Table 1: Details of data set of call option prices for BNPE and SAPE.

Start Date	Date of Maturity	Time to Maturity	Samples (BNPE)	Samples (SAPE)
2025-10-24	2025-11-21	27 days	47	33
	2025-12-19	55 days	51	52
	2026-01-16	83 days	34	29
	2026-03-20	146 days	28	28
	2026-06-19	237 days	30	29
	2026-09-18	328 days	28	28
	2026-12-18	419 days	18	15
	2027-12-17	601 days	18	15
	2028-06-16	783 days	18	15
	2028-12-15	965 days	18	15

Table 2: Stock prices at the time of data collection.

Collected	Underlying	s in €
2025-10-24	BNPE	68.72
	SAPE	242.00

7.2 Error measures

To evaluate the accuracy of the calibrated models, we compare model-implied prices with observed market prices using standard error metrics. Denoting by p the price of a financial instrument, where p^{Model} and p^{Market} denote the model and market prices respectively, consider the Mean Absolute Error (MAE), Root Mean Squared Error (RMSE), and Mean Absolute Percentage Error (MAPE) as error metrics, defined by (92) (93), and (94) respectively.

$$\text{MAE} = \frac{1}{N} \sum_{j=1}^N | p_j^{\text{Model}} - p_j^{\text{Market}} | \quad (92)$$

$$\text{RMSE} = \sqrt{\frac{1}{N} \sum_{j=1}^N (p_j^{\text{Model}} - p_j^{\text{Market}})^2} \quad (93)$$

$$\text{MAPE} = \frac{100}{N} \sum_{j=1}^N \left| \frac{p_j^{\text{Model}} - p_j^{\text{Market}}}{p_j^{\text{Market}}} \right|. \quad (94)$$

When it comes to the evaluation, the aforementioned error metrics quantify different kinds of error. MAE captures the average magnitude of pricing deviations without considering the direction of the deviation. This provides a measure for overall model accuracy. RMSE emphasizes larger discrepancies by means of squaring error before averaging, making it particularly sensitive to large mispricings. Finally, MAPE expresses errors relative to market prices, making it particularly useful for assessing whether low-priced instruments are accurately matched. Even small absolute deviations in such cases lead to large percentage errors, so MAPE highlights mispricings in regions where prices are small. Together, these measures offer a balanced evaluation of model performance, combining interpretability, sensitivity to extreme deviations, and scale invariance.

7.3 Calibration of the CIR++ model

Before we can calibrate the option pricing models, we need to estimate the parameters present in the Svensson ad CIR++ models, see (5) and (33). These parameters are obtained by fitting the model to market swaps and swaption prices using an optimization procedure described earlier. Once the short-rate parameters are calibrated, they are used as inputs for the subsequent calibration of the variance parameters in the FFT and PINN models.

Estimation of the Svensson curve parameters

As discussed in chapter 3, the Svensson model is needed for determining the deterministic shift function ψ in the CIR++ model (33). Define the set of parameters present in the Svensson discount curve model (4) and (5) by $\Theta_{\text{Svensson}} := (\beta_0, \beta_1, \beta_2, \beta_3, a_1, a_2)$, and recall that in the Svensson model, the zero-coupon bond is assumed to follow the expression

$$P^{\text{Svensson}}(\tau, T) = e^{-(T-\tau)y^{\text{Svensson}}(\tau, T)},$$

where the yield y^{Svensson} is described by the formula

$$\begin{aligned} y^{\text{Svensson}}(\tau, T) &= \beta_0 + \beta_1 \frac{1 - e^{-a_1(T-t)}}{a_1(T-t)} + \beta_2 \left(\frac{1 - e^{-a_1(T-t)}}{a_1(T-t)} - e^{-a_1(T-t)} \right) \\ &\quad + \beta_3 \left(\frac{1 - e^{-a_2(T-t)}}{a_2(T-t)} - e^{-a_2(T-t)} \right). \end{aligned}$$

Moreover, recall that the time- τ fair rate of a swap beginning at T_0 and maturing at T_n is given by (7), that is,

$$r_{\text{swap}}(\tau, T_n) = \frac{1 - P(\tau, T_n)}{\sum_{i=1}^n \delta_i P(\tau, T_i)},$$

where $\delta_i := T_i - T_{i-1}$. Since we use swaps in the form of OIS contracts, the fair swap rate $r_{\text{swap}}(\tau, T_n)$ is known. As a consequence, the discount curve $P(\tau, T_j)$ for $j = 1, \dots, n$ can therefore be computed iteratively with

$$P^{\text{Market}}(\tau, T_j) = \frac{1 - r_{\text{swap}}^{\text{OIS}}(\tau, T_j) \sum_{i=1}^{j-1} \delta_i P^{\text{Market}}(\tau, T_i)}{1 + \delta_j r_{\text{swap}}^{\text{OIS}}(\tau, T_j)}, \quad (95)$$

where $r_{\text{swap}}^{\text{OIS}}$ denotes the market OIS rate. Then the parameter set Θ_{Svensson} is found by solving the unconstrained minimization problem

$$\Theta_{\text{Svensson}}^* = \arg \min_{\Theta_{\text{Svensson}}} \frac{1}{n} \sum_{j=1}^n (P^{\text{Market}}(\tau, T_j) - P^{\text{Svensson}}(\tau, T_j))^2, \quad (96)$$

where $\Theta_{\text{Svensson}}^*$ is the optimal parameter set for the Svensson model.

Note that the unconstrained minimization in (96) is ill-conditioned, as highlighted by Banholzer et al. (2024), which may cause optimization algorithms to converge prematurely to suboptimal solutions. To mitigate this, we use the Svensson parameter set published by the ECB (2025) as an initial guess for $\Theta_{\text{Svensson}}^*$. These parameters are not used as the final solution to the minimization problem (96) because the ECB calibrates its curve to government zero-coupon bond prices, which embed market and credit risk and therefore tend to slightly overprice bonds. Nevertheless, they provide a highly informative starting point as bonds issued by the ECB are considered virtually risk-free, so that the optimal Svensson parameters for our setting are expected to lie close to those published by the ECB. The initial guess for the parameter set is reported in Table 3.

Table 3: Svensson curve parameters posted by the European Central Bank on October 24th, 2025.

Parameter	Value in %
β_0^{ECB}	1.128326
β_1^{ECB}	0.774661
β_2^{ECB}	-2.296025
β_3^{ECB}	7.721684
a_1^{ECB}	25.141534
a_2^{ECB}	8.498147

For the numerical implementation, we use the Limited-memory BFGS (L-BFGS) algorithm introduced by Liu and Nocedal (1989), a Quasi-Newton method well-suited for large-scale optimization problems due to its efficient memory usage and fast convergence properties. In Python, this algorithm is available through the `scipy.optimize.minimize` function.

The value for the resulting optimal parameter set $\Theta_{\text{Svensson}}^*$ obtained by solving the unconstrained minimization problem in (96) is found in table 4. Figure 6 presents a comparison between market zero-coupon bond prices and yields and the corresponding quantities implied by the calibrated Svensson model, together with the instantaneous forward rate curve generated by the parameters found in table 4. The three plots display, respectively, the zero-coupon bond prices, the zero-coupon yield curve, and the instantaneous forward curve for maturities from 1 to 30 years and illustrate the quality of fit to the observed OIS term structure.

Table 4: Optimal Svensson curve parameters on October 24th, 2025.

Parameter	Value in %
β_0^*	0.98635546
β_1^*	0.93036623
β_2^*	-0.34151371
β_3^*	5.72489906
a_1^*	53.35349837
a_2^*	7.26479511

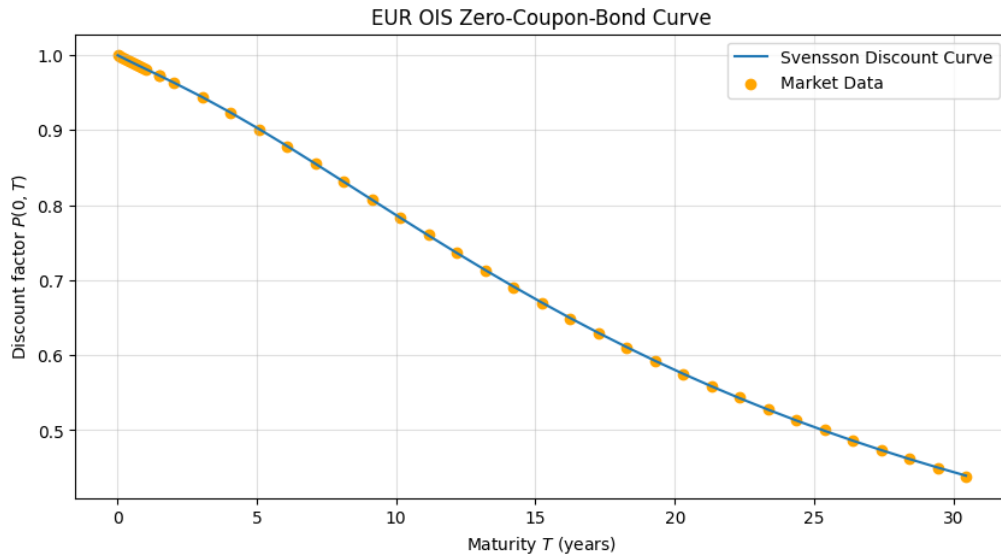
Estimation of the CIR++ parameters

Define the short-rate parameter set $\Theta_r := (x_0, \kappa_r, \theta_r, \sigma_r)$ and recall the CIR++ model introduced in chapter 3. Consider the swaption pricing formula (43), that is,

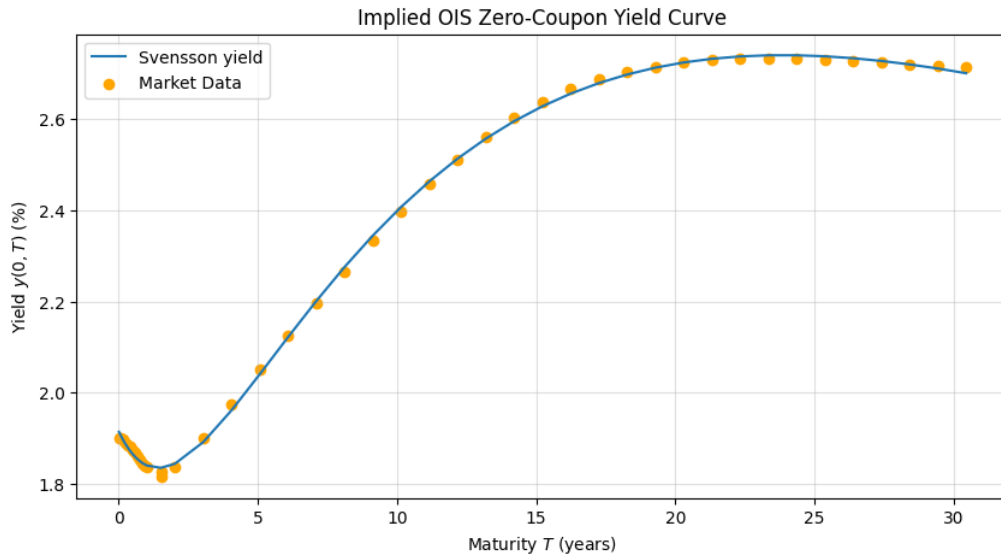
$$\mathbf{ps}(\tau, T_0, T_n) = \sum_{i=1}^n c_i \mathbf{zbc}(\tau, T_0, T_i, x_i),$$

where T_0 is the time of expiry of the swaption, T_n is the last payment date of the underlying swap, and \mathbf{zbc} denotes the price of a European option on a zero-coupon bond and is given by (40).

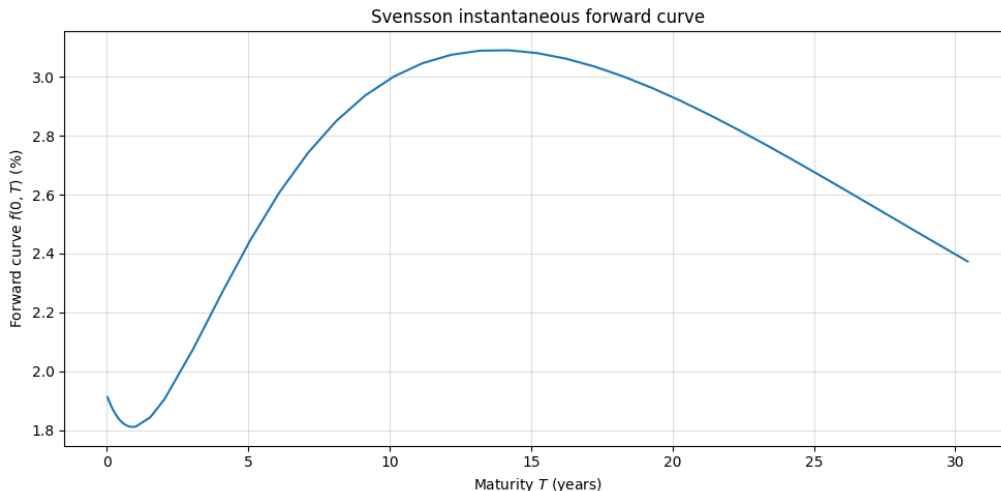
Figure 6: Zero-coupon bond prices, yields, and instantaneous forward rates for maturities from 1 to 30 years obtained from the Svensson model with parameter estimates found in table 4.



(a) Comparison of the Svensson zero-coupon bond prices (blue line) against market data (yellow dots).



(b) Comparison of the Svensson yield curve (blue line) against market data (yellow dots).



(c) Instantaneous forward rate of the Svensson model.

As mentioned in section 7.1, the market data for the swaptions contains a wide range of option expiries and underlying swap maturities, with expiries spanning from 1 year up to 15 years and swap tenors ranging from 1 year to 15 years. In other words, the time to maturity of the swaption, denoted by T_0 , varies from 1 to N , while the last payment date of the underlying swap, T_n , ranges from 1 to n . We then determine the optimal short-rate parameter set Θ_r^* , by minimizing the squared error between model and market prices across different time to maturities and swap payment dates. Mathematically speaking, Θ_r^* is the solution to the constrained minimization problem

$$\Theta_r^* = \arg \min_{\Theta_r} \frac{1}{n+N} \sum_{i=1}^N \sum_{j=1}^n (\mathbf{ps}^{\text{Model}}(\tau, T_i, T_j) - \mathbf{ps}^{\text{Market}}(\tau, T_i, T_j))^2, \quad (97)$$

such that the positivity constraint

$$\sigma_r^2 \leq 2\kappa_r \theta_r$$

is satisfied. In addition to the positivity constraint, we also restrict the parameters to be within some pre-specified range so that the parameters have an economically plausible interpretation. Specifically, we impose that

$$x_0 \in (0.001, 0.5), \quad \kappa_r \in (0.001, 0.5), \quad \theta_r \in (0.001, 0.05), \quad \sigma_r \in (0.001, 0.1).$$

The constrained minimization problem is then solved using the differential evolution algorithm introduced by Storn and Price (1997). It is a stochastic, evolutionary algorithm that seeks to find the optimal parameter set by iteratively trying to improve a candidate solution while satisfying eventual constraints. By design, it does not require the use of gradients and can search large areas within the parameter space. It is, however, worth noting that the algorithm requires larger numbers of function evaluations than conventional gradient-based techniques such as the L-BFGS-B algorithm. In the numerical implementation, we rely on the `differential_evolution` function found in Scipy's `scipy.optimize` package. The values for the optimal parameter set Θ_r^* along with the initial short rate $r = x_0 + \psi(\tau)$ are reported in table 5. Finally, the swaption pricing errors such as the MAE, RMSE, and MAPE can be found in table 6.

Table 5: CIR++ short-rate model parameters on October 24th, 2025.

Optimal Parameter	Value in %
r^*	1.916722
x_0^*	10.070984
κ_r^*	1.024475
θ_r^*	3.245518
σ_r^*	2.578739

Table 6: Error measures for the swaptions data set

Error metric	Value (%)
MAE	0.067888
RMSE	0.091902
MAPE	2.912893

7.4 Calibration of the option pricing models

Following the calibration of the Svensson and CIR++ models, this section focuses on estimating the remaining variance parameters required for option pricing. We assume that the parameters of the Svensson and CIR++ models are already fixed and given in tables 4 and 5 respectively, so the only unknowns are the variance-related parameters of the FFT and PINN models. We therefore begin by outlining the technical specifications for both pricing approaches and formulate the calibration as a constrained minimization problem. Then we calibrate the FFT and PINN models separately and report the results for both training data and out-of-sample data, which we refer to as test data, using European call options on BNPE and SAPE.

Option pricing model specifications

We begin by considering the FFT implementation, which follows the Carr and Madan (1999) framework seen in chapter 5. As we have seen, in addition to the initial conditions s , r , and ν , the FFT implementation depends on the damping factor α , the grid spacing ν and the number of discretization points N . In our case, we choose $\alpha = 1.5$, $\eta = 0.25$ and $N = 4'094$. The choice of parameters follows from the numerical experiment done by Carr and Madan (1999), where the authors choose similar parameters.

When it comes to the implementation of the PINN, we begin by considering the training procedure. Recall that the neural network architecture is by part determined by the number of layers l and hidden layers for each layer n_k for $k = 1, \dots, l$. In the implementation of their PINN, Hainaut and Casas (2024) choose a variety of networks and suggest that a 4-layer, 256-neuron residual PINN is a very good compromise for their numerical experiment. However, as they consider a constant short rate, as opposed to our stochastic short rate framework, our resulting PDE (84) is considerably more complex. We therefore increase the number of neurons at every hidden layer to the next power of two, that is, 512. We refer to this PINN as the 4×512 -model. The parameter ranges, as well as the number of samples and the training schedule for the 4×512 -model are reported in tables 7, 8, and 9 respectively. Lastly, the training performance of the PINN model is illustrated in figure 7 which shows the loss landscape of the PINN across the five training phases. The steady decline in total loss and residual loss shows successful convergence, while the plateau in later epochs suggests stability.

Table 7: Parameter ranges for the training procedure of the PINN.

Range of parameters and state variables for $K = 50$	
$s \in [0.1K, 3K]$	$\kappa_\nu \in [0.1, 5]$
$r \in [0.01, 0.03]$	$\theta_\nu \in [0.001, 0.5]$
$\nu \in [0.01, 0.3]$	$\sigma_\nu \in [0.01, 0.75]$
$T \in [0, 3]$	$\rho_2 \in (-1, 1)$
$t_j \in [0, T_j]$	

Table 8: Number of samples for the lower, upper and terminal boundaries as well as for the interior domain.

n_{lower}	n_{upper}	n_T	$n_{\mathcal{D}}$
10'000	10'000	10'000	50'000

Table 9: Learning rates and number of epochs used in the five training phases.

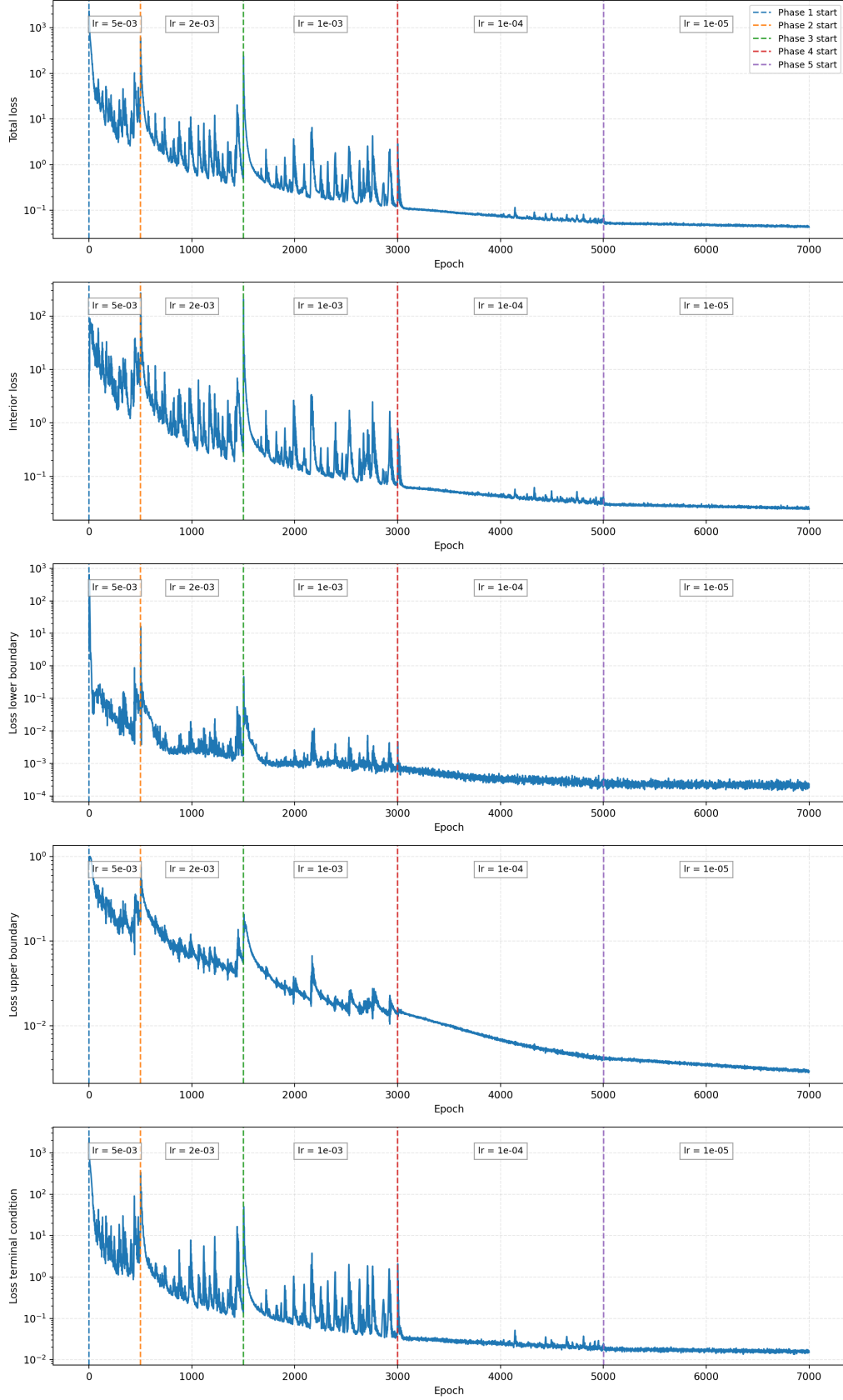
Phase	Learning rate	Epochs
1	0.005	500
2	0.002	1'000
3	0.001	1'500
4	0.0001	2'000
5	0.00001	2'000

Minimization problem

Assume that the PINN model has already been trained to approximate option prices by solving the underlying PDE (80). The next step is to calibrate the variance parameters so that the model prices align with observed market data.

Let $\Theta_\nu := (\nu, \kappa_\nu, \theta_\nu, \sigma_\nu, \rho_2)$ denote the unknown parameter set for the variance model of the stock and let c^{Model} and c^{Market} denote the model and market prices of a call option. In this case, c^{Model}

Figure 7: Loss landscape of the PINN during the training procedure. The notation "lr" refers to the learning rate used in each training phase. Vertical dashed lines indicate the epoch numbers where a new learning rate is introduced, marking the transition between phases.



denotes either the FFT or PINN call option function. Furthermore, assume that the market data contains M strikes and N maturities and index the strikes by k_m for $m = 1, \dots, M$ and the time of maturity by T_n for $n = 1, \dots, N$. Then, finding the optimal set of parameters Θ_ν^* translates to the following constrained minimization problem

$$\Theta_\nu^* = \arg \min_{\Theta_\nu} \frac{1}{N+M} \sum_{j=1}^N \sum_{k=1}^M \frac{(c^{\text{Model}}(\tau, s, r; T_j, K_k, \Theta_\nu) - c^{\text{Market}}(T_j, K_k))^2}{c^{\text{Market}}(T_j, K_k)} \quad (98)$$

such that

$$\sigma_\nu^2 \leq 2\kappa_\nu\theta_\nu,$$

and

$$\nu > 0, \quad \kappa_\nu > 0, \quad \theta_\nu > 0, \quad \sigma_\nu > 0, \quad \rho_2 \in (-1, 1).$$

When it comes to the practical implementation, we use the differential evolution algorithm and impose that the parameters lie within the following ranges

$$\nu \in (0.01, 0.3), \quad \kappa_\nu \in (0.1, 5), \quad \theta_\nu \in (0.001, 0.5), \quad \sigma_\nu \in (0.01, 0.75), \quad \rho_2 \in (-1, 1),$$

for both the FFT and PINN models.

Calibration results

We begin by presenting the calibration results for the FFT and PINN pricing models, obtained by solving the constrained minimization problem (98). The training and calibration times of the FFT and PINN pricing models on BNPE and SAPE data can be found in 10, where we note that the training and calibration process for the PINN model requires less than half the time needed to calibrate the FFT model. The corresponding optimal variance-related parameters ν^* , κ_ν^* , θ_ν^* , σ_ν^* , and ρ_2^* for both the FFT and PINN models are reported in Table 11 for European call options on BNPE and in Table 12 for options on SAPE. These results highlight some differences between the two approaches, particularly in the long-run variance θ_ν^* and volatility-of-variance σ_ν^* , where the PINN model tends to produce smaller values compared to its FFT counterpart.

Table 10: Approximate times for training and calibration of the FFT and PINN pricing models.

Stage	FFT time	PINN time
Training	—	35 min
Calibration	90 min	30 s

Table 11: Comparison of calibrated variance-related parameters for the FFT and PINN option pricing models for European call options on BNPE.

Parameter	Optimal FFT Model Value	Optimal PINN Model Value
ν^*	0.087031	0.053778
κ_ν^*	4.093108	1.059690
θ_ν^*	0.030860	0.012881
σ_ν^*	0.501914	0.165200
ρ_2^*	-0.008031	-0.448728

To check the robustness of the calibration and ensure that the models do not overfit, the dataset for the European call options was partitioned into 80% for training and 20% for testing. Both models are calibrated using the same training data and the out-of-sample data used to test the robustness of the models is identical for both the FFT and PINN models. Tables 13 and 14 summarize the error metrics for both models on the training and test sets of BNPE and SAPE call options respectively. For BNPE options, the FFT model achieves lower MAE and RMSE compared to the PINN model, indicating better absolute pricing accuracy. Moreover, the PINN model shows

Table 12: Comparison of calibrated variance-related parameters for the FFT and PINN option pricing models for European call options on SAPE.

Parameter	Optimal FFT Model Value	Optimal PINN Model Value
ν^*	0.063417	0.085265
κ_ν^*	4.150872	0.959796
θ_ν^*	0.067383	0.029323
σ_ν^*	0.747508	0.237246
ρ_2^*	-0.027635	-0.293631

Table 13: Error measures for BNPE training and test data sets

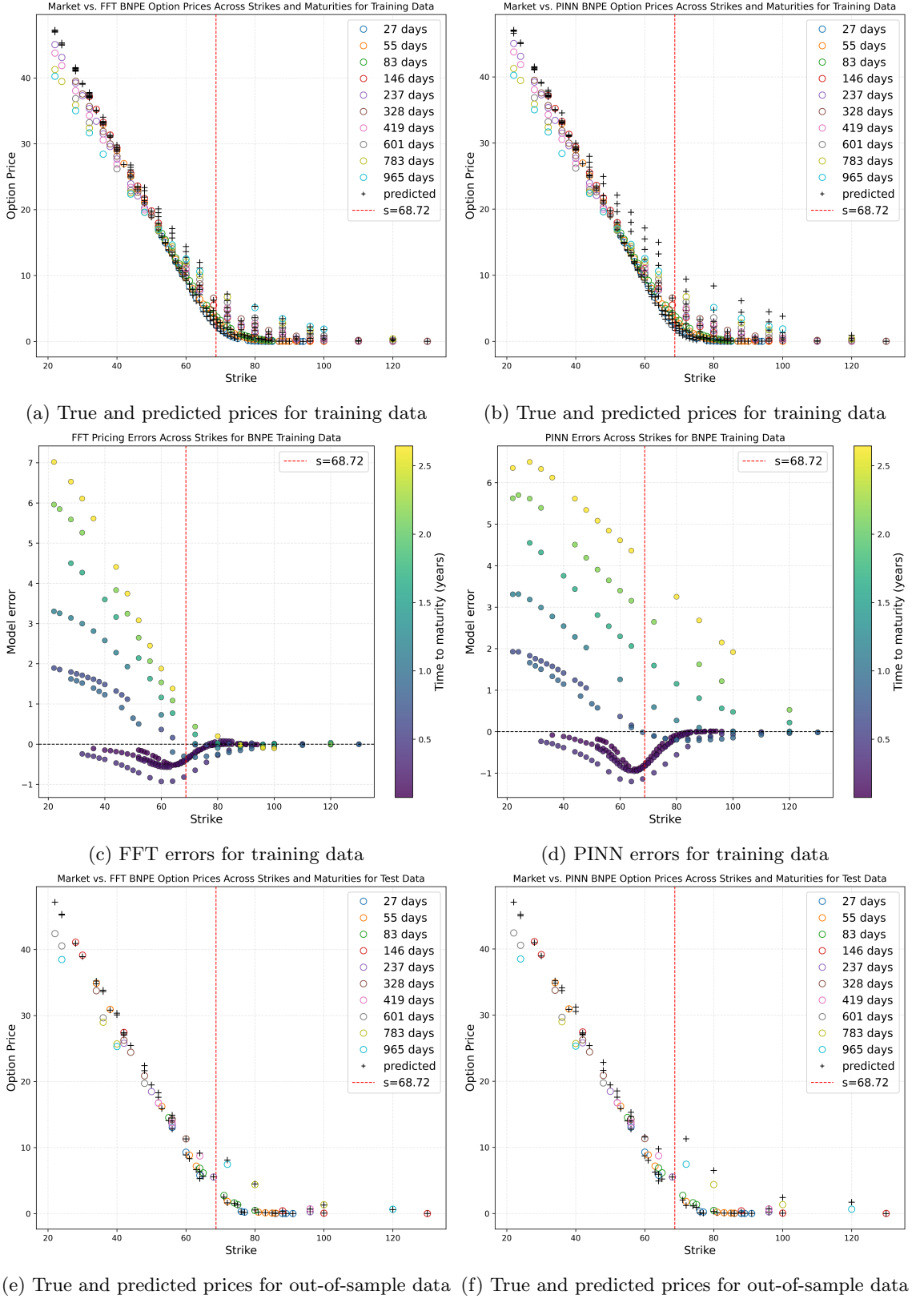
Training data			Test data		
Error metric	FFT error	PINN error	Error metric	FFT error	PINN error
MAE	0.847611	1.168454	MAE	0.931101	1.172423
RMSE	1.602870	1.862401	RMSE	1.819230	1.965502
MAPE	11.736420%	27.850090%	MAPE	13.285064%	27.356079%

Table 14: Error measures for SAPE training and test data sets

Training data			Test data		
Error metric	FFT error	PINN error	Error metric	FFT error	PINN error
MAE	0.484146	0.766512	MAE	0.475412	0.726603
RMSE	0.679406	1.131596	RMSE	0.637644	0.978481
MAPE	3.259376%	12.424769%	MAPE	2.798624%	10.336742%

significantly higher MAPE values, which suggests that relative errors are larger for out-of-the-money options. A similar pattern can be observed for SAPE options, where FFT consistently outperforms PINN in terms of MAE and RMSE.

Finally, figures 8 and 9 compare the FFT and PINN call option prices against market prices for European call options and show the corresponding pricing errors across strikes and maturities. The first row in each figure illustrates that both models capture the general shape of the option price curve, with prices decreasing as strike increases. However, we note that the PINN tends to deviate more than the FFT model, a behaviour also seen in the error tables 13 and 14. The second row in each figure shows the pricing error for the training data. FFT errors are relatively small, but tend to increase for smaller strikes, while PINN errors show a larger error dispersion. Moreover, both models exhibit larger pricing errors for when the time to maturity increases. Lastly, the third and fourth rows present out-of-sample results. We can observe that FFT maintains stable performance on the test set, wheras PINN shows higher variability and larger errors for extreme strikes. These patterns confirm the error metrics found in tables 13 and 14, where FFT achieves lower MAE and RMSE compared to PINN. Overall, the figures show that while both models reproduce the general price structure for both the training and test data, the FFT model provides more consistent accuracy across strikes and maturities.



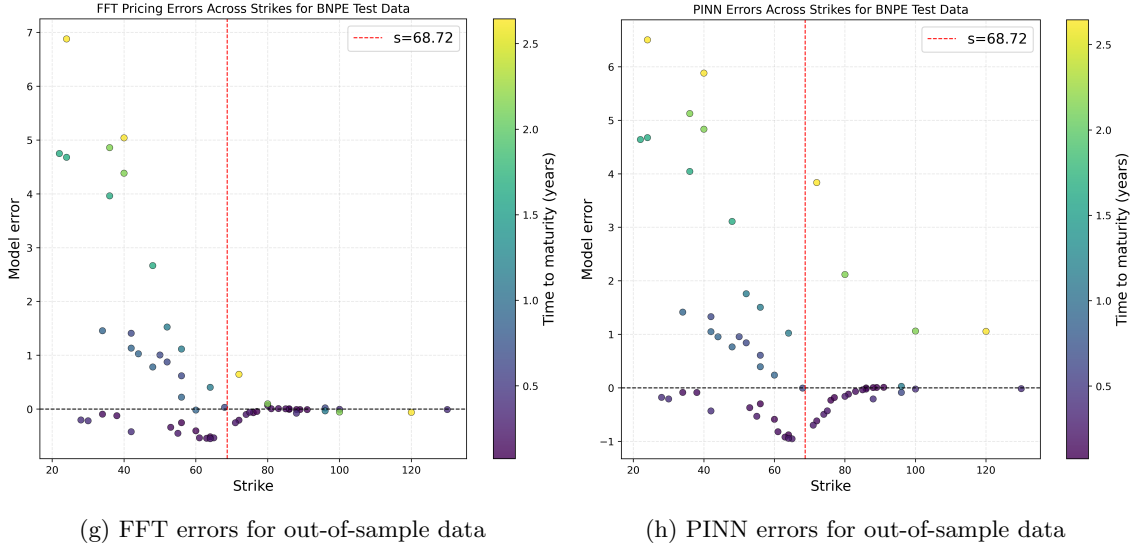
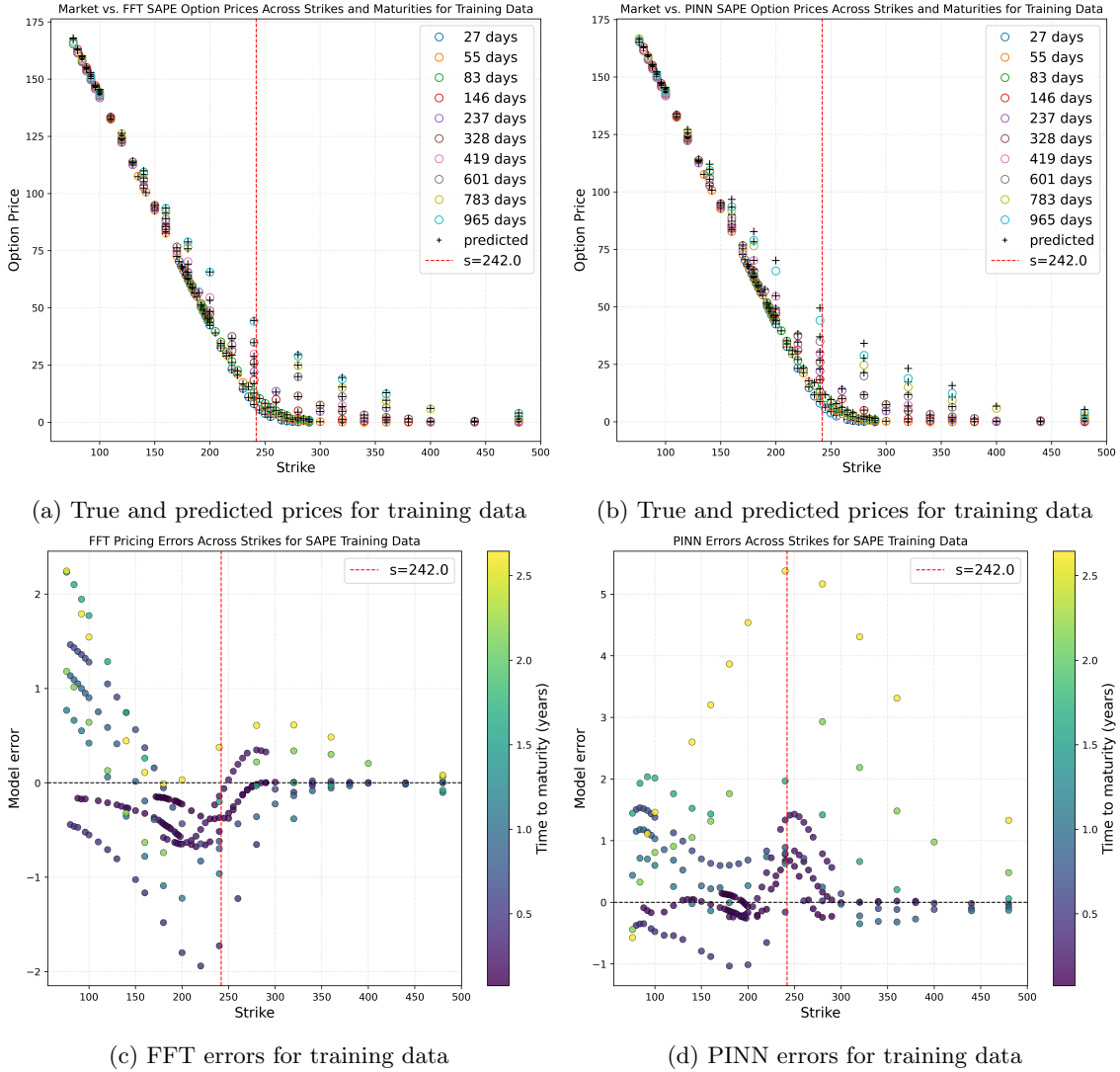
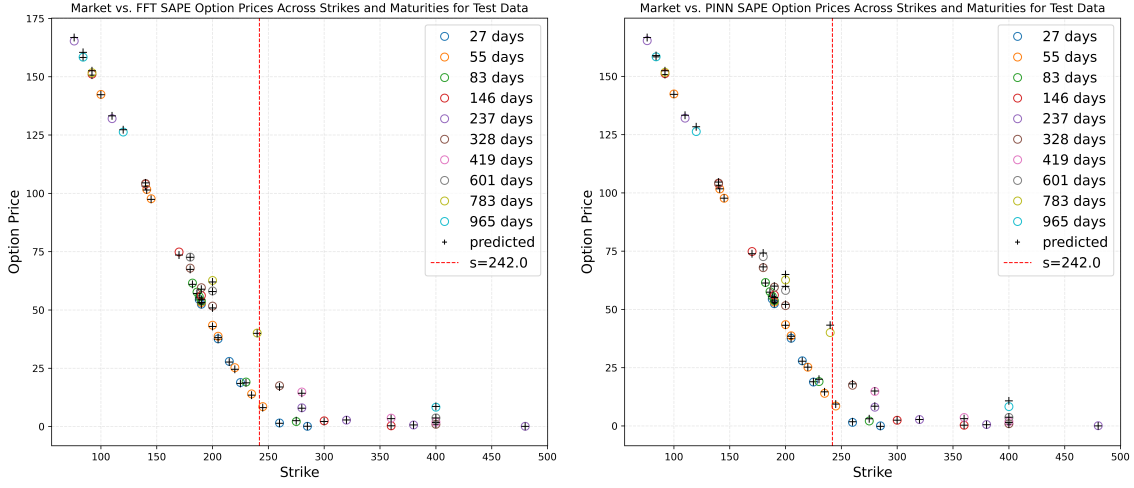
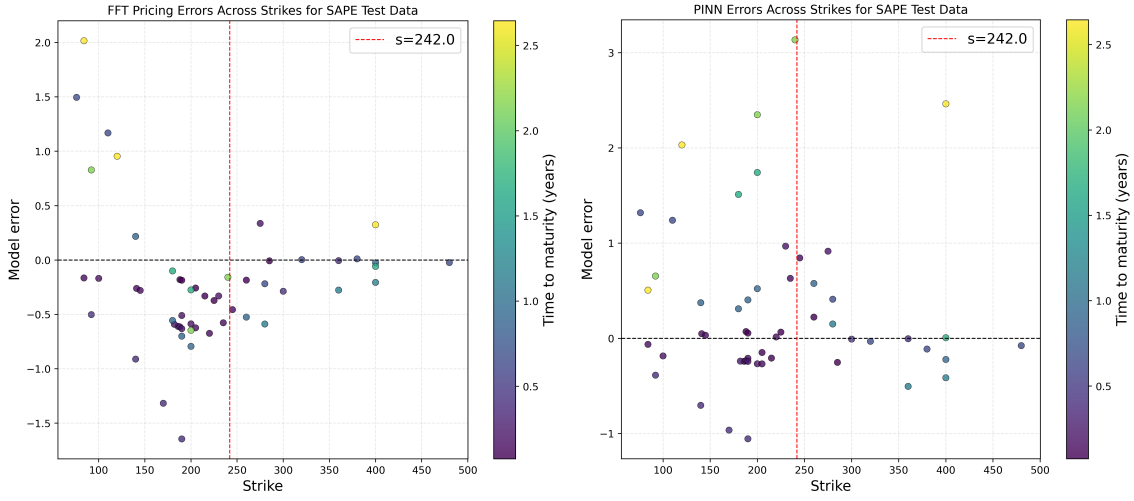


Figure 8: Comparison of FFT and PINN call option prices against market prices (rows 1 and 3) and their respective pricing errors (rows 2 and 4) across strikes for BNPE training and test data.





(e) True and predicted prices for out-of-sample data (f) True and predicted prices for out-of-sample data



(g) FFT errors for out-of-sample data

(h) PINN errors for out-of-sample data

Figure 9: Comparison of FFT and PINN call option prices against market prices (rows 1 and 3) and their respective pricing errors (rows 2 and 4) across strikes for SAPE training and test data.

8 Discussion

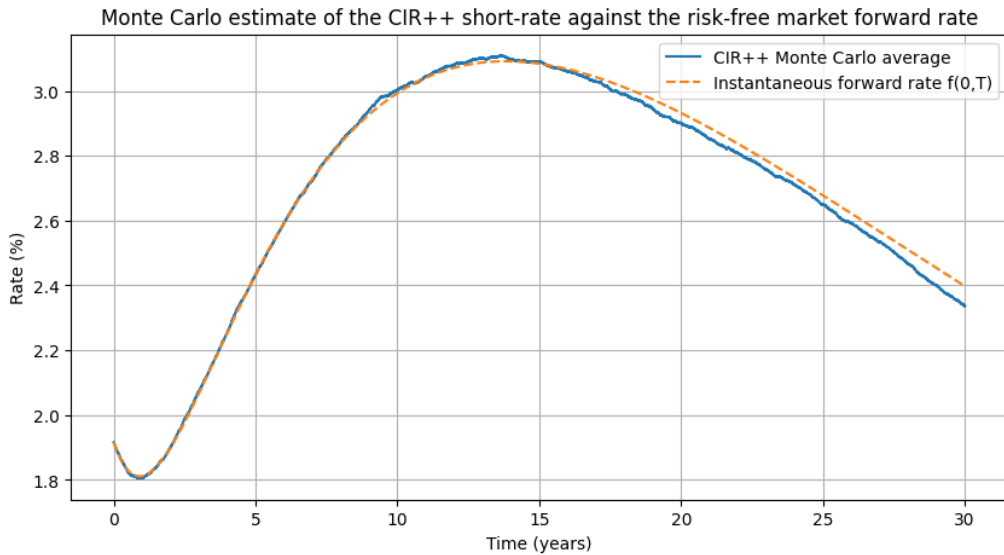
In this chapter, we analyze the results obtained from the calibration and pricing experiments. We assess the performance of the short-rate model and compare the accuracy and efficiency of the FFT and PINN approaches. Finally, we discuss the implications of these findings and highlight potential limitations and areas for improvement.

8.1 Short rate model evaluation

Beyond evaluating pricing accuracy through error metrics for swaptions, we assess the quality of the calibrated short-rate model by examining both the interpretability of its parameters and its consistency with theoretical properties particularly in view of proposition 3.3.

Proposition 3.3 states that for any $T > \tau$, the expected value of the short rate conditional on the filtration \mathcal{F}_τ and under \mathbb{Q}^T must equal the instantaneous forward rate $f(\tau, T)$. To validate this property, we simulate the CIR++ short-rate process under the T -forward measure (53) with parameters in table 5 and with 10'000 paths on a time grid with 10'951 points¹⁶. The numerical simulation is performed using the Euler-Maruyama method and we take the Monte Carlo mean at each timestep to get figure 10. The Euler-Maruyama scheme for the simulation of the short rate R can be found in appendix C. Figure 10 compares this Monte Carlo estimate (solid line) with the market-implied instantaneous forward curve under the Svensson model (dashed line) seen in figure 6. We see that the short-rate almost perfectly fits the forward rate, with a minor discrepancy at year 9 and a slight deviation from year 15. However, as our European call option data ranges from a month to 3 years, the discrepancies seen in figure 10 are not of concern to us as these happen well after year 3.

Figure 10: Monte Carlo estimate of the CIR++ short rate (solid line) compared with the risk-free market instantaneous forward rate $f(0, T)$ (dashed line) implied by the calibrated OIS term structure.



The error metrics for the swaption pricing model (43) compared to market data can be found in table 6. Both the MAE and RMSE indicate that absolute deviations are small for our short-rate model, with values of approximately 0.07% and 0.09% respectively. While these figures suggest good overall accuracy, it is important to note that pricing errors are not uniform across instruments. For instance swaptions with very low premiums of around 0.17% exhibit higher relative errors, sometimes approaching 30%, whereas instruments with larger premiums of 7% tend to be priced

¹⁶The choice of 10'951 points is deliberate as each point represents one calendar day, so that over a 30-year horizon the time grid covers $30 \times 365 + 1 = 10'951$ days, ensuring daily resolution for the simulation.

more accurately. This behaviour is in part due to the choice of the minimization function (97) used to calibrate the short rate model, as we seek to minimize the mean-square error and not the relative prices. Finally, the mean absolute percentage error (MAPE) of approximately 2.91% confirms that, on average, relative pricing errors remain rather small over the entire dataset.

Lastly, consider the values for the estimated values for the short-rate parameters r^* , κ_r^* , θ_r^* , and σ_r^* found in table 5. The initial short rate r is approximately 1.91%, which is consistent with ECB's policy rate on October 24, 2025. This shows that the model correctly reflects current market conditions at the calibration date. Moreover, recall that the CIR++ model is a mean-reverting process such that the parameters have economic interpretations. The speed of mean reversion, κ_r , determines the speed of mean-reversion towards the long-run equilibrium after shocks. In our case, $\kappa_r^* \approx 1.02$ which suggests that deviations from the long-run mean decay at moderate pace. This value implies that the short rate tends to revert toward equilibrium within roughly one year after shocks. The long-run mean θ_r^* is estimated at 3.25% and is noticeably higher than the current short rate. This indicates that the market anticipates a gradual upward drift in interest rates over the long term, reflecting expectations of normalization from historically low levels. Finally, the volatility parameter σ_r^* is approximately 2.58%, which represents moderate variability in the short rate process and is consistent with the relatively low uncertainty in the ECB's monetary policy outlook compared to more volatile markets.

In summary, the calibrated CIR++ model demonstrates theoretical consistency, interpretable parameters, and satisfactory pricing accuracy, making it a strong framework for modeling short rates.

8.2 Comparison of the FFT and PINN pricing models

When it comes to the comparison of the FFT against PINN pricing models for European call options, recall that we compare the models on identical short-rate parameters, data, constraints and objective. Both models are calibrated to market call prices by solving the constrained minimization problem (98) subject to the positivity constraint $\sigma_\nu^2 \leq 2\kappa_\nu\theta_\nu$ and bounds that keep parameters economically meaningful.

The resulting variance parameter estimates $\Theta_\nu^* = (\nu^*, \kappa_\nu^*, \theta_\nu^*, \sigma_\nu^*, \rho_2^*)$ show some large differences between the two approaches, see tables 11 and 12. For both underlyings, the PINN calibration shows a noticeably smaller long-run variance θ_ν^* and volatility-of-variance σ_ν^* than the FFT calibration, and it tends toward a lower mean-reversion κ_ν^* . In particular, the low mean-reversion is pronounced for BNPE and milder for SAPE. In terms of economical interpretation, the PINN therefore implies a smoother, less varying variance process than the FFT.

As a consequence, the models exhibit different error behaviour, see tables 13 and 14. Comparing the FFT model against the neural network model, one can observe that the FFT model is in overall more accurate both in-sample and out-of-sample. In particular, we note that the PINN model is worse at pricing options with smaller strikes when compared to the FFT model as can be seen in the MAPE errors. This occurs even though the objective function (98) puts a higher weight on low-priced options as we divide the error by the contracts' prices. In this case, the FFT model appears to handle this emphasis better than the current PINN configuration. The error plots in figures 8 and 9 confirm the metric-based findings. Both pricing models reproduce the monotone decline of call prices with the strike-maturity structure, yet FFT errors remain tightly clustered around smaller values than the PINN errors on both BNPE and SAPE data sets.

A contributing factor to the PINN's weaker performance compared to the FFT comes from the strike-rescaling used to re-purpose a network trained at a constant reference strike $K > 0$ to price option with a market strike $K' > 0$, see (85). Consider the option-pricing PDE (80), where the derivatives with respect to s are multiplied by quantities depending on s . Under the rescaling $s' := \frac{K}{K'}s$, we keep s and K fixed while varying the market strike K' , and observe that s' becomes small for large K' . This causes the PDE to be degenerate in the s' -direction as for small s' , both the drift, the diffusion, and the cross-variational terms depending of s' vanish. Consequently, the interior residual (89) is small and the optimizer under-penalizes errors in slope and curvature with respect to s' . Conversely, when K' is small, s' becomes large and the coefficients multiplying the

s' -gradient and s' -curvature grow by magnitudes of s' and $(s')^2$. The residual is therefore stiff for small K' such that small errors are amplified and the optimizer is driven to suppress curvature, yielding oversmoothed option price surfaces. After calibration, this can be seen in the form of lower estimates of the volatility-of-variance σ_ν and the long-run variance θ_ν . This effect can be seen in figure 9 and in particular in figure 8, where the PINN's curvature, or to be more precise the lack of it, becomes gradually more pronounced for smaller strikes and larger maturities. Moreover, note that we have limited ourselves to a feed-forward neural network with four layers and 512 hidden layers to solve the governing PDE using uniformly sampled data. It is therefore worth noting that different network architectures and sampling procedures may increase the PINNs accuracy.

On the FFT side, it is worth noting that the FFT pricing model itself is subject to numerical errors which may explain some of the errors seen in figures 8 and 9. Recall that the characteristic function under the T -forward measure requires solving a time-inhomogeneous Riccati system of ODEs, see proposition 5.11, where the functions Φ and Ψ_2 are computed numerically using a Runge-Kutta 4-5 method. Although this error is tolerance-driven, it is worth noting that reducing the tolerance results in a slower convergence, increasing the time needed to calibrate the FFT model. Lastly, the Fourier inversion in (62) is approximated on a finite grid with (78), where the integral over $[0, \infty)$ is truncated at $\beta = \eta N$. In our case, with $N = 4096$ and $\eta = 0.25$, the upper limit of the integral is 1024. Decreasing the grid's distance η and increasing N would give more precise estimates, but will take an infeasible amount of time when calibrating. Consequently, the choice of η and N represent a runtime-accuracy trade-off which one needs to consider when calibrating.

From a computational point of view, the runtime of both approaches differs noticeably. Although the FFT has no training phase, each underlying on each date must be calibrated by solving the Riccati ODEs Φ and Ψ_2 , in addition to computing the associated FFT grid. On the other hand, the PINN incurs a one-time training cost, after which the calibration process is very fast since calling the PINN takes constant time. Consequently, the entire training and calibration process the PINN takes around 35 minutes to run, while the FFT takes around 90 minutes for calibration, as seen in table 10. In simpler settings, such as Heston with a constant short rate where the numerical solution of ODEs is not required, the FFT provides fast and accurate European option prices. However, under more complex frameworks, the FFT model is still reliable but slows down a lot. Hence, for cases where one needs to price options for a broad universe of underlying stocks, PINNs provide a faster alternative than the FFT since pricing options after training the PINN is a task of a few seconds.

Overall, under the present setting, FFT delivers a better pricing accuracy and more stable out-of-sample behaviour on both BNPE and SAPE, whereas the PINN offers attractive speed once trained but tends to estimate smoother variance dynamics and exhibits larger percentage errors in the tails.

9 Conclusion

In this study, two approaches to pricing European options under a Heston-type variance with CIR++ stochastic short rates were compared, namely a Fast-Fourier-Transform-based (FFT) and a Physics-Informed-Neural-Networks-based (PINN) method. As there is little to no existing research on the Heston-CIR++ combination, we first developed necessary theory. In chapter 3, we constructed an affine term-structure model for the short rate, and derived a swaption formula used to calibrate the CIR++ parameters. In section 4, we derived the backward parabolic option-pricing PDE for the Heston-CIR++ setting, which served to train the PINN in chapter 6. Finally, in chapter 5, we obtained the characteristic function with the help of the affine transform formula and used the damped Carr-Madan inversion to end up with an FFT European call option pricing model.

When it comes to empirical findings, with short rate parameters estimated through Overnight Indexed Swaps (OIS) and swaptions, both models were tested on market data for European call options on BNP Paribas (BNPE) and SAP SE (SAPE). Across the in-sample and out-of-sample data, the FFT achieved lower errors than the PINN. This result is largely due to the PINN tending to learn smoother variance dynamics than the FFT and can be explained by the fact that we used only one strike price to train the PINN to then consider different strike prices by scaling the stock price accordingly. Computationally, however, the PINN evaluates in constant time and, in our setup, the training and calibration took around 35 minutes. On the other hand, the FFT took around 90 minutes for the calibration. Thus, the FFT sets the accuracy benchmark per asset and date, whereas PINN offers attractive speed at scale.

Future work should focus on strengthening the PINN approach and, in general, broadening the modeling scope. As discussed in chapter 7, training the network on log-prices of the underlying asset could improve the network's accuracy for small and large strikes, as this approach removes the dependence of PDE coefficients on the asset price. Another improvement could involve including gradient-based penalties into the loss function (90) to better capture slope and curvature as suggested by Czarnecki et al. (2017) and Yu et al. (2022). A hybrid strategy that integrates FFT-generated prices as additional training points may also improve long-maturity performance, though at the cost of increased runtime. Furthermore, a novel research conducted by Gao et al. (2025), wherein the authors introduce an *Adaptive Movement Sampling Physics-Informed Residual Network* (AM-PIRN) that dynamically re-distributes sampled points according to the evolving PDE residual, shows improved accuracy and robustness for the Heston option-pricing model compared to the standard PINN framework. It is worth noting, however, that the AM-PIRN is yet to be tested on real, market data and that the authors do not compare their model against a benchmark model such as the FFT model. Finally, extending the framework to include jump-diffusion models, such as Lévy models, would allow for a more realistic representation of volatility surfaces compared to pure Heston-type dynamics.

Bibliography

- Black, Fischer and Myron Scholes (1973). ‘The pricing of options and corporate liabilities’. In: *Journal of political economy* 81.3, pp. 637–654.
- Heston, Steven L. (1993). ‘A closed-form solution for options with stochastic volatility with applications to bond and currency options’. In: *The review of financial studies* 6.2, pp. 327–343.
- Carr, Peter and Dilip Madan (1999). ‘Option valuation using the fast Fourier transform’. In: *Journal of computational finance* 2.4, pp. 61–73.
- Cooley, James W. and John W. Tukey (1965). ‘An algorithm for the machine calculation of complex Fourier series’. In: *Mathematics of computation* 19.90, pp. 297–301.
- Raissi, Maziar, Paris Perdikaris and George Em Karniadakis (2017). ‘Physics informed deep learning (part i): Data-driven solutions of nonlinear partial differential equations’. In: *arXiv preprint arXiv:1711.10561*.
- Hainaut, Donatiens and Alex Casas (2024). ‘Option pricing in the Heston model with physics inspired neural networks’. In: *Annals of Finance* 20.3, pp. 353–376.
- Jarrow, Robert A. (2021). *Continuous-time asset pricing theory*. Springer.
- Brigo, Damiano and Fabio Mercurio (2006). *Interest Rate Models: Theory and Practice: With Smile, Inflation and Credit*. Second. Springer Finance. Springer Berlin, Heidelberg.
- Filipović, Damir (2009). *Term-Structure Models: A Graduate Course*. Springer Finance. Springer Berlin, Heidelberg.
- Evans, Lawrence C. (2013). *An Introduction to Stochastic Differential Equations*. Graduate Studies in Mathematics. American Mathematical Society.
- Delbaen, Freddy and Walter Schachermayer (2006). ‘A general version of the fundamental theorem of asset pricing (1994)’. In: *The Mathematics of Arbitrage*. Springer, pp. 149–205.
- Svensson, Lars E.O. (1994). *Estimating and interpreting forward interest rates: Sweden 1992-1994*.
- Brigo, Damiano and Fabio Mercurio (2001). ‘A deterministic–shift extension of analytically–tractable and time–homogeneous short–rate models’. In: *Finance and Stochastics* 5.3, pp. 369–387.
- Cox, John C., Jr. Ingersoll Jonathan E. and Stephen A. Ross (Mar. 1985). ‘A Theory of the Term Structure of Interest Rates’. In: *Econometrica* 53.2, pp. 385–407. DOI: 10.2307/1911242. URL: <https://www.jstor.org/stable/1911242>.
- Jeanblanc, Monique, Marc Yor and Marc Chesney (2009). *Mathematical Methods for Financial Markets*. Springer Finance. Springer-Verlag London Limited.
- Jamshidian, Farshid (1989). ‘An Exact Bond Option Formula’. In: *The Journal of Finance* 44.1, pp. 205–209. (Visited on 15th Dec. 2025).
- Jin, Xiaowei et al. (2021). ‘NSFnets (Navier-Stokes flow nets): Physics-informed neural networks for the incompressible Navier-Stokes equations’. In: *Journal of Computational Physics* 426, p. 109951.
- Norambuena, Ariel et al. (2024). ‘Physics-informed neural networks for quantum control’. In: *Physical Review Letters* 132.1.
- Cuomo, Salvatore et al. (2022). ‘Scientific machine learning through physics-informed neural networks: Where we are and what’s next’. In: *Journal of Scientific Computing* 92.3, p. 88.
- Lawal, Zaharaddeen Karami et al. (2022). ‘Physics-Informed Neural Network (PINN) Evolution and Beyond: A Systematic Literature Review and Bibliometric Analysis’. In: *Big Data and Cognitive Computing* 6.4, p. 140. DOI: 10.3390/bdcc6040140. URL: <https://doi.org/10.3390/bdcc6040140>.
- McCulloch, Warren S. and Walter Pitts (1943). ‘A logical calculus of the ideas immanent in nervous activity’. In: *The bulletin of mathematical biophysics* 5.4, pp. 115–133.
- Rosenblatt, Frank (1958). ‘The perceptron: a probabilistic model for information storage and organization in the brain.’ In: *Psychological review* 65.6.
- Rosenblatt, Frank et al. (1962). *Principles of neurodynamics: Perceptrons and the theory of brain mechanisms*. Vol. 55. Spartan books Washington, DC.
- Hornik, Kurt (1991). ‘Approximation capabilities of multilayer feedforward networks’. In: *Neural networks* 4.2, pp. 251–257.
- Leshno, Moshe et al. (1993). ‘Multilayer feedforward networks with a nonpolynomial activation function can approximate any function’. In: *Neural networks* 6.6, pp. 861–867.
- Sirignano, Justin and Konstantinos Spiliopoulos (2018). ‘DGM: A deep learning algorithm for solving partial differential equations’. In: *Journal of computational physics* 375, pp. 1339–1364.

-
- Baydin, Atilim Gunes et al. (2018). ‘Automatic differentiation in machine learning: a survey’. In: *Journal of machine learning research* 18.153, pp. 1–43.
- Damadi, Saeed et al. (2023). ‘The Backpropagation algorithm for a math student’. In: *2023 International Joint Conference on Neural Networks (IJCNN)*. IEEE, pp. 01–09.
- Kingma, Diederik P. (2014). ‘Adam: A method for stochastic optimization’. In: *arXiv preprint arXiv:1412.6980*.
- Bor, Gonchigsuren (2025). *OptionPricingProject*. URL: <https://github.com/goshabor/OptionPricingProject>.
- Banholzer, Dirk, Jörg Fliege and Ralf Werner (2024). ‘Revisiting the fitting of the Nelson–Siegel and Svensson models’. In: *Optimization* 73.10, pp. 3021–3053.
- ECB (2025). *Euro area yield curves*. https://www.ecb.europa.eu/stats/financial_markets_and_interest_rates/euro_area_yield_curves/html/index.en.html. Accessed: 2025-10-24.
- Liu, Dong C and Jorge Nocedal (1989). ‘On the limited memory BFGS method for large scale optimization’. In: *Mathematical programming* 45.1, pp. 503–528.
- Storn, Rainer and Kenneth Price (1997). ‘Differential evolution—a simple and efficient heuristic for global optimization over continuous spaces’. In: *Journal of global optimization* 11.4, pp. 341–359.
- Czarnecki, Wojciech M. et al. (2017). ‘Sobolev training for neural networks’. In: *Advances in neural information processing systems* 30.
- Yu, Jeremy et al. (2022). ‘Gradient-enhanced physics-informed neural networks for forward and inverse PDE problems’. In: *Computer Methods in Applied Mechanics and Engineering* 393, p. 114823.
- Gao, Qinjiao et al. (2025). ‘Adaptive Movement Sampling Physics-Informed Residual Network (AM-PIRN) for Solving Nonlinear Option Pricing models’. In: *arXiv preprint arXiv:2504.03244*.
- Björk, Tomas (2004). *Arbitrage Theory in Continuous Time*. Oxford University Press.

A Martingales and the martingale representation theorem

Define the filtered probability space $(\Omega, \mathcal{F}, \{\mathcal{F}_t\}_{t \in [0, T]}, \mathbb{P})$ for some finite T , and let X be a random process in continuous time. The following theory is taken from Björk (2004).

Definition A.1 (Martingale, see Björk (2004, Definition 4.6)). *The process $X = \{X(t)\}_{t \in [0, T]}$ is an \mathcal{F}_t -martingale if*

(i) *X is adapted to the filtration $\{\mathcal{F}_t\}_{t \in [0, T]}$.*

(ii) *For all t*

$$\mathbb{E}[|X(t)|] < \infty.$$

(iii) *For all s and t with $0 \leq s \leq t$ the following relation holds*

$$X(s) = \mathbb{E}_{\mathbb{P}}[X(t) \mid \mathcal{F}_s].$$

Theorem A.2 (Martingale representation theorem, see Björk (2004, Theorem 11.2)). *Let $M = \{M(t)\}_{t \in [0, T]}$ be a square-integrable martingale process with respect to the filtration $\{\mathcal{F}_t\}_{t \in [0, T]}$ generated by the standard Brownian motion $W \in \mathbb{R}$. Then, there exists an \mathcal{F}_t -adapted process $K = \{K(t)\}_{t \in [0, T]}$ such that*

(i)

$$\mathbb{E} \left[\int_0^T K_s^2 ds \right] < \infty \tag{99}$$

(ii)

$$\forall t \in [0, T], \quad M_t = M_0 + \int_0^t K_s dW_s \quad a.s. \tag{100}$$

Remark A.3. *The above result is the one-dimensional version of the martingale representation theorem stated in Björk (2004, Theorem 11.2), formulated here for a scalar Brownian motion and its natural filtration. In Björk (2004), the theorem is presented in a more general setting, but the essential structure is identical to theorem A.2.*

B Some Useful Theorems

In this appendix, well-known theorems used throughout the paper are presented.

B.1 Itô's Lemma

Lemma B.1 (Itô's Lemma in n dimensions, see Evans (2013, Chapter 4.4.2)). *Suppose that the stochastic process $\mathbf{X} \in \mathbb{R}^n$ has a stochastic differential*

$$d\mathbf{X}(t) = \mathbf{b}(t, \mathbf{X})dt + \mathbf{B}(t, \mathbf{X})d\mathbf{W}(t),$$

where $\mathbf{b} \in \mathbb{R}^n$, $\mathbf{B}(\mathbf{X}, t) \in \mathbb{R}^{n \times m}$, and $\mathbf{W} \in \mathbb{R}^m$. Let $u : \mathbb{R} \times [0, T] \rightarrow \mathbb{R}$ be continuous, with continuous partial derivatives $\partial_t u$, $\partial_{x_j} u$, $\partial_{x_j x_k} u$ for $j, k = 1, \dots, n$. Then

$$du(t, \mathbf{X}(t)) = \partial_t u dt + \sum_{j=1}^n \partial_{x_j} u d\mathbf{X}_j(t) + \frac{1}{2} \sum_{j,k=1}^n \partial_{x_j x_k} u \sum_{\ell=1}^m \mathbf{B}_{j\ell} \mathbf{B}_{k\ell} dt,$$

where the argument of the partial derivatives of u is $(\mathbf{X}(t), t)$.

B.2 The Feynman-Kac Theorem

Theorem B.2 (The Feynman-Kac Theorem, see Björk (2004, Proposition 5.5)). *Let τ be the initial time of a stochastic process and assume that the function g is a solution to the boundary value problem*

$$\begin{aligned} \partial_\tau g(\tau, x) + \mu(\tau, x) \partial_x g + \frac{1}{2} \sigma^2(\tau, x) \partial_{xx} g(\tau, x) &= 0, \\ g(T, x) &= h(x). \end{aligned}$$

Assume furthermore that the process

$$\sigma(t, X(t)) \partial_x g(t, X(t))$$

is in L^2 , where X is defined below. Then, g has the representation

$$g(\tau, x) = \mathbb{E}[h(X(T)) \mid X(\tau) = x],$$

where X satisfies the SDE

$$\begin{aligned} dX(t) &= b(t, X(t)) dt + \sigma(t, X(t)) dW(t), \\ X(\tau) &= x. \end{aligned}$$

B.3 Girsanov's Change of Measure Theorem

Theorem B.3 (Girsanov's Theorem, see Jarrow (2021, Theorem 5)). *Let W be a standard Brownian motion on $(\Omega, \mathcal{F}, \{\mathcal{F}\}_{t \in [0, T]}, \mathbb{P})$ and let $\theta = \{\theta(t)\}_{t \in [\tau, T]}$ be an adapted process satisfying the Novikov condition*

$$\mathbb{E}_{\mathbb{P}} \left[e^{\frac{1}{2} \int_{\tau}^T \theta^2(u) du} \right] < \infty, \tag{101}$$

Then, the process $L = \{L(t)\}_{t \in [\tau, T]}$ defined by

$$L(t) = e^{-\frac{1}{2} \int_{\tau}^t \theta^2(u) du - \int_{\tau}^t \theta_u dW(u)} \tag{102}$$

is a martingale under the \mathbb{P} -measure. Moreover, under the probability measure \mathbb{Q} equivalent to \mathbb{P} on \mathcal{F}_T , defined by

$$\frac{d\mathbb{Q}}{d\mathbb{P}} = L(T) \quad \text{on } \mathcal{F}_T,$$

the process

$$W^{\mathbb{Q}}(t) = W^{\mathbb{P}}(t) + \int_{\tau}^t \theta(u) du \quad (103)$$

is an \mathcal{F}_t -Brownian motion under \mathbb{Q} .

Remark B.4. The above result is a slight modification of the theorem given in Jarrow (2021, Theorem 5). In all essence, however, both theorems are equivalent.

B.4 Bayes' Theorem

Theorem B.5 (Bayes' Theorem, see Björk (2004, Proposition B.41)). Assume that X is a random variable on $(\Omega, \mathcal{F}, \mathbb{P})$, and let \mathbb{Q} be another probability measure on (Ω, \mathcal{F}) with Radon-Nikodym derivative

$$L = \frac{d\mathbb{Q}}{d\mathbb{P}} \quad \text{on } \mathcal{F}.$$

Assume that $X \in L^1(\Omega, \mathcal{F}, \mathbb{Q})$ and that \mathcal{G} is a sigma-algebra with $\mathcal{G} \subseteq \mathcal{F}$. Then

$$\mathbb{E}_{\mathbb{Q}}[X | \mathcal{G}] = \frac{\mathbb{E}_{\mathbb{P}}[L \cdot X | \mathcal{G}]}{\mathbb{E}_{\mathbb{P}}[L | \mathcal{G}]}, \quad \mathbb{Q} - \text{a.s..} \quad (104)$$

C Numerical simulation of SDEs and Monte Carlo approximation

C.1 Euler–Maruyama approximation to SDEs

Consider the probability space $(\Omega, \mathcal{F}, \{\mathcal{F}\}_{t \in [\tau, T]}, \mathbb{Q}^T)$ and recall that the short-rate dynamics of the CIR++ process under the given probability space are given by

$$dR(t) = (\kappa_r(\theta_r - R(t) + \psi(t)) + \psi'(t) - \sigma_r^2(R(t) - \psi(t))b^2(t, T)) dt + \sigma_r \sqrt{R(t) - \psi(t)} dW^{R, \mathbb{Q}^T}(t),$$

with $R(\tau) = r$ as the initial condition and where $x_0, \kappa_r, \theta_r, \sigma_r > 0$ are real-valued, constant parameters, $\psi(t)$ is a deterministic function of t , and $r = x_0 + \psi(\tau)$. With $R(t) = \tilde{X}(t) + \psi(t)$ for $t \in [\tau, T]$, the model reads as

$$\begin{cases} d\tilde{X}(t) = (\kappa_r(\theta_r - \tilde{X}(t)) - \sigma_r^2 b^2(t, T)\tilde{X}(t)) dt + \sigma_r \sqrt{\tilde{X}(t)} dW^{R, \mathbb{Q}}(t), & \tilde{X}(\tau) = x_0 \\ R(t) = \tilde{X}(t) + \psi(t), & R(\tau) = r. \end{cases}$$

Due to the lack of a closed-form solution for the CIR++ process, a numerical simulation is needed. Therefore, consider the Euler–Maruyama scheme used for the simulation of R , found in algorithm 1.

Algorithm 1 Euler–Maruyama scheme for the simulation of CIR++ short-rate paths under \mathbb{Q}^T

Input: Parameter vector $\Theta_r = (x_0, \kappa_r, \theta_r, \sigma_r)$

Initial time τ and maturity T

Number of time points n_{grid}

Number of simulated paths n_{sim}

Output: Time grid $(t_k)_{k=0}^{n_{\text{grid}}}$ and short-rate paths $R_{t_k}^{(j)}$, $j = 1, \dots, n_{\text{sim}}$, $k = 0, \dots, n_{\text{grid}}$

1: **Construct** equidistant time grid $t_k \leftarrow k\Delta t$ for $k = 0, \dots, n_{\text{grid}}$, where $\Delta t \leftarrow \frac{T-\tau}{n_{\text{grid}}}$

2: **Initialise** matrices $\tilde{X} \in \mathbb{R}^{n_{\text{sim}} \times (n_{\text{grid}}+1)}$ and $R \in \mathbb{R}^{n_{\text{sim}} \times (n_{\text{grid}}+1)}$

3: **Set** $\tilde{X}_{t_0}^{(j)} \leftarrow x_0$ for all $j = 1, \dots, n_{\text{sim}}$

4: **Generate** independent Gaussian increments $\Delta W_k^{(j)} \sim \mathcal{N}(0, \Delta t)$ for $j = 1, \dots, n_{\text{sim}}$ and $k = 0, \dots, n_{\text{grid}}$

5: **for** $k = 1$ **to** n_{grid} **do**

6: **for** $j = 1$ **to** n_{sim} **do**

7: $\tilde{X}_{t_k}^{(j)} \leftarrow \tilde{X}_{t_{k-1}}^{(j)} + (\kappa_r(\theta_r - \tilde{X}_{t_{k-1}}^{(j)}) - \sigma_r^2 b^2(t_{k-1}, T)\tilde{X}_{t_{k-1}}^{(j)})\Delta t + \sigma_r \sqrt{\tilde{X}_{t_{k-1}}^{(j)}} \Delta W_{t_{k-1}}^{(j)}.$

8: **end for**

9: **end for**

10: **Compute** short-rate paths $R_{t_k}^{(j)} \leftarrow \tilde{X}_{t_k}^{(j)} + \psi(t_k)$ for all $j = 1, \dots, n_{\text{sim}}$, $k = 0, \dots, N$

11: **Return** time grid $(t_k)_{k=0}^N$ and matrix R .

C.2 Monte–Carlo approximation

Once the short-rate dynamics have been discretized by the Euler–Maruyama scheme in algorithm 1, expectations under the forward measure \mathbb{Q}^T are computed by Monte–Carlo averaging. Let $R_{t_k}^{(j)}$, $j = 1, \dots, n_{\text{sim}}$ denote the simulated CIR++ short-rate paths on the time grid $t_0, \dots, t_{n_{\text{grid}}}$ returned by the algorithm. Moreover, recall that by proposition 3.3, the \mathbb{Q}^T -expectation of $R(t_k)$ conditional on \mathcal{F}_τ must be equal to the instantaneous forward rate $f(\tau, t_k)$, that is,

$$f(\tau, t_k) = \mathbb{E}_{\mathbb{Q}^T}[R(t_k) | \mathcal{F}_\tau], \quad k = 0, \dots, n_{\text{grid}}.$$

Then the Monte–Carlo estimator of $f(\tau, t_k)$ is given by

$$\hat{f}(\tau, t_k) = \frac{1}{n_{\text{sim}}} \sum_{j=1}^{n_{\text{sim}}} R_{t_k}^{(j)}, \quad k = 0, \dots, n_{\text{grid}}.$$

D Market data

In this appendix, we present the market data used for the practical implementation. Specifically, one can find market data for financial contracts such as OIS, swaptions, and European call options on stocks of BNP Paribas, and of SAP SE. Note that the data presented below is, by the terms and conditions of the London Stock Exchange Group, *not to be freely distributed*.

D.1 OIS data

Table 15: EUR OIS par swap rates on October 24th, 2025. The suffixes "W", "M", and "Y" means week, month(s) and year(s), respectively.

Start Date	End Date	Swap Tenor	Swap rate (%)
2025-10-24	2025-10-31	1W	1.928
	2025-11-24	1M	1.927
	2025-12-24	2M	1.928
	2026-01-26	3M	1.922
	2026-02-24	4M	1.917
	2026-03-24	5M	1.913
	2026-04-24	6M	1.912
	2026-07-24	9M	1.919
	2026-10-26	1Y	1.927
	2027-10-25	2Y	2.014
	2028-10-24	3Y	2.116
	2029-10-24	4Y	2.212
	2030-10-24	5Y	2.297
	2031-10-24	6Y	2.366
	2032-10-25	7Y	2.420
	2033-10-24	8Y	2.461
	2034-10-24	9Y	2.493
	2035-10-24	10Y	2.517
	2036-10-26	11Y	2.534
	2037-10-25	12Y	2.546
	2038-10-25	13Y	2.555
	2039-10-24	14Y	2.561
	2040-10-24	15Y	2.566
	2041-10-24	16Y	2.685
	2042-10-24	17Y	2.702
	2043-10-26	18Y	2.717
	2044-10-24	19Y	2.729
	2045-10-24	20Y	2.738
	2046-10-24	21Y	2.744
	2047-10-24	22Y	2.748
	2048-10-26	23Y	2.751
	2049-10-25	24Y	2.752
	2050-10-24	25Y	2.752
	2051-10-24	26Y	2.752
	2052-10-24	27Y	2.751
	2053-10-24	28Y	2.749
	2054-10-26	29Y	2.748
	2055-10-25	30Y	2.747

D.2 Swaptions data

Table 16: Market and model swaption prices (in percent) on October 24th, 2025. The suffix "Y" means year(s).

Date of Maturity	Tenor	Strike (%)	Price (%)	Model Price (%)	Model Error (%)
2026-10-24	1Y	2.043	0.172	0.239	0.067
	2Y	2.143	0.387	0.445	0.059
	3Y	2.235	0.596	0.646	0.050
	4Y	2.315	0.807	0.854	0.047
	5Y	2.388	1.023	1.069	0.045
	6Y	2.458	1.227	1.278	0.051
	7Y	2.527	1.431	1.472	0.040
	8Y	2.590	1.633	1.655	0.022
	9Y	2.650	1.833	1.818	0.015
	10Y	2.706	2.034	1.962	0.072
	11Y	2.757	2.217	2.090	0.126
	12Y	2.802	2.400	2.208	0.192
	13Y	2.839	2.580	2.324	0.256
	14Y	2.871	2.754	2.431	0.323
	15Y	2.895	2.925	2.547	0.379
2027-10-24	1Y	2.245	0.296	0.333	0.037
	2Y	2.334	0.604	0.656	0.052
	3Y	2.410	0.910	0.983	0.073
	4Y	2.479	1.207	1.313	0.106
	5Y	2.547	1.510	1.633	0.123
	6Y	2.615	1.802	1.933	0.131
	7Y	2.676	2.091	2.218	0.127
	8Y	2.735	2.376	2.477	0.102
	9Y	2.790	2.663	2.712	0.049
	10Y	2.839	2.956	2.926	0.030
	11Y	2.882	3.213	3.126	0.087
	12Y	2.917	3.464	3.319	0.145
	13Y	2.947	3.706	3.500	0.206
	14Y	2.969	3.941	3.687	0.254
	15Y	2.985	4.170	3.870	0.300
2028-10-24	1Y	2.425	0.384	0.419	0.035
	2Y	2.495	0.771	0.841	0.070
	3Y	2.561	1.146	1.262	0.116
	4Y	2.627	1.511	1.671	0.160
	5Y	2.694	1.871	2.055	0.184
	6Y	2.755	2.223	2.420	0.196
	7Y	2.812	2.571	2.756	0.185
	8Y	2.866	2.914	3.064	0.150
	9Y	2.914	3.256	3.348	0.092
	10Y	2.956	3.601	3.613	0.012
	11Y	2.989	3.907	3.869	0.038
	12Y	3.017	4.199	4.109	0.090
	13Y	3.036	4.481	4.353	0.128
	14Y	3.050	4.754	4.590	0.164
	15Y	3.058	5.020	4.824	0.196
2029-10-24	1Y	2.567	0.452	0.502	0.049
	2Y	2.632	0.901	1.001	0.100
	3Y	2.698	1.332	1.485	0.153
	4Y	2.766	1.749	1.941	0.192
	5Y	2.826	2.162	2.375	0.213
	6Y	2.883	2.563	2.778	0.215

Date of Maturity	Swap Tenor	Strike (%)	Price (%)	Model Price (%)	Model Error (%)
2030-10-24	7Y	2.937	2.953	3.148	0.195
	8Y	2.984	3.339	3.492	0.153
	9Y	3.024	3.713	3.814	0.101
	10Y	3.055	4.097	4.124	0.028
	11Y	3.081	4.441	4.417	0.024
	12Y	3.098	4.766	4.710	0.056
	13Y	3.109	5.080	4.995	0.086
	14Y	3.114	5.385	5.274	0.112
	15Y	3.116	5.677	5.545	0.132
	1Y	2.698	0.511	0.568	0.057
	2Y	2.766	1.014	1.119	0.105
	3Y	2.836	1.489	1.639	0.151
	4Y	2.896	1.952	2.136	0.184
	5Y	2.952	2.407	2.598	0.191
	6Y	3.005	2.839	3.025	0.186
2031-10-24	7Y	3.050	3.261	3.423	0.162
	8Y	3.089	3.674	3.797	0.123
	9Y	3.118	4.075	4.156	0.081
	10Y	3.141	4.482	4.495	0.014
	11Y	3.155	4.847	4.833	0.013
	12Y	3.163	5.193	5.161	0.032
	13Y	3.166	5.528	5.481	0.047
	14Y	3.165	5.847	5.791	0.056
	15Y	3.161	6.156	6.089	0.067
	1Y	2.836	0.555	0.612	0.056
	2Y	2.908	1.097	1.191	0.094
	3Y	2.965	1.608	1.743	0.135
	4Y	3.021	2.105	2.260	0.155
	5Y	3.072	2.591	2.739	0.148
2032-10-24	6Y	3.115	3.053	3.187	0.135
	7Y	3.152	3.499	3.609	0.110
	8Y	3.178	3.934	4.014	0.079
	9Y	3.199	4.361	4.396	0.035
	10Y	3.209	4.788	4.775	0.013
	11Y	3.214	5.173	5.142	0.031
	12Y	3.214	5.539	5.499	0.040
	13Y	3.210	5.887	5.845	0.042
	14Y	3.203	6.224	6.177	0.047
	15Y	3.194	6.548	6.496	0.052
	1Y	2.982	0.590	0.633	0.043
	2Y	3.033	1.166	1.239	0.073
	3Y	3.086	1.708	1.806	0.098
	4Y	3.136	2.233	2.334	0.100
2033-10-24	5Y	3.177	2.745	2.829	0.084
	6Y	3.210	3.224	3.295	0.071
	7Y	3.233	3.694	3.742	0.047
	8Y	3.251	4.150	4.164	0.014
	9Y	3.258	4.595	4.582	0.013
	10Y	3.259	5.041	4.986	0.055
	11Y	3.255	5.444	5.378	0.066
	12Y	3.248	5.820	5.757	0.063
	13Y	3.238	6.183	6.121	0.063
	14Y	3.227	6.532	6.470	0.062
	15Y	3.213	6.866	6.805	0.061
	1Y	3.086	0.615	0.654	0.040
	2Y	3.141	1.216	1.269	0.053

Date of Maturity	Swap Tenor	Strike (%)	Price (%)	Model Price (%)	Model Error (%)
2034-10-24	3Y	3.190	1.779	1.842	0.064
	4Y	3.229	2.325	2.381	0.056
	5Y	3.260	2.850	2.889	0.039
	6Y	3.280	3.347	3.376	0.029
	7Y	3.294	3.832	3.837	0.005
	8Y	3.297	4.301	4.291	0.010
	9Y	3.295	4.759	4.729	0.030
	10Y	3.287	5.218	5.154	0.063
	11Y	3.277	5.626	5.565	0.061
	12Y	3.264	6.014	5.958	0.056
	13Y	3.250	6.385	6.336	0.049
	14Y	3.234	6.741	6.698	0.043
	15Y	3.218	7.083	7.041	0.042
	1Y	3.197	0.635	0.659	0.024
	2Y	3.244	1.256	1.276	0.020
2035-10-24	3Y	3.280	1.837	1.856	0.019
	4Y	3.307	2.393	2.403	0.010
	5Y	3.323	2.930	2.928	0.002
	6Y	3.333	3.442	3.425	0.017
	7Y	3.331	3.938	3.914	0.024
	8Y	3.325	4.419	4.385	0.034
	9Y	3.314	4.888	4.841	0.047
	10Y	3.299	5.348	5.282	0.067
	11Y	3.284	5.766	5.704	0.062
	12Y	3.267	6.160	6.108	0.052
	13Y	3.248	6.537	6.496	0.041
	14Y	3.230	6.899	6.864	0.035
	15Y	3.212	7.242	7.212	0.029
	1Y	3.293	0.652	0.657	0.006
	2Y	3.324	1.292	1.277	0.015
2036-10-24	3Y	3.347	1.880	1.862	0.018
	4Y	3.357	2.446	2.423	0.023
	5Y	3.363	2.996	2.955	0.041
	6Y	3.357	3.516	3.476	0.040
	7Y	3.346	4.022	3.979	0.043
	8Y	3.331	4.513	4.465	0.048
	9Y	3.313	4.985	4.934	0.050
	10Y	3.294	5.451	5.383	0.068
	11Y	3.274	5.873	5.814	0.060
	12Y	3.254	6.272	6.226	0.045
	13Y	3.233	6.653	6.617	0.036
	14Y	3.213	7.015	6.988	0.026
	15Y	3.194	7.359	7.336	0.023
	1Y	3.355	0.665	0.657	0.007
	2Y	3.375	1.308	1.278	0.030

Date of Maturity	Swap Tenor	Strike (%)	Price (%)	Model Price (%)	Model Error (%)
2037-10-24	14Y	3.185	7.076	7.077	0.002
	15Y	3.167	7.425	7.421	0.004
	1Y	3.395	0.666	0.656	0.010
	2Y	3.392	1.317	1.285	0.032
	3Y	3.392	1.918	1.882	0.036
	4Y	3.375	2.492	2.466	0.026
	5Y	3.356	3.042	3.027	0.015
	6Y	3.333	3.563	3.571	0.008
	7Y	3.309	4.077	4.094	0.017
	8Y	3.285	4.569	4.594	0.025
	9Y	3.261	5.047	5.074	0.027
	10Y	3.237	5.520	5.533	0.013
	11Y	3.213	5.944	5.968	0.024
	12Y	3.190	6.351	6.381	0.030
	13Y	3.169	6.739	6.769	0.030
2038-10-24	14Y	3.150	7.108	7.131	0.023
	15Y	3.132	7.459	7.465	0.007
	1Y	3.389	0.670	0.661	0.009
	2Y	3.391	1.323	1.289	0.035
	3Y	3.368	1.926	1.902	0.024
	4Y	3.345	2.500	2.492	0.008
	5Y	3.319	3.051	3.063	0.012
	6Y	3.293	3.572	3.612	0.040
	7Y	3.268	4.082	4.137	0.055
	8Y	3.242	4.573	4.640	0.067
	9Y	3.216	5.049	5.121	0.072
	10Y	3.192	5.526	5.577	0.051
	11Y	3.168	5.952	6.010	0.059
	12Y	3.146	6.360	6.417	0.058
	13Y	3.126	6.747	6.797	0.050
2039-10-24	14Y	3.109	7.117	7.149	0.032
	15Y	3.093	7.469	7.476	0.008
	1Y	3.392	0.672	0.657	0.014
	2Y	3.356	1.326	1.300	0.026
	3Y	3.330	1.929	1.917	0.012
	4Y	3.301	2.505	2.514	0.009
	5Y	3.272	3.047	3.088	0.041
	6Y	3.245	3.569	3.637	0.068
	7Y	3.218	4.077	4.163	0.086
	8Y	3.191	4.565	4.666	0.100
	9Y	3.166	5.042	5.142	0.101
	10Y	3.142	5.515	5.595	0.080
	11Y	3.120	5.944	6.020	0.076
	12Y	3.100	6.350	6.418	0.067
	13Y	3.082	6.738	6.786	0.048
2040-10-24	14Y	3.066	7.107	7.129	0.022
	15Y	3.052	7.461	7.448	0.014
	1Y	3.319	0.671	0.670	0.000
	2Y	3.297	1.325	1.315	0.010
	3Y	3.268	1.931	1.937	0.006
	4Y	3.240	2.499	2.535	0.037
	5Y	3.213	3.039	3.108	0.068
	6Y	3.186	3.558	3.656	0.097
	7Y	3.159	4.063	4.179	0.116
	8Y	3.134	4.550	4.676	0.126
	9Y	3.109	5.020	5.148	0.128

Date of Maturity	Swap Tenor	Strike (%)	Price (%)	Model Price (%)	Model Error (%)
	10Y	3.087	5.492	5.591	0.099
	11Y	3.068	5.922	6.006	0.084
	12Y	3.051	6.327	6.390	0.063
	13Y	3.035	6.714	6.749	0.035
	14Y	3.021	7.084	7.082	0.002
	15Y	3.008	7.434	7.390	0.045

D.3 European call option data

European call option data for BNP Paribas

Table 17: Option data for BNPE on October 24, 2025 for spot stock price $s = 68.72\text{€}$.

Ticker	Start Date	Date of Maturity	Instrument	Price	Strike Price
BNPE	2025-10-24	2025-11-21	/BNPE520K5.EX	16.94	52.00
			/BNPE530K5.EX	15.96	53.00
			/BNPE540K5.EX	14.99	54.00
			/BNPE550K5.EX	14.02	55.00
			/BNPE560K5.EX	13.06	56.00
			/BNPE570K5.EX	12.10	57.00
			/BNPE580K5.EX	11.15	58.00
			/BNPE590K5.EX	10.21	59.00
			/BNPE600K5.EX	9.29	60.00
			/BNPE610K5.EX	8.38	61.00
			/BNPE620K5.EX	7.49	62.00
			/BNPE630K5.EX	6.63	63.00
			/BNPE640K5.EX	5.80	64.00
			/BNPE650K5.EX	5.01	65.00
			/BNPE660K5.EX	4.27	66.00
			/BNPE670K5.EX	3.58	67.00
			/BNPE680K5.EX	2.96	68.00
			/BNPE690K5.EX	2.40	69.00
			/BNPE700K5.EX	1.91	70.00
			/BNPE710K5.EX	1.50	71.00
			/BNPE720K5.EX	1.16	72.00
			/BNPE730K5.EX	0.88	73.00
			/BNPE740K5.EX	0.66	74.00
			/BNPE750K5.EX	0.49	75.00
			/BNPE760K5.EX	0.33	76.00
			/BNPE770K5.EX	0.23	77.00
			/BNPE780K5.EX	0.16	78.00
			/BNPE790K5.EX	0.11	79.00
			/BNPE800K5.EX	0.07	80.00
			/BNPE810K5.EX	0.05	81.00
			/BNPE820K5.EX	0.03	82.00
			/BNPE830K5.EX	0.02	83.00
			/BNPE840K5.EX	0.01	84.00
			/BNPE850K5.EX	0.01	85.00
			/BNPE860K5.EX	0.01	86.00
			/BNPE870K5.EX	0.01	87.00
			/BNPE880K5.EX	0.01	88.00
			/BNPE890K5.EX	0.01	89.00
			/BNPE900K5.EX	0.01	90.00
			/BNPE910K5.EX	0.01	91.00
			/BNPE920K5.EX	0.01	92.00
			/BNPE930K5.EX	0.01	93.00
			/BNPE940K5.EX	0.01	94.00
	2025-12-19		/BNPE520L5.EX	17.38	52.00
			/BNPE530L5.EX	16.42	53.00
			/BNPE540L5.EX	15.45	54.00
			/BNPE550L5.EX	14.48	55.00
			/BNPE560L5.EX	13.52	56.00
			/BNPE570L5.EX	12.56	57.00

Ticker	Start Date	Date of Maturity	Instrument	Price	Strike Price
			/BNPE580L5.EX	11.61	58.00
			/BNPE590L5.EX	10.67	59.00
			/BNPE600L5.EX	9.74	60.00
			/BNPE610L5.EX	8.82	61.00
			/BNPE620L5.EX	7.92	62.00
			/BNPE630L5.EX	7.05	63.00
			/BNPE640L5.EX	6.20	64.00
			/BNPE650L5.EX	5.38	65.00
			/BNPE660L5.EX	4.60	66.00
			/BNPE670L5.EX	3.87	67.00
			/BNPE680L5.EX	3.19	68.00
			/BNPE690L5.EX	2.58	69.00
			/BNPE700L5.EX	2.03	70.00
			/BNPE710L5.EX	1.57	71.00
			/BNPE720L5.EX	1.19	72.00
			/BNPE730L5.EX	0.89	73.00
			/BNPE740L5.EX	0.66	74.00
			/BNPE750L5.EX	0.48	75.00
			/BNPE760L5.EX	0.34	76.00
			/BNPE770L5.EX	0.24	77.00
			/BNPE780L5.EX	0.17	78.00
			/BNPE790L5.EX	0.12	79.00
			/BNPE800L5.EX	0.08	80.00
			/BNPE810L5.EX	0.05	81.00
			/BNPE820L5.EX	0.04	82.00
			/BNPE830L5.EX	0.03	83.00
			/BNPE840L5.EX	0.02	84.00
			/BNPE850L5.EX	0.02	85.00
			/BNPE860L5.EX	0.01	86.00
			/BNPE870L5.EX	0.01	87.00
			/BNPE880L5.EX	0.01	88.00
			/BNPE890L5.EX	0.01	89.00
			/BNPE900L5.EX	0.01	90.00
			/BNPE910L5.EX	0.01	91.00
			/BNPE920L5.EX	0.01	92.00
			/BNPE930L5.EX	0.01	93.00
			/BNPE940L5.EX	0.01	94.00
			/BNPE950L5.EX	0.01	95.00
			/BNPE960L5.EX	0.01	96.00
	2026-01-16		/BNPE520C6.EX	17.92	52.00
			/BNPE530C6.EX	16.96	53.00
			/BNPE540C6.EX	16.00	54.00
			/BNPE550C6.EX	15.03	55.00
			/BNPE560C6.EX	14.07	56.00
			/BNPE570C6.EX	13.11	57.00
			/BNPE580C6.EX	12.16	58.00
			/BNPE590C6.EX	11.22	59.00
			/BNPE600C6.EX	10.29	60.00
			/BNPE610C6.EX	9.38	61.00
			/BNPE620C6.EX	8.48	62.00
			/BNPE630C6.EX	7.61	63.00
			/BNPE640C6.EX	6.76	64.00
			/BNPE650C6.EX	5.95	65.00
			/BNPE660C6.EX	5.18	66.00
			/BNPE670C6.EX	4.45	67.00
			/BNPE680C6.EX	3.78	68.00

Ticker	Start Date	Date of Maturity	Instrument	Price	Strike Price
2026-03-20			/BNPE690C6.EX	3.17	69.00
			/BNPE700C6.EX	2.62	70.00
			/BNPE710C6.EX	2.15	71.00
			/BNPE720C6.EX	1.74	72.00
			/BNPE730C6.EX	1.40	73.00
			/BNPE740C6.EX	1.11	74.00
			/BNPE750C6.EX	0.87	75.00
			/BNPE760C6.EX	0.67	76.00
			/BNPE770C6.EX	0.51	77.00
			/BNPE780C6.EX	0.38	78.00
			/BNPE790C6.EX	0.29	79.00
			/BNPE800C6.EX	0.22	80.00
			/BNPE810C6.EX	0.17	81.00
			/BNPE820C6.EX	0.13	82.00
			/BNPE830C6.EX	0.10	83.00
			/BNPE840C6.EX	0.08	84.00
			/BNPE520C6.EX	18.40	52.00
			/BNPE530C6.EX	17.44	53.00
			/BNPE540C6.EX	16.48	54.00
			/BNPE550C6.EX	15.51	55.00
			/BNPE560C6.EX	14.55	56.00
			/BNPE570C6.EX	13.59	57.00
			/BNPE580C6.EX	12.64	58.00
			/BNPE590C6.EX	11.70	59.00
			/BNPE600C6.EX	10.77	60.00
			/BNPE610C6.EX	9.85	61.00
			/BNPE620C6.EX	8.95	62.00
			/BNPE630C6.EX	8.07	63.00
			/BNPE640C6.EX	7.22	64.00
			/BNPE650C6.EX	6.40	65.00
			/BNPE660C6.EX	5.62	66.00
			/BNPE670C6.EX	4.88	67.00
			/BNPE680C6.EX	4.20	68.00
			/BNPE690C6.EX	3.58	69.00
			/BNPE700C6.EX	3.03	70.00
			/BNPE710C6.EX	2.55	71.00
			/BNPE720C6.EX	2.13	72.00
			/BNPE730C6.EX	1.76	73.00
			/BNPE740C6.EX	1.44	74.00
			/BNPE750C6.EX	1.17	75.00
			/BNPE760C6.EX	0.94	76.00
			/BNPE770C6.EX	0.75	77.00
			/BNPE780C6.EX	0.59	78.00
			/BNPE790C6.EX	0.46	79.00
2026-06-19			/BNPE520F6.EX	18.88	52.00
			/BNPE530F6.EX	17.93	53.00
			/BNPE540F6.EX	16.96	54.00
			/BNPE550F6.EX	16.00	55.00
			/BNPE560F6.EX	15.04	56.00
			/BNPE570F6.EX	14.08	57.00
			/BNPE580F6.EX	13.12	58.00
			/BNPE590F6.EX	12.17	59.00
			/BNPE600F6.EX	11.23	60.00
			/BNPE610F6.EX	10.30	61.00
			/BNPE620F6.EX	9.38	62.00
			/BNPE630F6.EX	8.48	63.00

Ticker	Start Date	Date of Maturity	Instrument	Price	Strike Price
2026-09-18			/BNPE640F6.EX	7.60	64.00
			/BNPE650F6.EX	6.75	65.00
			/BNPE660F6.EX	5.93	66.00
			/BNPE670F6.EX	5.15	67.00
			/BNPE680F6.EX	4.42	68.00
			/BNPE690F6.EX	3.75	69.00
			/BNPE700F6.EX	3.14	70.00
			/BNPE710F6.EX	2.59	71.00
			/BNPE720F6.EX	2.10	72.00
			/BNPE730F6.EX	1.67	73.00
			/BNPE740F6.EX	1.29	74.00
			/BNPE750F6.EX	0.97	75.00
			/BNPE760F6.EX	0.70	76.00
			/BNPE770F6.EX	0.48	77.00
			/BNPE780F6.EX	0.31	78.00
			/BNPE790F6.EX	0.19	79.00
			/BNPE520I6.EX	19.34	52.00
			/BNPE530I6.EX	18.38	53.00
			/BNPE540I6.EX	17.42	54.00
			/BNPE550I6.EX	16.46	55.00
			/BNPE560I6.EX	15.50	56.00
			/BNPE570I6.EX	14.54	57.00
			/BNPE580I6.EX	13.58	58.00
			/BNPE590I6.EX	12.63	59.00
			/BNPE600I6.EX	11.69	60.00
			/BNPE610I6.EX	10.76	61.00
			/BNPE620I6.EX	9.84	62.00
			/BNPE630I6.EX	8.94	63.00
			/BNPE640I6.EX	8.06	64.00
			/BNPE650I6.EX	7.21	65.00
			/BNPE660I6.EX	6.39	66.00
			/BNPE670I6.EX	5.61	67.00
			/BNPE680I6.EX	4.88	68.00
			/BNPE690I6.EX	4.20	69.00
			/BNPE700I6.EX	3.59	70.00
			/BNPE710I6.EX	3.04	71.00
			/BNPE720I6.EX	2.55	72.00
			/BNPE730I6.EX	2.13	73.00
			/BNPE740I6.EX	1.77	74.00
			/BNPE750I6.EX	1.47	75.00
			/BNPE760I6.EX	1.22	76.00
			/BNPE770I6.EX	1.02	77.00
			/BNPE780I6.EX	0.85	78.00
			/BNPE790I6.EX	0.72	79.00
2026-12-18			/BNPE520L6.EX	19.68	52.00
			/BNPE530L6.EX	18.72	53.00
			/BNPE540L6.EX	17.76	54.00
			/BNPE550L6.EX	16.80	55.00
			/BNPE560L6.EX	15.84	56.00
			/BNPE570L6.EX	14.88	57.00
			/BNPE580L6.EX	13.92	58.00
			/BNPE590L6.EX	12.97	59.00
			/BNPE600L6.EX	12.03	60.00
			/BNPE610L6.EX	11.10	61.00
			/BNPE620L6.EX	10.18	62.00
			/BNPE630L6.EX	9.28	63.00

Ticker	Start Date	Date of Maturity	Instrument	Price	Strike Price
		/BNPE640L6.EX	8.40	64.00	
		/BNPE650L6.EX	7.55	65.00	
		/BNPE660L6.EX	6.73	66.00	
		/BNPE670L6.EX	5.95	67.00	
		/BNPE680L6.EX	5.22	68.00	
		/BNPE690L6.EX	4.54	69.00	
		/BNPE700L6.EX	3.93	70.00	
	2027-06-18	/BNPE520F7.EX	20.08	52.00	
		/BNPE530F7.EX	19.12	53.00	
		/BNPE540F7.EX	18.16	54.00	
		/BNPE550F7.EX	17.20	55.00	
		/BNPE560F7.EX	16.24	56.00	
		/BNPE570F7.EX	15.28	57.00	
		/BNPE580F7.EX	14.32	58.00	
		/BNPE590F7.EX	13.37	59.00	
		/BNPE600F7.EX	12.43	60.00	
		/BNPE610F7.EX	11.50	61.00	
		/BNPE620F7.EX	10.58	62.00	
		/BNPE630F7.EX	9.68	63.00	
		/BNPE640F7.EX	8.80	64.00	
		/BNPE650F7.EX	7.95	65.00	
		/BNPE660F7.EX	7.13	66.00	
		/BNPE670F7.EX	6.35	67.00	
		/BNPE680F7.EX	5.62	68.00	
		/BNPE690F7.EX	4.94	69.00	
		/BNPE700F7.EX	4.33	70.00	
	2027-12-17	/BNPE520L7.EX	20.43	52.00	
		/BNPE530L7.EX	19.47	53.00	
		/BNPE540L7.EX	18.51	54.00	
		/BNPE550L7.EX	17.55	55.00	
		/BNPE560L7.EX	16.59	56.00	
		/BNPE570L7.EX	15.63	57.00	
		/BNPE580L7.EX	14.67	58.00	
		/BNPE590L7.EX	13.72	59.00	
		/BNPE600L7.EX	12.78	60.00	
		/BNPE610L7.EX	11.85	61.00	
		/BNPE620L7.EX	10.93	62.00	
		/BNPE630L7.EX	10.03	63.00	
		/BNPE640L7.EX	9.15	64.00	
		/BNPE650L7.EX	8.30	65.00	
		/BNPE660L7.EX	7.48	66.00	
		/BNPE670L7.EX	6.70	67.00	
		/BNPE680L7.EX	5.97	68.00	
		/BNPE690L7.EX	5.29	69.00	
	2028-06-16	/BNPE520F8.EX	20.76	52.00	
		/BNPE530F8.EX	19.80	53.00	
		/BNPE540F8.EX	18.84	54.00	
		/BNPE550F8.EX	17.88	55.00	
		/BNPE560F8.EX	16.92	56.00	
		/BNPE570F8.EX	15.96	57.00	
		/BNPE580F8.EX	15.00	58.00	
		/BNPE590F8.EX	14.05	59.00	
		/BNPE600F8.EX	13.11	60.00	
		/BNPE610F8.EX	12.18	61.00	
		/BNPE620F8.EX	11.26	62.00	
		/BNPE630F8.EX	10.36	63.00	

Ticker	Start Date	Date of Maturity	Instrument	Price	Strike Price
			/BNPE640F8.EX	9.48	64.00
			/BNPE650F8.EX	8.63	65.00
			/BNPE660F8.EX	7.81	66.00
			/BNPE670F8.EX	7.03	67.00
			/BNPE680F8.EX	6.30	68.00
			/BNPE690F8.EX	5.62	69.00

European call option data on SAP

Table 18: Option data for SAPE on October 24, 2025 for spot stock price $s = 242\text{€}$.

Ticker	Start Date	Date of Maturity	Instrument	Price	Strike Price
SAPE	2025-10-24	2025-11-21	/SAPE1720bK5.EX	70.39	172.00
			/SAPE1740bK5.EX	68.40	174.00
			/SAPE1760bK5.EX	66.40	176.00
			/SAPE1780bK5.EX	64.41	178.00
			/SAPE1800bK5.EX	62.41	180.00
			/SAPE1820bK5.EX	60.42	182.00
			/SAPE1840bK5.EX	58.43	184.00
			/SAPE1860bK5.EX	56.44	186.00
			/SAPE1880bK5.EX	54.45	188.00
			/SAPE1900bK5.EX	52.46	190.00
			/SAPE1920bK5.EX	50.47	192.00
			/SAPE1940bK5.EX	48.48	194.00
			/SAPE1960bK5.EX	46.50	196.00
			/SAPE1980bK5.EX	44.52	198.00
			/SAPE2000bK5.EX	42.54	200.00
			/SAPE2050bK5.EX	37.62	205.00
			/SAPE2100bK5.EX	32.75	210.00
			/SAPE2150bK5.EX	27.96	215.00
			/SAPE2200bK5.EX	23.30	220.00
			/SAPE2250bK5.EX	18.87	225.00
			/SAPE2300bK5.EX	14.78	230.00
			/SAPE2350bK5.EX	11.15	235.00
			/SAPE2400bK5.EX	8.09	240.00
			/SAPE2450bK5.EX	5.70	245.00
			/SAPE2500bK5.EX	3.97	250.00
			/SAPE2550bK5.EX	2.73	255.00
			/SAPE2600bK5.EX	1.89	260.00
			/SAPE2650bK5.EX	1.32	265.00
			/SAPE2700bK5.EX	0.93	270.00
			/SAPE2750bK5.EX	0.66	275.00
			/SAPE2800bK5.EX	0.46	280.00
			/SAPE2850bK5.EX	0.32	285.00
			/SAPE2900bK5.EX	0.23	290.00
			/SAPE2950bK5.EX	0.16	295.00
			/SAPE3000bK5.EX	0.11	300.00
			/SAPE3100bK5.EX	0.06	310.00
	2025-12-19		/SAPE1760bL5.EX	68.01	176.00
			/SAPE1780bL5.EX	66.03	178.00
			/SAPE1800bL5.EX	64.04	180.00
			/SAPE1820bL5.EX	62.06	182.00
			/SAPE1840bL5.EX	60.08	184.00

Ticker	Start Date	Date of Maturity	Instrument	Price	Strike Price
			/SAPE1860bL5.EX	58.10	186.00
			/SAPE1880bL5.EX	56.13	188.00
			/SAPE1900bL5.EX	54.16	190.00
			/SAPE1920bL5.EX	52.19	192.00
			/SAPE1940bL5.EX	50.23	194.00
			/SAPE1960bL5.EX	48.28	196.00
			/SAPE1980bL5.EX	46.33	198.00
			/SAPE2000bL5.EX	44.39	200.00
			/SAPE2050bL5.EX	39.69	205.00
			/SAPE2100bL5.EX	35.11	210.00
			/SAPE2150bL5.EX	30.64	215.00
			/SAPE2200bL5.EX	26.33	220.00
			/SAPE2250bL5.EX	22.22	225.00
			/SAPE2300bL5.EX	18.38	230.00
			/SAPE2350bL5.EX	14.86	235.00
			/SAPE2400bL5.EX	11.71	240.00
			/SAPE2450bL5.EX	8.99	245.00
			/SAPE2500bL5.EX	6.74	250.00
			/SAPE2550bL5.EX	4.92	255.00
			/SAPE2600bL5.EX	3.52	260.00
			/SAPE2650bL5.EX	2.48	265.00
			/SAPE2700bL5.EX	1.72	270.00
			/SAPE2750bL5.EX	1.19	275.00
			/SAPE2800bL5.EX	0.82	280.00
			/SAPE2850bL5.EX	0.58	285.00
			/SAPE2900bL5.EX	0.41	290.00
			/SAPE3000bL5.EX	0.22	300.00
			/SAPE3200bL5.EX	0.06	320.00
	2026-01-16		/SAPE1720bC6.EX	71.79	172.00
			/SAPE1740bC6.EX	69.80	174.00
			/SAPE1760bC6.EX	67.81	176.00
			/SAPE1780bC6.EX	65.83	178.00
			/SAPE1800bC6.EX	63.84	180.00
			/SAPE1820bC6.EX	61.85	182.00
			/SAPE1840bC6.EX	59.87	184.00
			/SAPE1860bC6.EX	57.90	186.00
			/SAPE1880bC6.EX	55.93	188.00
			/SAPE1900bC6.EX	53.97	190.00
			/SAPE1920bC6.EX	52.01	192.00
			/SAPE1940bC6.EX	50.07	194.00
			/SAPE1960bC6.EX	48.15	196.00
			/SAPE1980bC6.EX	46.25	198.00
			/SAPE2000bC6.EX	44.37	200.00
			/SAPE2050bC6.EX	39.78	205.00
			/SAPE2100bC6.EX	35.35	210.00
			/SAPE2150bC6.EX	31.02	215.00
			/SAPE2200bC6.EX	26.84	220.00
			/SAPE2250bC6.EX	22.86	225.00
			/SAPE2300bC6.EX	19.13	230.00
			/SAPE2350bC6.EX	15.71	235.00
			/SAPE2400bC6.EX	12.65	240.00
			/SAPE2450bC6.EX	9.99	245.00
			/SAPE2500bC6.EX	7.74	250.00
			/SAPE2550bC6.EX	5.86	255.00
			/SAPE2600bC6.EX	4.32	260.00
			/SAPE2650bC6.EX	3.09	265.00

Ticker	Start Date	Date of Maturity	Instrument	Price	Strike Price
			/SAPE2700bC6.EX	2.11	270.00
			/SAPE2750bC6.EX	1.36	275.00
			/SAPE2800bC6.EX	0.83	280.00
			/SAPE2850bC6.EX	0.48	285.00
			/SAPE2900bC6.EX	0.27	290.00
			/SAPE2950bC6.EX	0.14	295.00
			/SAPE3000bC6.EX	0.07	300.00
	2026-03-20		/SAPE1720bC6.EX	73.44	172.00
			/SAPE1740bC6.EX	71.45	174.00
			/SAPE1760bC6.EX	69.46	176.00
			/SAPE1780bC6.EX	67.47	178.00
			/SAPE1800bC6.EX	65.49	180.00
			/SAPE1820bC6.EX	63.50	182.00
			/SAPE1840bC6.EX	61.52	184.00
			/SAPE1860bC6.EX	59.54	186.00
			/SAPE1880bC6.EX	57.57	188.00
			/SAPE1900bC6.EX	55.60	190.00
			/SAPE1920bC6.EX	53.64	192.00
			/SAPE1940bC6.EX	51.69	194.00
			/SAPE1960bC6.EX	49.74	196.00
			/SAPE1980bC6.EX	47.81	198.00
			/SAPE2000bC6.EX	45.90	200.00
			/SAPE2050bC6.EX	41.39	205.00
			/SAPE2100bC6.EX	37.02	210.00
			/SAPE2150bC6.EX	32.76	215.00
			/SAPE2200bC6.EX	28.65	220.00
			/SAPE2250bC6.EX	24.72	225.00
			/SAPE2300bC6.EX	21.02	230.00
			/SAPE2350bC6.EX	17.60	235.00
			/SAPE2400bC6.EX	14.52	240.00
			/SAPE2450bC6.EX	11.80	245.00
			/SAPE2500bC6.EX	9.48	250.00
			/SAPE2550bC6.EX	7.55	255.00
			/SAPE2600bC6.EX	5.96	260.00
			/SAPE2650bC6.EX	4.65	265.00
			/SAPE2700bC6.EX	3.57	270.00
			/SAPE2750bC6.EX	2.70	275.00
			/SAPE2800bC6.EX	1.99	280.00
			/SAPE2850bC6.EX	1.44	285.00
			/SAPE2900bC6.EX	1.02	290.00
			/SAPE2950bC6.EX	0.73	295.00
			/SAPE3000bC6.EX	0.52	300.00
			/SAPE3100bC6.EX	0.23	310.00
			/SAPE3200bC6.EX	0.11	320.00
			/SAPE3400bC6.EX	0.03	340.00
			/SAPE3600bC6.EX	0.01	360.00
			/SAPE3800bC6.EX	0.01	380.00
			/SAPE4000bC6.EX	0.00	400.00
			/SAPE4400bC6.EX	0.00	440.00
			/SAPE4800bC6.EX	0.00	480.00
	2026-05-15		/SAPE1720bC6.EX	75.00	172.00
			/SAPE1740bC6.EX	73.01	174.00
			/SAPE1760bC6.EX	71.01	176.00
			/SAPE1780bC6.EX	69.03	178.00
			/SAPE1800bC6.EX	67.04	180.00
			/SAPE1820bC6.EX	65.06	182.00

Ticker	Start Date	Date of Maturity	Instrument	Price	Strike Price
			/SAPE1840bC6.EX	63.08	184.00
			/SAPE1860bC6.EX	61.11	186.00
			/SAPE1880bC6.EX	59.14	188.00
			/SAPE1900bC6.EX	57.18	190.00
			/SAPE1920bC6.EX	55.22	192.00
			/SAPE1940bC6.EX	53.27	194.00
			/SAPE1960bC6.EX	51.33	196.00
			/SAPE1980bC6.EX	49.40	198.00
			/SAPE2000bC6.EX	47.48	200.00
			/SAPE2050bC6.EX	43.02	205.00
			/SAPE2100bC6.EX	38.74	210.00
			/SAPE2150bC6.EX	34.52	215.00
			/SAPE2200bC6.EX	30.39	220.00
			/SAPE2250bC6.EX	26.41	225.00
			/SAPE2300bC6.EX	22.62	230.00
			/SAPE2350bC6.EX	19.09	235.00
			/SAPE2400bC6.EX	15.84	240.00
			/SAPE2450bC6.EX	12.92	245.00
			/SAPE2500bC6.EX	10.35	250.00
			/SAPE2550bC6.EX	8.13	255.00
			/SAPE2600bC6.EX	6.26	260.00
			/SAPE2650bC6.EX	4.71	265.00
			/SAPE2700bC6.EX	3.44	270.00
			/SAPE2750bC6.EX	2.42	275.00
			/SAPE2800bC6.EX	1.63	280.00
			/SAPE2850bC6.EX	1.02	285.00
			/SAPE2900bC6.EX	0.63	290.00
			/SAPE2950bC6.EX	0.40	295.00
			/SAPE3000bC6.EX	0.25	300.00
			/SAPE3100bC6.EX	0.10	310.00
			/SAPE3200bC6.EX	0.05	320.00
			/SAPE3400bC6.EX	0.01	340.00
			/SAPE3600bC6.EX	0.01	360.00
			/SAPE3800bC6.EX	0.00	380.00
			/SAPE4000bC6.EX	0.00	400.00
			/SAPE4400bC6.EX	0.00	440.00
			/SAPE4800bC6.EX	0.00	480.00
	2026-09-18		/SAPE1720bC6.EX	77.33	172.00
			/SAPE1740bC6.EX	75.34	174.00
			/SAPE1760bC6.EX	73.35	176.00
			/SAPE1780bC6.EX	71.37	178.00
			/SAPE1800bC6.EX	69.38	180.00
			/SAPE1820bC6.EX	67.40	182.00
			/SAPE1840bC6.EX	65.42	184.00
			/SAPE1860bC6.EX	63.45	186.00
			/SAPE1880bC6.EX	61.48	188.00
			/SAPE1900bC6.EX	59.52	190.00
			/SAPE1920bC6.EX	57.56	192.00
			/SAPE1940bC6.EX	55.61	194.00
			/SAPE1960bC6.EX	53.67	196.00
			/SAPE1980bC6.EX	51.74	198.00
			/SAPE2000bC6.EX	49.82	200.00
			/SAPE2050bC6.EX	45.39	205.00
			/SAPE2100bC6.EX	41.14	210.00
			/SAPE2150bC6.EX	36.98	215.00
			/SAPE2200bC6.EX	32.91	220.00

Ticker	Start Date	Date of Maturity	Instrument	Price	Strike Price
			/SAPE2250bC6.EX	28.97	225.00
			/SAPE2300bC6.EX	25.20	230.00
			/SAPE2350bC6.EX	21.66	235.00
			/SAPE2400bC6.EX	18.38	240.00
			/SAPE2450bC6.EX	15.40	245.00
			/SAPE2500bC6.EX	12.74	250.00
			/SAPE2550bC6.EX	10.40	255.00
			/SAPE2600bC6.EX	8.38	260.00
			/SAPE2650bC6.EX	6.65	265.00
			/SAPE2700bC6.EX	5.19	270.00
			/SAPE2750bC6.EX	3.98	275.00
			/SAPE2800bC6.EX	2.99	280.00
			/SAPE2850bC6.EX	2.20	285.00
			/SAPE2900bC6.EX	1.57	290.00
			/SAPE2950bC6.EX	1.10	295.00
			/SAPE3000bC6.EX	0.76	300.00
			/SAPE3100bC6.EX	0.34	310.00
			/SAPE3200bC6.EX	0.16	320.00
			/SAPE3400bC6.EX	0.05	340.00
			/SAPE3600bC6.EX	0.02	360.00
			/SAPE3800bC6.EX	0.01	380.00
			/SAPE4000bC6.EX	0.00	400.00
			/SAPE4400bC6.EX	0.00	440.00
			/SAPE4800bC6.EX	0.00	480.00
	2027-01-15		/SAPE1720bC7.EX	78.70	172.00
			/SAPE1740bC7.EX	76.71	174.00
			/SAPE1760bC7.EX	74.73	176.00
			/SAPE1780bC7.EX	72.74	178.00
			/SAPE1800bC7.EX	70.75	180.00
			/SAPE1820bC7.EX	68.77	182.00
			/SAPE1840bC7.EX	66.79	184.00
			/SAPE1860bC7.EX	64.82	186.00
			/SAPE1880bC7.EX	62.85	188.00
			/SAPE1900bC7.EX	60.89	190.00
			/SAPE1920bC7.EX	58.93	192.00
			/SAPE1940bC7.EX	56.98	194.00
			/SAPE1960bC7.EX	55.03	196.00
			/SAPE1980bC7.EX	53.09	198.00
			/SAPE2000bC7.EX	51.15	200.00
			/SAPE2050bC7.EX	46.75	205.00
			/SAPE2100bC7.EX	42.51	210.00
			/SAPE2150bC7.EX	38.39	215.00
			/SAPE2200bC7.EX	34.39	220.00
			/SAPE2250bC7.EX	30.55	225.00
			/SAPE2300bC7.EX	26.90	230.00
			/SAPE2350bC7.EX	23.48	235.00
			/SAPE2400bC7.EX	20.34	240.00
			/SAPE2450bC7.EX	17.52	245.00
			/SAPE2500bC7.EX	15.03	250.00
			/SAPE2550bC7.EX	12.86	255.00
			/SAPE2600bC7.EX	10.97	260.00
			/SAPE2650bC7.EX	9.33	265.00
			/SAPE2700bC7.EX	7.92	270.00
			/SAPE2750bC7.EX	6.70	275.00
			/SAPE2800bC7.EX	5.65	280.00
			/SAPE2850bC7.EX	4.76	285.00

Ticker	Start Date	Date of Maturity	Instrument	Price	Strike Price
			/SAPE2900bC7.EX	4.01	290.00
			/SAPE2950bC7.EX	3.39	295.00
			/SAPE3000bC7.EX	2.88	300.00
			/SAPE3100bC7.EX	2.12	310.00
			/SAPE3200bC7.EX	1.56	320.00
			/SAPE3400bC7.EX	0.78	340.00
			/SAPE3600bC7.EX	0.40	360.00
			/SAPE3800bC7.EX	0.22	380.00
			/SAPE4000bC7.EX	0.12	400.00
			/SAPE4400bC7.EX	0.04	440.00
			/SAPE4800bC7.EX	0.02	480.00
	2027-12-17		/SAPE1720bC7.EX	84.24	172.00
			/SAPE1740bC7.EX	82.25	174.00
			/SAPE1760bC7.EX	80.27	176.00
			/SAPE1780bC7.EX	78.28	178.00
			/SAPE1800bC7.EX	76.30	180.00
			/SAPE1820bC7.EX	74.32	182.00
			/SAPE1840bC7.EX	72.35	184.00
			/SAPE1860bC7.EX	70.37	186.00
			/SAPE1880bC7.EX	68.40	188.00
			/SAPE1900bC7.EX	66.44	190.00
			/SAPE1920bC7.EX	64.47	192.00
			/SAPE1940bC7.EX	62.52	194.00
			/SAPE1960bC7.EX	60.57	196.00
			/SAPE1980bC7.EX	58.63	198.00
			/SAPE2000bC7.EX	56.70	200.00
			/SAPE2050bC7.EX	52.34	205.00
			/SAPE2100bC7.EX	48.09	210.00
			/SAPE2150bC7.EX	43.93	215.00
			/SAPE2200bC7.EX	39.88	220.00
			/SAPE2250bC7.EX	35.96	225.00
			/SAPE2300bC7.EX	32.21	230.00
			/SAPE2350bC7.EX	28.66	235.00
			/SAPE2400bC7.EX	25.35	240.00
			/SAPE2450bC7.EX	22.30	245.00
			/SAPE2500bC7.EX	19.54	250.00
			/SAPE2550bC7.EX	17.06	255.00
			/SAPE2600bC7.EX	14.86	260.00
			/SAPE2650bC7.EX	12.92	265.00
			/SAPE2700bC7.EX	11.23	270.00
			/SAPE2750bC7.EX	9.77	275.00
			/SAPE2800bC7.EX	8.51	280.00
			/SAPE2850bC7.EX	7.42	285.00
			/SAPE2900bC7.EX	6.49	290.00
			/SAPE2950bC7.EX	5.69	295.00
			/SAPE3000bC7.EX	5.01	300.00
			/SAPE3100bC7.EX	3.97	310.00
			/SAPE3200bC7.EX	3.16	320.00
			/SAPE3400bC7.EX	1.92	340.00
			/SAPE3600bC7.EX	1.17	360.00
			/SAPE3800bC7.EX	0.76	380.00
			/SAPE4000bC7.EX	0.52	400.00
			/SAPE4400bC7.EX	0.24	440.00
			/SAPE4800bC7.EX	0.12	480.00
	2029-12-21		/SAPE400bL9.EX	203.61	40.00
			/SAPE480bL9.EX	197.05	48.00

Ticker	Start Date	Date of Maturity	Instrument	Price	Strike Price
			/SAPE560bL9.EX	190.55	56.00
			/SAPE640bL9.EX	184.09	64.00
			/SAPE720bL9.EX	177.63	72.00
			/SAPE800bL9.EX	171.28	80.00
			/SAPE840bL9.EX	162.99	84.00
			/SAPE920bL9.EX	156.19	92.00
			/SAPE1000bL9.EX	149.48	100.00
			/SAPE1200bL9.EX	133.19	120.00
			/SAPE1400bL9.EX	117.74	140.00
			/SAPE1600bL9.EX	103.30	160.00
			/SAPE1800bL9.EX	90.01	180.00
			/SAPE2000bL9.EX	77.96	200.00
			/SAPE2400bL9.EX	57.75	240.00
			/SAPE2800bL9.EX	42.44	280.00
			/SAPE3200bL9.EX	31.21	320.00
			/SAPE3600bL9.EX	23.12	360.00
			/SAPE4000bL9.EX	17.31	400.00
			/SAPE4800bL9.EX	10.07	480.00
	2028-06-16		/SAPE400bF8.EX	204.46	40.00
			/SAPE480bF8.EX	198.03	48.00
			/SAPE560bF8.EX	191.65	56.00
			/SAPE640bF8.EX	185.31	64.00
			/SAPE720bF8.EX	179.00	72.00
			/SAPE800bF8.EX	172.72	80.00
			/SAPE840bF8.EX	158.40	84.00
			/SAPE920bF8.EX	151.13	92.00
			/SAPE1000bF8.EX	143.94	100.00
			/SAPE1200bF8.EX	126.32	120.00
			/SAPE1400bF8.EX	109.43	140.00
			/SAPE1600bF8.EX	93.52	160.00
			/SAPE1800bF8.EX	78.84	180.00
			/SAPE2000bF8.EX	65.64	200.00
			/SAPE2400bF8.EX	44.11	240.00
			/SAPE2800bF8.EX	28.94	280.00
			/SAPE3200bF8.EX	18.89	320.00
			/SAPE3600bF8.EX	12.43	360.00
			/SAPE4000bF8.EX	8.31	400.00
			/SAPE4800bF8.EX	3.94	480.00
